

POLITECNICO DI TORINO

Master's Degree in Civil Engineering



Master Thesis

**The Bridged Crack model with n fibers:
Cyclic loading, hysteresis, and shake-down**

Tutors

Prof. Alberto CARPINTERI

Ing. Federico ACCORNERO

Candidate

Giulio BAFFA GIUSA

Academic Year 2016-2017

Abstract

Brittle matrix fiber reinforced materials are characterized by enhanced strength, ductility and cracking resistance thanks to the bridging action exerted by the fiber reinforcements. These materials are often used in structures subjected to cyclic loading. The analysis of their behaviour in this condition and the phenomena of hysteresis and shake-down are the subjects of the present dissertation.

In the first part, the different approaches that have been formulated to analyse them are reviewed. Then the Bridged Crack model is described, and it is utilized in order to perform the present study. In particular, it is examined in detail especially with regard to the problem of cyclic loading. This model takes into account both compatibility and equilibrium equations, and it allows to clearly explore the influence of several different parameters in fiber reinforced materials. The problem of a composite rectangular-section beam subjected to bending is analysed. The matrix is elastic-perfectly brittle, whereas the fibers are characterized by a rigid-perfectly plastic law, that can represent either yielding or reinforcement slippage. The value of the moment that produces the fiber plasticization and the one that causes the crack propagation are evaluated. The crack propagation is taken into account assuming an approach based on linear elastic fracture mechanics and a review of stress intensity factors formulas is carried out in order to check their influence on the result. The case of cyclic loading is analysed starting from the monotonic loading: more precisely, load history is divided into monotonic steps, and each step is considered setting the deformation deriving from the previous one, as the initial condition.

In the second part, three different algorithms are illustrated. They simulate the behaviour of the system subjected to monotonic loading (Crack Length Control Scheme) or to cyclic loading (Loading Control, Rotation Control). The structure of the algorithms is described in detail and then the results of some applications are discussed. The comparison between the three algorithms lets immediately understand the effect of snap-back and snap-through instabilities. If a moment-rotation curve obtained with the Crack Length Control Scheme is superimposed over the same curve obtained by the Rotation Control algorithm, a loading drop is present (snap-back). If the same operation is repeated considering the Loading Control instead of the deformation one, a jump is visible for a constant value of bending moment (snap-through).

Then, the results in terms of moment-rotation response, reinforcements reactions, crack openings, plastic and cracking moments are shown. In addition to them, the shape of unloading-reloading cycle is analysed in relation to hysteresis and shake-down, that is the load level necessary to obtain the fiber plasticization in compression when the structure is unloaded. The shake-down moment of a fiber is exactly the double of the respectively plastic moment.

The numerical issues deriving from the singularity that arises if a fiber is too close to the crack tip is discussed, and a minimum distance to avoid the problem is found. Then, the effect of the number of points used in the algorithm to describe the response of the system is considered.

The brittleness number, N_p , is introduced to describe the behaviour of the system. The brittleness number is directly proportional to the ultimate fiber force and inversely proportional to the matrix Fracture Toughness. The higher the brittleness number is, the more ductile the system response will be.

If shake-down occurs, it is possible to have hysteresis and energy dissipation. For low values of N_p the shake-down moment is lower than the fracture propagation one. On the contrary, for high values of N_p , the instable fracture propagation precedes shake-down, and energy dissipation is not possible.

Increasing the number of fibers, it is possible to keep the reinforcement percentage constant by decreasing the area of each fiber. In this case, fracture propagation moment increases slightly while the shake-down moment decreases rapidly. It should be remarked that the behaviour obtained using a high number of fibers tends to the one derived from a model with a continuous reinforcement expressed as a cohesive law.

The profile of crack faces is analysed during the whole loading and unloading cycle, checking the performance of the model. In this way, it is possible to fully observe the rigid-perfectly plastic law of the reinforcements. The crack at the fiber level remains closed until plasticization is attained.

Future developments of this analysis could take into account the matrix strength both in tension and compression, using the cohesive crack model and the overlapping model.

Table of contents

Abstract.....	I
Introduction.....	1
1. Modelling of fiber reinforced materials	2
1.1 Fiber reinforced materials.....	2
1.2 Review of the models	2
1.3 Bridged crack model.....	3
1.3.1 Geometry and hypotheses	3
1.3.2 Shape functions and stress intensity factor	4
1.3.3 Compliances of a cracked beam element.....	7
1.3.4 Crack openings.....	8
1.3.5 Rotation	9
1.3.6 Compatibility equation	9
1.3.7 Plastic moments	11
1.3.8 Crack propagation condition.....	12
1.3.9 Forces and bending moment at crack propagation.....	12
1.3.10 Brittleness number and dimensionless analysis	13
1.3.11 Ultimate bending moment.....	14
1.4 Cyclic loading	15
1.4.1 Composite structures subjected to cyclic loading	15
1.4.2 Compatibility equations	15
1.4.3 Shake down moments (one single fiber model).....	16
1.4.4 Shape functions for fatigue problems	18
2. Hysteretic behaviour of fiber reinforced material: the case of multiple fibers	19
2.1 Monotonic loading	19
2.1.1 Crack Length Control Scheme (CLCS).....	19
2.1.2 Case studies.....	22
2.1.3 Numerical errors.....	28
2.2 Cyclic loading	29
2.2.1 Force-controlled algorithm.....	29
2.2.2 Rotation-controlled algorithm.....	32
2.2.3 Moment-rotation response and shake-down moments.....	34
2.2.4 Snap-back and snap-through instability.....	36

2.2.5 Energy dissipation	37
2.2.6 Influence of brittleness number, crack depth and fiber number	37
2.2.7 Case studies: loading control	48
2.2.8 Case studies: rotation control	56
2.2.9 Scale effects	60
2.2.10 Numerical errors	65
2.2.11 Future developments	67
Conclusion.....	69
References	70
Appendix – MATLAB code	75
Appendix 1 – Crack Length Control Scheme	75
Appendix 2 – Force-controlled algorithm.....	77
Appendix 3 – Rotation-controlled algorithm	80
Appendix 4 – Shape functions	83
Appendix 5 – Compliances	84

Introduction

The dissertation deals with the behaviour of fiber reinforced materials subjected to cyclic loading. This condition gives rise to the phenomena of hysteresis and shake-down, that are fundamental to study the energy dissipation of the system.

The first part is focused on the modelling of these materials. In section [1.1] a description of their improved mechanical properties is given and in section [1.2] the different models used to study their behaviour are reviewed. In section [1.3] the Bridged Crack model is chosen to perform the analysis and it is described in detail regarding the problem of monotonic loading. In section [1.4] the model is extended to the case of cyclic loading.

The second part is about the numerical algorithms and the results of the analysis. In section [2.1] the Crack Length Control Scheme is illustrated in relation to the problem of monotonic loading. In section [2.2] the force and rotation controlled algorithms are analysed and the influence of mechanical and geometric parameters on the system behaviour is discussed.

1. Fiber reinforced material modelling

In this chapter the characteristics of fiber reinforced materials and the models used for their analysis are illustrated in section [1.1] and [1.2]. Then the Bridged Crack model is chosen to study their behaviour and it is explained in detail in section [1.3]. Eventually its application to the case of cyclic loading is discussed in section [1.4].

1.1 Fiber reinforced materials

A composite material is obtained through the combination of two or more different constituents, whose interfaces remain recognizable. The properties of the composite are usually enhanced in comparison with the ones of the initial materials. They are used in many different applications and they are usually optimized to achieve a particular balance of properties for a given range of applications.

From a mechanical point of view, it is possible to distinguish a matrix in which a reinforcement material is spread.

Different classifications of composite materials are possible. One of the most used is that based on the matrix characterization. In this case three different groups are identified: polymer, ceramic and metal matrix composites. Another one is based on the shape of the strengthening phase and it is possible to distinguish three classes: grained composites, fiber reinforced composites and laminar composites.

In this dissertation only the case of fibrous composite with brittle matrix is considered. The presence of fibers improves strength, ductility, cracking resistance and fatigue strength.

Reinforced concrete is a well-known example of this class of composites. The matrix is characterized by low tensile strength and poor fracture toughness, but the presence of reinforcements acts against the nucleation of cracks thanks to their bridging action. At the same time the matrix offers resistance to the corrosion of reinforcements.

1.2 Review of the models

Independently of the matrix, fibrous composites present a common feature: the bridging action exerted by the fibers. This behaviour is the focus of the mechanical models used for the analysis of these materials on the basis of fracture mechanics.

There are several ways to classify the models: for example those based on the fiber type (continuous or discontinuous fibers), on the cracking regime (multiple cracking or single crack), on the crack opening conditions (steady-state or non steady-state cracking), on the matrix properties (perfectly brittle or strain-softening), on the bridging actions (continuous or discontinuous), on the loading condition (tensile loading, compressive loading, bending).

The models based on interface mechanics and fracture mechanics are the most common.

In the first case the focus is on the interface between the matrix and the fibers. The bond is studied with micromechanical models, that sometimes take into account the principle of fracture mechanics too.

The second family can be divided into two types: the Bridged Crack model and the cohesive crack model. They have been unified in a single formulation (Carpinteri, Massabò, 1996) and it has been demonstrated that they predict the same overall behaviour.

The cohesive crack model, in accordance with the ones proposed by Barenblatt (1962) for the analysis of brittle heterogeneous materials and then by Dugdale (1960) for the analysis of ductile materials, replaces the bridging zone by a fictitious crack, where a closing action is present (cohesive law).

On the contrary the Bridged Crack model considers localized closing tractions.

The first model assumes a finite stress field at the crack tip, while in the second case the stress field is singular.

1.3 Bridged crack model

The Bridged Crack model was proposed initially for the case of a monotonic loading applied to beams with a single reinforcement (Carpinteri, 1984). Later it was extended to the case of multiple reinforcements (Carpinteri, Massabò, 1996, 1997) and to the one of cyclic loading with a single reinforcement (Carpinteri, 1984) or two reinforcements (Carpinteri, Puzzi, 2003).

1.3.1 Geometry and hypotheses

The Bridged Crack model considers a fiber reinforced rectangular-section beam subjected to the bending moment M and with an edge crack. The dimensions of the beam (h , b), the initial crack depth a and the position of the fibers c_i are shown in Figure 1.1. Only the fibers crossing the crack are active and their number is equal to m .

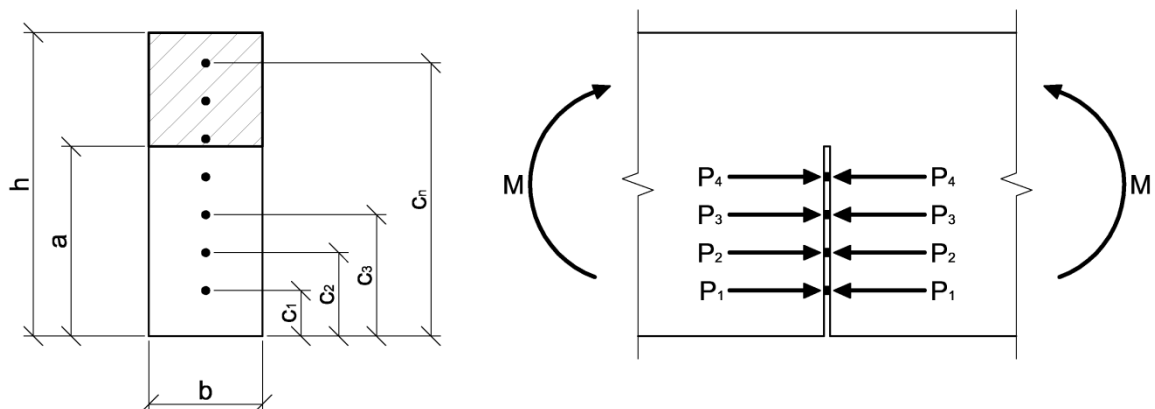


Figure 1.1: Geometry of the fiber reinforced beam.

It is possible to define the normalized crack depth (Eq. (1.1)) and the normalized position of a generic reinforcement (Eq. (1.2)) with respect to the bottom of the beam.

$$\xi = a/h \quad (1.1)$$

$$\zeta_i = c_i/h \quad (1.2)$$

The reinforcements exert a bridging action across the crack described by the forces P_i .

The matrix is assumed elastic-perfectly brittle and it is described by the fracture toughness K_{IC} and by the Young Modulus E , while the reinforcements are considered rigid-perfectly plastic and their ultimate force is equal to $P_{P,i}$. The rigid-perfectly plastic law of the fibers can describe either their slippage or their yielding. In the first case the value of $P_{P,i}$ is related to frictional bonding force between the matrix and the reinforcement, while in the second it represents the force that makes the fiber plastically flow. This force is proportional to the area of the reinforcement A_i and to the yielding stress $\sigma_{y,i}$ of its material (Eq.(1.3)). The same value is assumed both in tension and in compression.

$$P_{P,i} = A_i \sigma_{y,i} \quad (1.3)$$

In other words this means that the elastic deformation of the fiber is disregarded.

The beam is made of a composite material, but its matrix is homogeneous and isotropic if it is considered isolated.

The model takes into account both equilibrium and compatibility equations. If the beam section length vanishes, its compliance is due only to the cracked section. So, it is necessary to evaluate the compliance of a cracked element in order to calculate the openings of the crack and the rotation of the section. The model disregards the contribution to the deformability given by the beam which the cracked section belongs to.

1.3.2 Shape functions and stress intensity factor

In this section the formulas of the stress intensity factor are reported. They are a measure of the singular stress field in the crack tip proximity. They will be needed to calculate the compliances of a cracked element and to take into account the crack propagation based on linear elastic fracture mechanics. Only the crack opening (Mode I) is considered while the problem of the shear and the crack sliding (Mode II) is disregarded.

The stress intensity factors due respectively to the bending moment and to a concentrated force applied on the crack face (Tada, Paris Irwin, 1985) are:

$$K_{IM} = \frac{M}{h^{3/2}b} Y_M(\xi) \quad (1.4)$$

$$K_{IP} = \frac{P}{h^{1/2}b} Y_P(\xi, \zeta_i) \quad (1.5)$$

In the previous equations the shape functions Y_M and Y_P appear. They depend on the crack depth and their value can be found in different stress intensity factors handbook.

For example, the shape function for the bending moment Y_M is defined by different authors in various way.

- Tada, Paris, Irwin (1985)

$$Y_M(\xi) = \begin{cases} 6(1,99\xi^{0,5} - 2,47\xi^{1,5} + 12,97\xi^{2,5} - 23,17\xi^{3,5} + 24,8\xi^{4,5}) & \xi \leq 0,6 \\ 3,99(1 - \xi)^{-1,5} & \xi > 0,6 \end{cases} \quad (1.6)$$

- Wilson (1970) ($1/2 \leq \xi \leq 4/5$)

$$Y_M(\xi) = \frac{6\sqrt{\pi}}{(1 - \xi)^{3/2}} c \quad (1.7)$$

$$c = 0,375 \quad (1.8)$$

- Paris, Sih (1965) ($\xi < 1$)

$$Y_M(\xi) = \frac{6\sqrt{\pi}}{(1 - \xi)^{3/2}} c \quad (1.9)$$

$$c = \frac{2(\pi - 2)}{3(\pi^2 - 8)} \quad (1.10)$$

- Sinclair, Messner, Meda (1996) ($\xi < 1$)

$$Y_M(\xi) = \frac{6\sqrt{\pi}}{(1 - \xi)^{3/2}} c \quad (1.11)$$

$$c = 0,375 + \frac{0,108}{10^4} \left[e^{24\left(\frac{4}{3}\xi - 1\right)} - 1 \right] \quad (1.12)$$

- Guinea, Pastor, Planas, Elices (1998) ($\xi < 1$)

$$Y_M(\xi) = \frac{6\sqrt{\xi}}{(1 - \xi)^{3/2}(1 + 3\xi)} p_\infty \quad (1.13)$$

$$p_\infty = 1,99 + 0,83\xi - 0,31\xi^2 + 0,14\xi^3 \quad (1.14)$$

A comparison between Eq. (1.6) and (1.13) is shown in Figure 1.2. It can be noticed that the values of the shape functions are almost identical for $\xi > 0,2$ and in any case the little difference does not affect the numerical results of the analysis. The shape function Y_M has a vertical asymptote at $\xi = 1$.

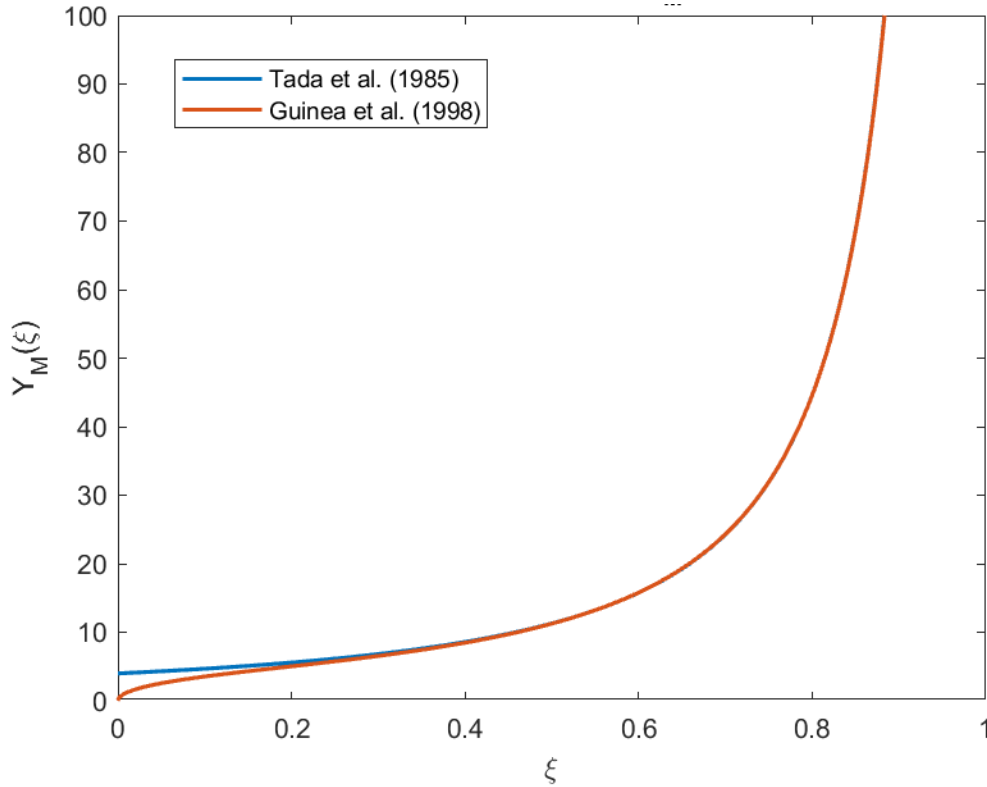


Figure 1.2: Shape function $Y_M(\xi)$ according to Eq. (1.6) and (1.13).

The other equation graphs are very similar to the one of Eq. (1.6), even if they are valid only for a limited range of crack depth values. All the results shown in the present analysis are attained using Eq. (1.13). Eq. (1.6) should not be used because of its discontinuity in $\xi = 0,6$, that gives rise to numerical problems.

Regarding the shape function for the load Y_p only the following expression is considered in the analysis (Tada, Paris, Irwin, 1985):

$$Y_p(\xi, \zeta_i) = \frac{2}{\sqrt{\pi\xi}} \frac{1}{(1-\xi)^{1,5} \sqrt{1 - \left(\frac{\zeta_i}{\xi}\right)^2}} G(\xi, \zeta_i) \quad \xi \geq \zeta_i \quad (1.15)$$

$$G(\xi, \zeta_i) = g_1(\xi) + g_2(\xi) \frac{\zeta_i}{\xi} + g_3(\xi) \left(\frac{\zeta_i}{\xi}\right)^2 + g_4(\xi) \left(\frac{\zeta_i}{\xi}\right)^3 \quad (1.16)$$

$$g_1(\xi) = 0,46 + 3,06\xi + 0,84(1-\xi)^5 + 0,66\xi^2(1-\xi)^2 \quad (1.17)$$

$$g_2(\xi) = -3,52\xi^2 \quad (1.18)$$

$$g_3(\xi) = 6,17 - 28,22\xi + 34,54\xi^2 - 14,39\xi^3 - (1-\xi)^{1,5} - 5,88(1-\xi)^5 - 2,64\xi^2(1-\xi)^2 \quad (1.19)$$

$$g_4(\xi) = -6,63 + 25,16\xi - 31,04\xi^2 + 14,41\xi^3 + 2(1-\xi)^{1,5} + 5,04(1-\xi)^5 + 1,98\xi^2(1-\xi)^2 \quad (1.20)$$

In Figure 1.3 the graph of Y_p is shown for different positions of the fiber. It is characterized by two vertical asymptotes: one located at the position of the fiber and another one located at $\xi = 1$.

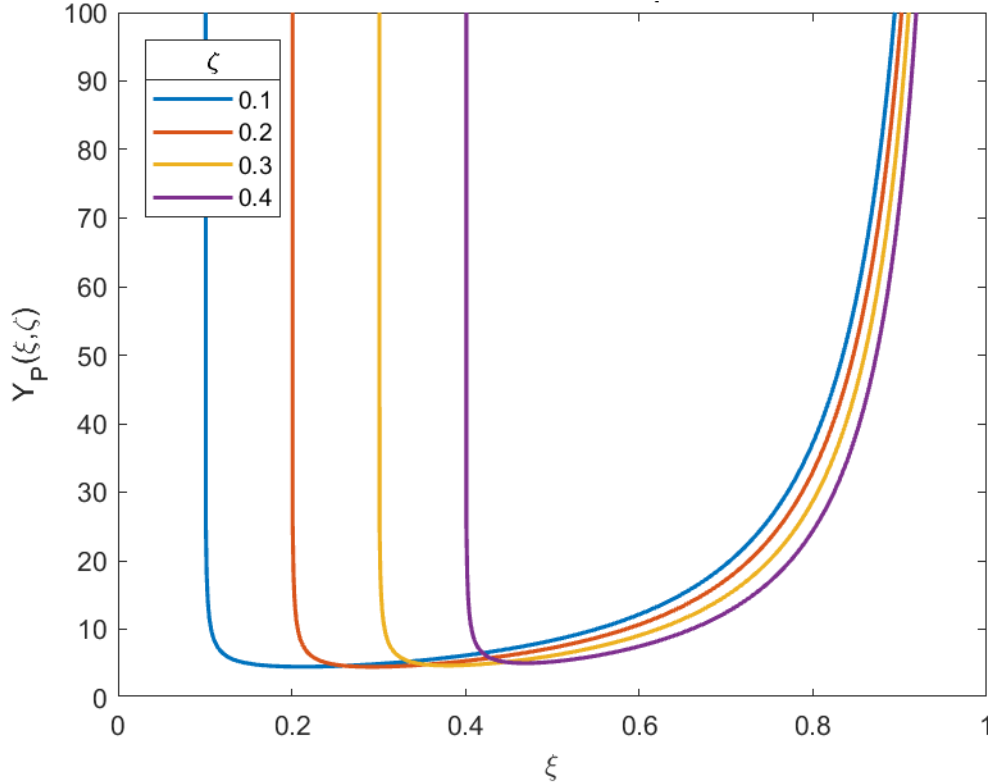


Figure 1.3: Shape function $Y_P(\xi, \zeta_i)$ according to Eq. (1.15).

1.3.3 Compliances of a cracked beam element

If the beam has only one fiber, the rotation ϕ and the crack opening w are connected to the bending moment M and the reinforcement reaction P by the compliance matrix.

$$\begin{Bmatrix} \phi \\ w \end{Bmatrix} = \begin{bmatrix} \lambda_{MM} & \lambda_{MP} \\ \lambda_{PM} & \lambda_{PP} \end{bmatrix} \begin{Bmatrix} M \\ P \end{Bmatrix} \quad (1.21)$$

The matrix in Eq. (1.21) is symmetric because $\lambda_{MP} = \lambda_{PM}$ for the Betty's theorem.

By using Clapeyron's theorem and superposition principle it is possible to evaluate the energy variation.

$$-\Delta W = \frac{1}{2} M \phi + \frac{1}{2} P w \quad (1.22)$$

$$-\Delta W = \frac{1}{2} \lambda_{MM} M^2 + \frac{1}{2} \lambda_{PP} P^2 + \lambda_{MP} M P \quad (1.23)$$

Then, the strain energy release rate and the relation between \mathcal{G}_I and K_I are introduced.

$$\mathcal{G}_I = -\frac{dW}{dA} \quad (1.24)$$

$$\mathcal{G}_I = \frac{K_I^2}{E} \quad (1.25)$$

Now the energy variation can be expressed by:

$$\begin{aligned}
-\Delta W &= \int_0^a G_I b \, dh = \int_0^a \frac{K_I^2}{E} b \, dh = \int_0^a \frac{(K_{IM} + K_{IP})^2}{E} b \, dh \\
&= \int_0^a \frac{K_{IM}^2}{E} b \, dh + \int_0^a \frac{K_{IP}^2}{E} b \, dh + 2 \int_0^a \frac{K_{IM} K_{IP}}{E} b \, dh
\end{aligned} \tag{1.26}$$

Then using Eq. (1.4) and Eq. (1.5)

$$-\Delta W = \frac{M^2}{b^2 h E} \int_0^\xi Y_M^2(\xi) d\xi + \frac{P^2}{h E} \int_0^\xi Y_P^2(\xi) d\xi + \frac{2MP}{bh E} \int_0^\xi Y_M(\xi) Y_P(\xi) d\xi \tag{1.27}$$

The expressions of the compliances are attained by comparing Eq.(1.23) and Eq. (1.27) and using the identity principle of polynomials.

$$\lambda_{MM} = \frac{2}{E h^2 b} \int_0^\xi Y_M^2(\xi) d\xi \tag{1.28}$$

$$\lambda_{MP} = \frac{2}{hb E} \int_0^\xi Y_P(\xi) Y_M(\xi) d\xi \tag{1.29}$$

$$\lambda_{PP} = \frac{2}{b E} \int_0^\xi Y_P^2(\xi) d\xi \tag{1.30}$$

In the case of more than one fiber the following relations can be obtained (Massabò, 1997).

$$\lambda_{MM} = \frac{2}{E h^2 b} \int_0^\xi Y_M^2(\xi) d\xi \tag{1.31}$$

$$\lambda_{iM} = \frac{2}{hb E} \int_{\zeta_i}^\xi Y_P(\xi, \zeta_i) Y_M(\xi) d\xi \tag{1.32}$$

$$\lambda_{ij} = \frac{2}{b E} \int_{\max(\zeta_i, \zeta_j)}^\xi Y_P(\xi, \zeta_i) Y_P(\xi, \zeta_j) d\xi \tag{1.33}$$

The integral of Eq. (1.32) and Eq. (1.33) are improper because the integrand has a singularity at the lower bound of integration. In the first case the singularity is only apparent, while in the second it is not removable when $i = j$. However, in this second case it is possible to consider a distribution of stresses instead of a concentrated force to model the fiber action (Massabò, 1997) achieving the following equation:

$$\lambda_{ii} = \frac{2}{b E} \int_{\zeta_i + \delta}^\xi Y_P^2(\xi, \zeta_i) d\xi \tag{1.34}$$

Where δ is a cut-off distance that can be assumed equal to 10^{-5} .

1.3.4 Crack openings

The crack openings at the level of the reinforcements can be evaluated by using the superposition principle: it is necessary to sum the contribution due to the bending moment and the one due to the concentrated forces applied on the crack faces (Eq. (1.35)).

$$w_i = \lambda_{iM}M - \sum_{j=1}^m \lambda_{ij}P_j \quad (1.35)$$

In the previous equation the minus sign is related to the fact that a positive bending moment tries to open the crack, while a positive force tries to close the crack. The compliance λ_{iM} is the displacement at the fiber level i due to a unit bending moment, while the compliance λ_{ij} is the displacement at the fiber level i due to a unit force applied at the fiber level j .

Equation (1.35) can be rewritten in matrix form:

$$\{w\} = \{\lambda_M\}M - [\lambda]\{P\} \quad (1.36)$$

where $\{w\}$ is the vector of the crack openings at the level of the reinforcements, $\{\lambda_M\}$ is the vector of the compliance λ_{iM} , $[\lambda]$ is the symmetric square matrix of the compliance λ_{ij} and $\{P\}$ is the vector of the fiber reactions.

It is also possible to evaluate the crack opening at the generic level ζ (Eq. (1.37)) and it can be useful to draw the entire profile of the crack faces.

$$w(\zeta) = \lambda_{\zeta M}M - \sum_{j=1}^m \lambda_{\zeta j}P_j \quad (1.37)$$

1.3.5 Rotation

The rotation of the section is calculated in the same way as the crack openings:

$$\phi = \lambda_{MM}M - \sum_{j=1}^m \lambda_{jM}P_j \quad (1.38)$$

where the compliance λ_{MM} is the rotation due to a unit bending moment, while the compliance λ_{jM} is the rotation due to a unit force applied at the fiber level j .

Again Eq. (1.38) can be written in matrix form:

$$\phi = \lambda_{MM}M - \{\lambda_M\}^T\{P\} \quad (1.39)$$

where $\{\lambda_M\}$ is the vector of the compliance λ_{jM} and $\{P\}$ is the vector of the fiber reactions.

1.3.6 Compatibility equation

The problem is statically indeterminate because the forces in the fibers are unknown and so the compatibility equation is introduced to solve it.

Because of the hypothesis of rigid-perfectly plastic law of the fibers, the crack openings at their level remain equal to zero until the ultimate force $P_{p,i}$ is reached in one of them. These m conditions are expressed by:

$$\{w\} = \{\lambda_M\}M - [\lambda]\{P\} = \{0\} \quad (1.40)$$

If the bending moment is known, the reactions in the reinforcements $\{P\}$ can be calculated by solving the linear system:

$$[\lambda]\{P\} = \{\lambda_M\}M \quad (1.41)$$

When a generic fiber i reaches its ultimate force, the crack openings at its level starts increasing and the previous compatibility equation is not valid any more. The force in the fiber becomes known and equal to $P_{P,i}$, while the corresponding opening displacement w_i becomes unknown. However, the compatibility equation is valid for the $m - 1$ fibers, that are not yielded, and also the number of static unknowns is equal to $m - 1$. So, it is possible to solve again the problem whose size is reduced by one.

Considering a generic situation and naming f (free displacements) the plasticized fibers and c (constrained displacements) the elastic fibers, it is possible to split the problem in two parts: one statically indeterminate and one statically determinate.

$$\begin{Bmatrix} w_f \\ w_c \end{Bmatrix} = \begin{Bmatrix} \lambda_{Mf} \\ \lambda_{Mc} \end{Bmatrix} M - \begin{bmatrix} \lambda_{ff} & \lambda_{fc} \\ \lambda_{cf} & \lambda_{cc} \end{bmatrix} \begin{Bmatrix} P_f \\ P_c \end{Bmatrix} \quad (1.42)$$

The displacements of the elastic fibers $\{w_c\}$ and the ultimate forces of the yielded fibers $\{P_f\}$ are known and equal respectively to $\{0\}$ and $\{P_{P,f}\}$.

If the second equation of (1.42) is considered:

$$\{w_c\} = \{\lambda_{Mc}\}M - ([\lambda_{cf}]\{P_{P,f}\} + [\lambda_{cc}]\{P_c\}) = \{0\} \quad (1.43)$$

it is possible to find the value of the forces in the elastic fibers $\{P_c\}$ by solving the linear system:

$$[\lambda_{cc}]\{P_c\} = \{\lambda_{Mc}\}M - [\lambda_{cf}]\{P_{P,f}\} \quad (1.44)$$

Then, considering the first equation of (1.42) with the conditions $\{P_f\} = \{P_{P,f}\}$ and $\{w_c\} = \{0\}$ and substituting the value of $\{P_c\}$ from (1.44), it is possible to compute the displacements of the plasticized fibers $\{w_f\}$.

$$\{w_f\} = \{\lambda_{Mf}\}M - ([\lambda_{ff}]\{P_{P,f}\} + [\lambda_{fc}]\{P_c\}) \quad (1.45)$$

In any case it is necessary to know the plasticized reinforcements a priori and this means that the problem should be solved step by step. The procedure used in this analysis will be explained in the section of the numerical algorithm.

From an overall point of view the problem presents $2m$ unknowns in a first stage: m static unknowns, the reactions $\{P\}$, and m kinematic unknowns, the displacements $\{w\}$. Thanks to the m compatibility conditions all the kinematic unknowns become known and so the problem can be solved using the m equations of system (1.41). At a subsequent stage characterized by the yielding of one fiber, the number of static unknowns is reduced by one, because the force in this fiber becomes known and

equal to its limit value. The number of compatibility conditions is reduced by one too, because the yielded fiber displacement starts increasing and it remains unknown. Anyway, the problem can be solved using the $m - 1$ equations of system (1.44) to find the reactions and Eq. (1.45) to find the only unknown displacement.

1.3.7 Plastic moments

If all the fibers are still in the elastic field, the bending moment value, that makes only one fiber yield, can be calculated by imposing each reinforcement reaction equal to its ultimate force. The first fiber, that plasticizes, is the one corresponding to the minimum bending moment. In order to find this value, the ultimate forces $P_{P,i}$ are substituted in each equation of (1.41) and then the bending moments are computed. The first plastic moment is the minimum.

First of all, the reactions are calculated from Eq. (1.41).

$$\{P\} = [\lambda]^{-1}\{\lambda_M\}M \quad (1.46)$$

$$P_i = [\lambda]_i^{-1}\{\lambda_M\}M \quad (1.47)$$

Then the condition $P_i = P_{P,i}$ is considered and the correspondingly bending moment is evaluated.

$$P_{P,i} = [\lambda]_i^{-1}\{\lambda_M\}M_{P,i} \quad (1.48)$$

$$M_{P,i} = \frac{P_{P,i}}{[\lambda]_i^{-1}\{\lambda_M\}} \quad (1.49)$$

As previously remarked the first plastic moment is the minimum among these values.

$$M_{P,1} = \min_{i=1,m} \frac{P_{P,i}}{[\lambda]_i^{-1}\{\lambda_M\}} \quad (1.50)$$

In the previous equations the subscript i of the matrix $[\lambda]^{-1}$ indicates that only the i row is considered.

At a following stage, when at least one fiber is yielded, it is possible to do the same but considering Eq. (1.44) instead of Eq. (1.41).

$$\{P_c\} = [\lambda_{cc}]^{-1}\{\lambda_{Mc}\}M - [\lambda_{cf}]\{P_{P,f}\} \quad (1.51)$$

$$P_i = [\lambda_{cc}]_i^{-1}\{\lambda_{Mc}\}M - [\lambda_{cf}]\{P_{P,f}\} \quad (1.52)$$

Then the condition $P_i = P_{P,i}$ is considered and the correspondingly bending moment is evaluated.

$$P_{P,i} = [\lambda_{cc}]_i^{-1}\{\lambda_{Mc}\}M_{P,i} - [\lambda_{cf}]\{P_{P,f}\} \quad (1.53)$$

$$M_{P,i} = \frac{P_{P,i} + [\lambda_{cc}]_i^{-1}[\lambda_{cf}]\{P_{P,f}\}}{[\lambda_{cc}]_i^{-1}\{\lambda_{Mc}\}} \quad (1.54)$$

So, the j -th plastic moment is given by the equation:

$$M_{P,j} = \min_{i=1,n_c} \frac{P_{P,i} + [\lambda_{cc}]_i^{-1} [\lambda_{cf}] \{P_{P,f}\}}{[\lambda_{cc}]_i^{-1} \{\lambda_{Mc}\}} \quad j = 2, \dots, m \quad (1.55)$$

1.3.8 Crack propagation condition

The crack propagation condition is evaluated regarding linear elastic fracture mechanics. The crack propagates when the stress intensity factor K_I reaches its critical value, that is the fracture toughness of the material K_{IC} .

$$K_I = K_{IC} \quad (1.56)$$

The stress intensity factor is the sum of two contributions: one due to the applied bending moment and another due to the reactions of reinforcements.

$$K_I = K_{I,M} - \sum_{i=1}^m K_{I,i} \quad (1.57)$$

The minus sign is related to the fact that a positive bending moment acts opening the crack, while a positive force acts closing it. Eq. (1.57) can be rewritten taking into account the expressions of the stress intensity factors for the moment and the force given in [1.3.2] and by using the scalar product for the summation.

$$K_I = \frac{M}{h^{3/2}b} Y_M - \frac{\{Y_P\}^T \{P\}}{h^{1/2}b} = K_{IC} \quad (1.58)$$

where $\{Y_P\}$ is the vector of the shape functions related to the concentrated forces.

The stress intensity factor due to bending moment is only function of the normalized crack depth, while the one related to the forces is function of the normalized position of the fiber too.

$$Y_M = Y_M(\xi) \quad (1.59)$$

$$Y_{P,i} = Y_P(\xi, \zeta_i) \quad (1.60)$$

The value of the moment, that makes the crack propagate, is:

$$M_F = \frac{h^{3/2}b}{Y_M} \left(K_{IC} + \frac{\{Y_P\}^T \{P\}}{h^{1/2}b} \right) = \frac{h^{3/2}b}{Y_M} K_{IC} + \frac{h}{Y_M} \{Y_P\}^T \{P\} = R_1 + R_2 \{Y_P\}^T \{P\} \quad (1.61)$$

In the previous equation the parameters R_1 and R_2 are introduced in order to write the relation in a more compact way.

1.3.9 Forces and bending moment at crack propagation

The value of the moment M_F causing fracture propagation is function of the reinforcement reactions $\{P\}$ (Eq. (1.58)), but these forces are function of the applied bending moment because of the compatibility equation.

So, by imposing the condition $M = M_F$ it is possible to calculate the values of the fiber reactions at crack propagation.

If all the fibers are in the elastic field, this result can be attained substituting the value of the moment from Eq. (1.61) in Eq. (1.41).

$$[\lambda]\{P\} = \{\lambda_M\}(R_1 + R_2\{Y_P\}^T\{P\}) \quad (1.62)$$

Then the following linear system is obtained:

$$([\lambda] - R_2\{\lambda_M\}\{Y_P\}^T)\{P\} = R_1\{\lambda_M\} \quad (1.63)$$

If at least one fiber is plasticized, it is necessary to use Eq. (1.44) instead of Eq. (1.41).

$$[\lambda_{cc}]\{P_c\} = \{\lambda_{Mc}\}(R_1 + R_2\{Y_P\}^T\{P\}) - [\lambda_{cf}]\{P_{P,f}\} \quad (1.64)$$

In order to obtain a linear system, the vectors $\{Y_P\}$ and $\{P\}$ are split into two parts as done before in the case of Eq. (1.42).

$$[\lambda_{cc}]\{P_c\} = \{\lambda_{Mc}\} \left[R_1 + R_2 \left(\{Y_{P,f}\}^T \{P_{P,f}\} + \{Y_{P,c}\}^T \{P_c\} \right) \right] - [\lambda_{cf}]\{P_{P,f}\} \quad (1.65)$$

Eventually the following linear system is achieved:

$$\left([\lambda_{cc}] - R_2\{\lambda_{Mc}\}\{Y_{P,c}\}^T \right) \{P_c\} = \{\lambda_{Mc}\} \left(R_1 + R_2\{Y_{P,f}\}^T \{P_{P,f}\} \right) - [\lambda_{cf}]\{P_{P,f}\} \quad (1.66)$$

By solving system (1.63) or (1.66) the values of the forces at crack propagation are found. In the second case the condition $\{P_f\} = \{P_{P,f}\}$ is still valid and it lets calculate all the reactions and not only the ones of the elastic fibers $\{P_c\}$.

Then, by substituting back the values of the forces $\{P\}$ in Eq. (1.61), it is possible to attain the value of the applied bending moment, that makes the crack advance.

1.3.10 Brittleness number and dimensionless analysis

If all the reinforcements are equal, Eq. (1.58) can be rewritten in the following form

$$\frac{M_F}{K_{IC}h^{3/2}b} = \frac{1}{Y_M(\xi)} \left(1 + \frac{N_P}{\rho} \sum_{i=1}^m \rho_i \alpha_i(\xi, \zeta_i) Y_P(\xi, \zeta_i) \right) \quad (1.67)$$

where

$$N_P = \frac{\rho \sigma_y h^{1/2}}{K_{IC}} = \frac{m P_{P,i}}{K_{IC} h^{1/2} b} \quad (1.68)$$

$$\rho_i = \frac{A_i}{bh} \quad (1.69)$$

$$\rho = \frac{mA_i}{bh} \quad (1.70)$$

$$\alpha_i(\xi, \zeta_i) = \frac{P_i}{P_{P,i}} \quad (1.71)$$

The nondimensional parameter N_p is named brittleness number (Carpinteri 1981, 1984) and its value is responsible for the behaviour of the system. The higher N_p is, the more ductile the behaviour of the structure will be and vice versa. This issue will be analysed in detail in sections [2.1.2], [2.2.6] and [2.2.7].

In the results of the present work also the following quantities will be sometimes normalized.

$$\tilde{M} = \frac{M}{K_{IC}h^{3/2}b} \quad (1.72)$$

$$\tilde{P} = \frac{P}{K_{IC}h^{1/2}b} \quad (1.73)$$

$$\tilde{\phi} = \frac{\phi E h^{1/2}}{K_{IC}} \quad (1.74)$$

$$\tilde{w} = \frac{wE}{K_{IC}h^{1/2}} \quad (1.75)$$

If the properties are different from one reinforcement to another, Eq. (1.68) can be generalized in the following way:

$$N_p = \frac{\sum_{i=1}^m P_{P,i}}{K_{IC}h^{1/2}b} \quad (1.76)$$

1.3.11 Ultimate bending moment

When the section is completely cracked and the depth of the fracture is equal to the beam height, it is possible to compute the ultimate bending moment the structure is able to bear.

At this final stage characterized by large displacements all the fibers are plasticized in tension, while the resultant of compressions is applied in a single point as shown in Figure 1.4.

If all the fibers are equal and ζ_G is the normalized depth of their barycentre, the ultimate bending moment is given by:

$$M_u = mP_P b_U = mP_P h(1 - \zeta_G) = N_p K_{IC} h^{3/2} b(1 - \zeta_G) \quad (1.77)$$

This value is slightly overestimate because the arm reduction due to the rotation ϕ is disregarded. In any case this situation is only hypothetical because the point of the matrix, where the reaction is applied, should bear an infinite stress.

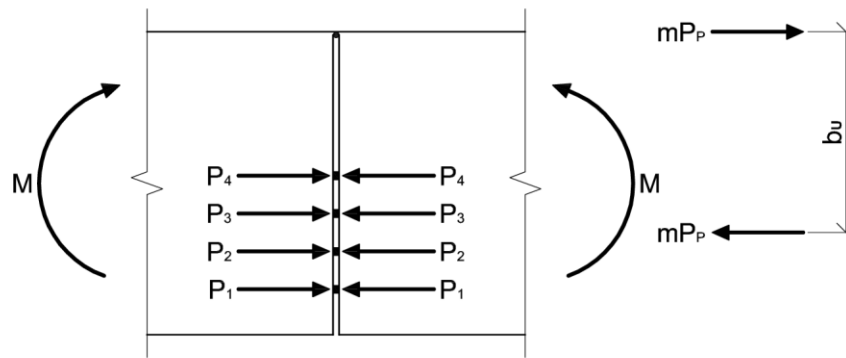


Figure 1.4: Geometry corresponding to the ultimate bending moment.

M_u can be computed also with different types of fibers, considering the equilibrium around the point of the matrix where the compression reaction is applied.

1.4 Cyclic loading

In this section the Bridged Crack model will be extended to the case of cyclic loading, starting from the equations illustrated for the monotonic loading.

1.4.1 Composite structures subjected to cyclic loading

Fiber reinforced materials are often used in structures subjected to fatigue problem. The bridging action of the fibers acts against crack propagation also in this situation.

1.4.2 Compatibility equations

The formulas obtained for the case of monotonic loading can be generalized for the case of cyclic loading observing that it is possible to divide a generic load history in different parts, each one characterized by an increasing or decreasing load starting from an initial condition (Puzzi, 2004) as shown in Figure 1.5.

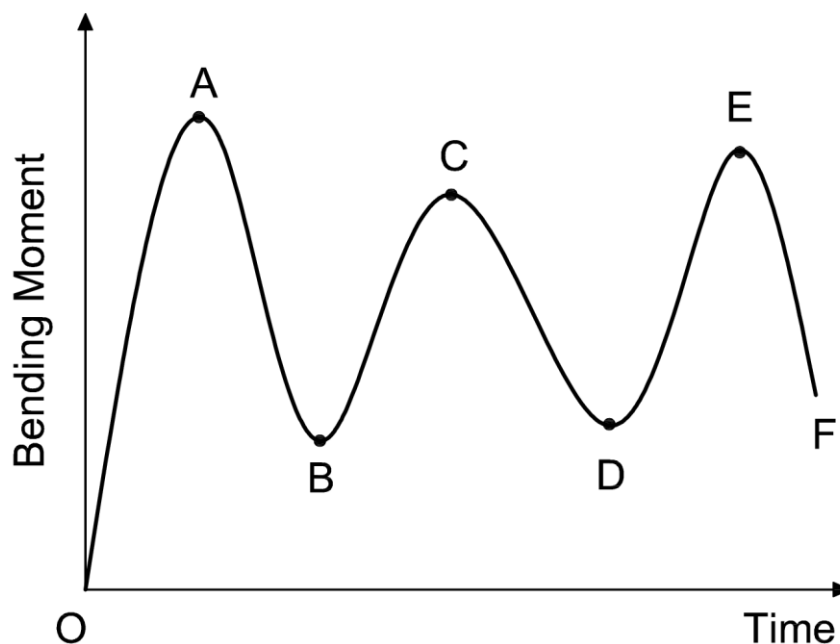


Figure 1.5: Decomposition of load history into monotonic parts.

So, Eq. (1.40) can be rewritten in its incremental form by subtracting this equation written with the initial conditions (subscript 0) from the one written at a generic stage.

$$\{w\} - \{w_0\} = \{\lambda_M\}(M - M_0) - [\lambda]({P} - \{P_0\}) = \{0\} \quad (1.78)$$

It is valid only if all the reinforcements are in the elastic field. The initial conditions are equal to the respective values at the end of the previous loading part. If one reinforcement is yielded, it is possible to do the same with Eq. (1.42) with the conditions $P_{f,i} = \pm P_{P,f,i}$ and $\{w_c\} = \{w_{0,c}\}$.

$$\begin{Bmatrix} w_f \\ w_c \end{Bmatrix} - \begin{Bmatrix} w_{0,f} \\ w_{0,c} \end{Bmatrix} = \begin{Bmatrix} \lambda_{Mf} \\ \lambda_{Mc} \end{Bmatrix} (M - M_0) - \begin{bmatrix} \lambda_{ff} & \lambda_{fc} \\ \lambda_{cf} & \lambda_{cc} \end{bmatrix} \left(\begin{Bmatrix} P_f \\ P_c \end{Bmatrix} - \begin{Bmatrix} P_{0,f} \\ P_{0,c} \end{Bmatrix} \right) \quad (1.79)$$

The sign \pm depends on the direction of loading: the positive and negative values are attained respectively in the loading and unloading phase. The second condition is explained in [1.4.3]. Then the problem can be solved as done before for the case of monotonic loading in [1.3.6] and the crack propagation can be taken into account as explained in [1.3.8].

Also the rotation is computed considering the difference of two equations.

$$\begin{aligned} \phi - \phi_0 &= \lambda_{MM}(M - M_0) - \sum_{j=1}^m \lambda_{jM}(P_j - P_{0,j}) \\ &= \lambda_{MM}(M - M_0) - \{\lambda_M\}^T (\{P\} - \{P_0\}) \end{aligned} \quad (1.80)$$

1.4.3 Shake down moments (one single fiber model)

If the value of the applied bending moment decreases, the forces in the reinforcements do the same. At a certain point they could become negative and the fibers could undergo yielding in compression if their ultimate force is attained.

This can be explained considering that the matrix tries to close completely the crack if the structure is unloaded, but the reinforcements act against it if they yielded during the loading phase. This happens because the crack openings at the level of the yielded fibers cannot decrease until the plastic force in the reinforcements is achieved as a consequence of their rigid-perfectly plastic law.

The value of the bending moment, that is necessary to overcome during the loading phase to attain the inverse plasticization of a fiber, is called shake-down moment.

If the case of a single fiber is considered, this means that the crack opening due to the moment and to the yielded fiber during the loading phase should be equal to the one due only to the fiber opening reaction when the beam is unloaded (Figure 1.6). So, the following compatibility condition is obtained:

$$w(M) - w(P_p) = w(P) \quad (1.81)$$

The shake-down moment is the minimum value of the moment for which $P = P_p$.

$$w(M_{SD}) - w(P_P) = w(P_P) \quad (1.82)$$

$$w(M_{SD}) = 2 w(P_P) \quad (1.83)$$

Considering the compatibility condition at the fiber yielding in tension, it is possible to demonstrate that the shake-down moment is the double of the plastic moment.

$$w(M_P) - w(P_P) = 0 \quad (1.84)$$

$$w(M_{SD}) = 2 w(M_P) \quad (1.85)$$

Because of the problem linearity, the previous equation can be rewritten in the following way:

$$M_{SD} = 2M_P \quad (1.86)$$

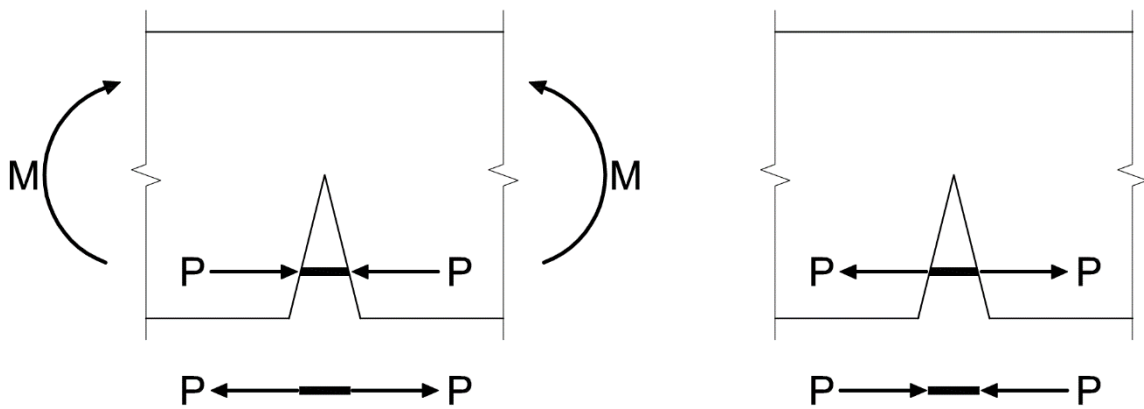


Figure 1.6: Shake-down condition

This can be generalized to the case of m fibers considering Eq. (1.78) and imposing for each fiber one by one the condition $P_i = -P_{P,i}$. The lowest moment calculated is the value of the first shake-down moment. This procedure is similar to the one applied to the plastic moment in [1.3.7].

$$M_{SD,1} = \min_{i=1,m} \frac{2P_{P,i}}{[\lambda]_i^{-1}\{\lambda_M\}} \quad (1.87)$$

It is important to notice that the value of M_{SD} is the double of the correspondent plastic moment. The factor 2 in Eq. (1.87) is given by the difference $P_i - P_{P,i}$ that in this case is equal to $-2P_{P,i}$.

$$M_{SD,1} = 2M_{P,1} \quad (1.88)$$

The next shake-down moments can be evaluated with the same procedure, but considering Eq. (1.79) instead of Eq. (1.78).

$$M_{SD,j} = \min_{i=1,n_c} \frac{2P_{P,i} + 2[\lambda_{cc}]_i^{-1}\{\lambda_{cf}\}\{P_{P,f}\}}{[\lambda_{cc}]_i^{-1}\{\lambda_{Mc}\}} \quad j = 2, \dots, m \quad (1.89)$$

Again the shake-down moment is exactly the double of the correspondent plastic moment.

$$M_{SD,j} = 2M_{P,j} \quad j = 2, \dots, m \quad (1.90)$$

In the case of a cyclic load with a minimum different from zero, it is possible to demonstrate the following relation between the plastic and the shake-down moments.

$$M_{SD,j} = M_{min} + 2M_{P,j} \quad (1.91)$$

The demonstration of Eq. (1.87) and (1.89) is reported in [2.2.3].

1.4.4 Shape functions for fatigue problems

If the system is subjected to cyclic loading and fatigue, the choice of the shape function could be crucial, because a small difference in its value leads to a large one in the life calculation.

Deep cracks should be taken into account and consequently the shape function needs to be able to capture the system behaviour as ξ tends to one.

2. Hysteretic behaviour of fiber reinforced material: the case of multiple fibers

In this chapter the behaviour of the structure subjected to a cyclic loading is analysed both for force and deformation control. Also the case of a monotonic loading controlled by increasing crack length (Crack Length Control Scheme) is examined in order to check the results obtained for the cyclic loading. In this way it is possible to underline the snap-back and snap-through instabilities, that appear respectively in the case of deformation and force control. The numerical algorithm is described in detail for these three cases respectively in sections [2.1] and [2.2] and the correspondingly results are illustrated.

2.1 Monotonic loading

In this section the problem of a monotonic loading applied controlling the crack length is analysed. Using this technique, it is possible to describe completely the softening branches even with a positive slope of the moment-rotation response of the system.

2.1.1 Crack Length Control Scheme (CLCS)

The presented procedure is based on the fact that the value of the applied bending moment should be equal to the cracking moment in order to make fracture advance. So, for each value of the crack depth, starting from an initial value and up to a stopping value fixed in advance, the cracking moment is computed using the expressions shown in [1.3.9]. The relation between the bending moment and the crack depth is obtained. Then, to describe the moment-rotation response it is necessary to notice that a fiber can attain its ultimate force even if the crack is not advancing and this changes the stiffness of the system and the slope of the graph. So, the plastic moments of all the reinforcements should be computed for a given depth of the crack, but only the ones lower than the cracking moment and higher than one computed for the previous depth should be taken into account. These values of moments and their respective rotations are added to the graph. The plastic moments are evaluated regarding [1.3.7].

Now the numerical algorithm is described in detail. The following input parameters have to be considered:

- Beam geometry
 - b – section thickness
 - h – section depth
 - a_{start} – crack initial depth (or ξ_{start} - normalized initial crack depth)
- Reinforcements geometry
 - m – number of fibers
 - c_{min} – position of first fiber (or ζ_{min} – normalized position of first fiber)
 - c_{max} – position of last fiber (or ζ_{max} – normalized position of last fiber)
- Matrix material
 - E – Young Modulus

- K_{IC} – matrix fracture toughness
- Reinforcement material
 - $P_{P,i}$ – fiber ultimate force

The value of the ultimate force of the fiber can be given directly or it can be computed starting from these additional parameters (round fiber):

- r_i – fiber radius
- $\sigma_{y,i}$ – fiber yielding tension

$$P_{P,i} = (\pi r_i^2) \sigma_{y,i} \quad (2.1)$$

The fibers are considered equally spaced between c_{min} and c_{max} , but it is possible to define the position of each reinforcement too.

Further parameters are necessary to define the crack depths for which the cracking moment will be computed:

- a_{stop} – stopping crack depth (or ξ_{stop} - normalized stopping crack depth)
- $\Delta\xi$ – normalized crack depth increment at each calculation step

For each value of the crack depth it is necessary to find the active fibers crossing the crack. If the crack tip is too close to a fiber, the crack length should be increased of a fraction of $\Delta\xi$ in order to avoid numerical issues because of the shape function $Y_P(\xi, \zeta_i)$ singularity in correspondence of a fiber. This problem is analysed in detail in [2.1.3]. The active fibers are identified by the following relation:

$$\zeta_i < \xi^{(k)} \quad (2.2)$$

Where the apex k indicates the generic calculation step.

Then, using Eq. (1.13) and (1.15) the shape functions for the bending moment $Y_M(\xi^{(k)})$ and for the reactions $Y_P(\xi^{(k)}, \zeta_i)$ are attained.

The compliances are evaluated with Eq. (1.31), (1.32), (1.33) and (1.34) considering only the active fibers and if necessary they are arranged in a matrix or in a vector.

$$\lambda_{MM}^{(k)} = \lambda_{MM}(E, b, h, \xi^{(k)}) \quad (2.3)$$

$$\{\lambda_M^{(k)}\} = \{\lambda_M(E, b, h, \xi^{(k)}, \zeta_i)\} \quad (2.4)$$

$$[\lambda^{(k)}] = [\lambda(E, b, \xi^{(k)}, \zeta_i, \zeta_j)] \quad (2.5)$$

The problem partition described in [1.3.6] is introduced using two vectors $\{c\}$ and $\{f\}$ containing respectively the indexes of the elastic and plasticized fibers. At the beginning of each step k all the reinforcements are in the elastic field. So $\{c\}$ is the vector of the active fibers, while $\{f\}$ is empty. Hence it is possible to obtain $\{\lambda_{M,c}\}$, $\{\lambda_{M,f}\}$, $[\lambda_{cc}]$, $[\lambda_{cf}] = [\lambda_{fc}]$ and $[\lambda_{ff}]$.

The values of the reactions at crack propagation are attained solving linear system (1.63). If at least a force in one fiber is higher than its ultimate value, the most loaded fiber is considered yielded, its force is set equal to $P_{p,i}$, $\{c\}$ and $\{f\}$ are update and consequently the partitioned matrix or vector of compliances are updated too. The reactions at crack propagation are calculated again, but now using Eq. (1.66). Until all the forces are lower or equal to their ultimate value, it is necessary to repeat the calculation, updating the yielded fibers. At the end the bending moment $M_F^{(k)}$ and the rotation $\phi_F^{(k)}$ are achieved with Eq. (1.61) and (1.39).

Now using a similar iterative procedure, the plastic moments and the respective rotations are evaluated by using Eq. (1.50), Eq. (1.55) and Eq. (1.39). Only the moments, that respect the following condition, are taken into account:

$$M_F^{(k-1)} < M_{p,i}^{(k)} < M_F^{(k)} \quad (2.6)$$

Then the crack length can be updated and the procedure can be repeated with the new value.

$$\xi^{(k+1)} = \xi^{(k)} + \Delta\xi \quad (2.7)$$

At each step the crack openings could be computed too. This can be done with Eq. (1.37).

It is possible to summarize the algorithm in the following way:

1. Initialization
2. For each value of crack depth $\xi^{(k)}$
 - a. Calculation of shape functions and compliances
 - b. Initialization of $\{c\}$ and $\{f\}$
 - c. Iterative procedure to find the cracking moment $M_F^{(k)}$
 - i. Computation of cracking forces with Eq. (1.63) or (1.66)
 - ii. Update $\{c\}$ and $\{f\}$, partitioned matrix and vector and reactions of yielded fibers
 - iii. Stop if all the reactions are lower or equal to their ultimate value
 - d. Computation of $M_F^{(k)}$ and $\phi_F^{(k)}$ with Eq. (1.61) and (1.39)
 - e. Computation of plastic moments with Eq. (1.50) and (1.55) and rotations with Eq. (1.39)
 - f. Add plastic moments that satisfy Eq. (2.6)
3. Update crack depth according to Eq. (2.7) and return to 2 if $\xi^{(k+1)} < \xi_{stop}$
4. Plot $M - \phi$ values

This algorithm has been implemented in MATLAB language and the code is reported in Appendix 1.

2.1.2 Case studies

Even if the analysis of the crack length control scheme is carried out only to check the results coming from the algorithms developed for cyclic loading, in this section some results obtained with this method are shown.

For example a beam with three equally spaced fibers is considered and its characteristics are summarized in Table 2.1. The mechanical properties correspond to those of a medium resistance concrete.

b	[cm]	25
h	[cm]	40
a/h		0,1
E	[GPa]	30
K_{IC}	[daN/cm ^{3/2}]	100
σ_y	[MPa]	450
m		3
ζ_{min}		0,1
ζ_{max}		0,3
r_i	[mm]	3,86
N_p		0,40

Table 2.1: Input data.

The crack propagation is considered up to $\xi_{stop} = 0,7$, while the other parameter $\Delta\xi$ is discussed in [2.1.3].

The response of the structure is evaluated both in terms of moment-rotation (Figure 2.1) and moment-crack depth (Figure 2.2).

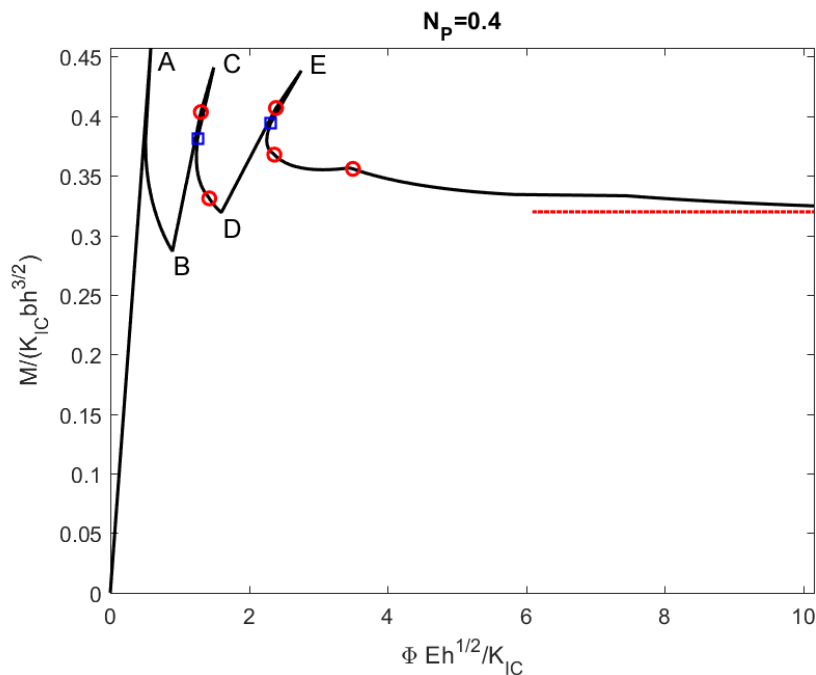


Figure 2.1: Moment-rotation diagram.

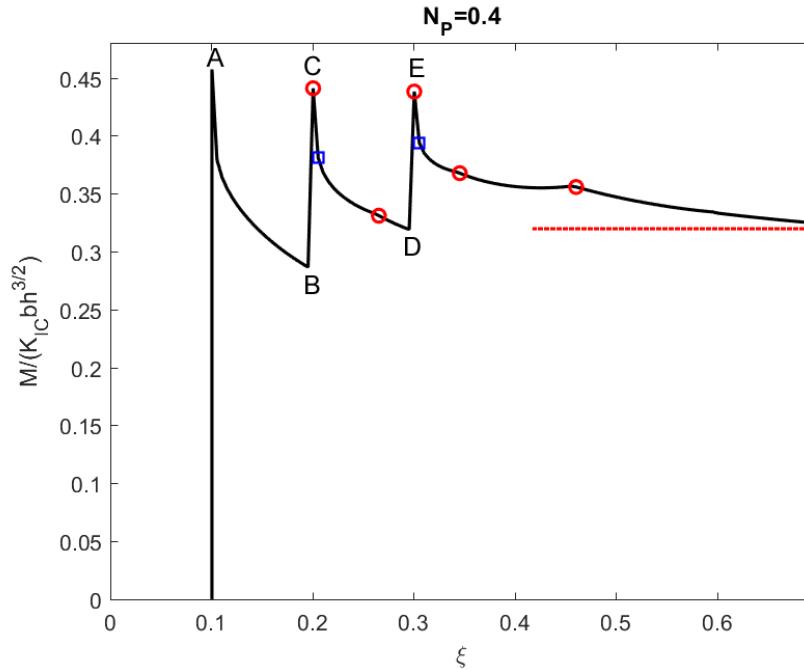


Figure 2.2: Moment-crack depth diagram.

In Figure 2.1 the branch between the origin and point A is elastic. The crack does not propagate and so in Figure 2.2 this corresponds to a vertical line. From A to B the fracture starts propagating in an unstable way because the bending moment decreases, while the deformation is increasing. In point B the fracture intersects a new fiber, that stops the propagation. So from B to C a second elastic branch is encountered and in this part the first fiber attains its ultimate load (red circle). Then the crack propagates again from C to D. In this part the load in the first fiber becomes lower than the ultimate one (blu square), but immediately after this value is reached again (red circle). In point D the third fiber does not let the crack propagate and a new elastic segment is present between D and E. After point E the fracture starts propagating again, the second fiber shows the same behaviour of the first one in part C-D. In the last red circle the third fiber attains its limit. For large deformation it is possible to see that the bending moment tends to its ultimate value (dotted red line) calculated as explained in [1.3.11].

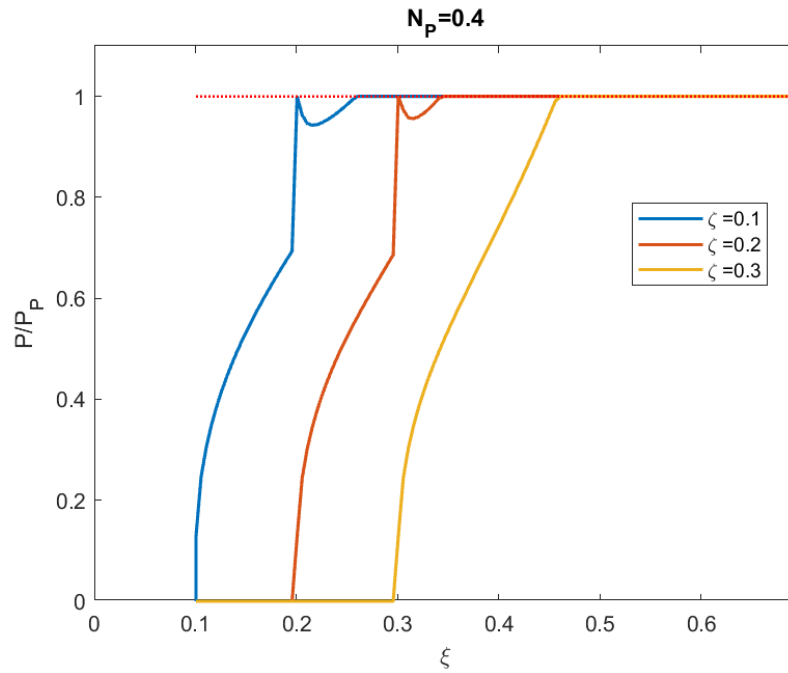


Figure 2.3: Fiber reactions.

In Figure 2.3 the value of the fiber reactions is shown. It can be used in order to check the behaviour already described in Figure 2.1 and Figure 2.2. At the beginning only the first fiber is active and its load increases, while the crack propagates. The second and the third fibers become active only when the crack overcomes them. It happens respectively in $\xi = 0.2$ and $\xi = 0.3$. It is possible to see the small load drops in the first and second fiber. At the end all the reinforcements reach their limit force, that is represented by the dotted red line.

Eventually the analysis of the crack opening profile is considered. According to [1.3.4] the crack openings are evaluated not only at the fibers level, but also along the entire crack length. In Figure 2.4, Figure 2.5 and Figure 2.6 the shape of the fracture is drawn for different value of the crack depth $\xi^{(k)}$. It is possible to notice the continuous crack propagation and the fiber bridging effect too.

The fibers in the elastic field are represented in green and they keep closed the crack, while the yielded fibers are represented in orange and they let the crack openings growing at their level.

In the previous graphs the maximum crack depth was equal to 0,7, while now for the sake of brevity only the figures up to 0,5 are reported. In any case all the fibers are plasticized when this value is reached.

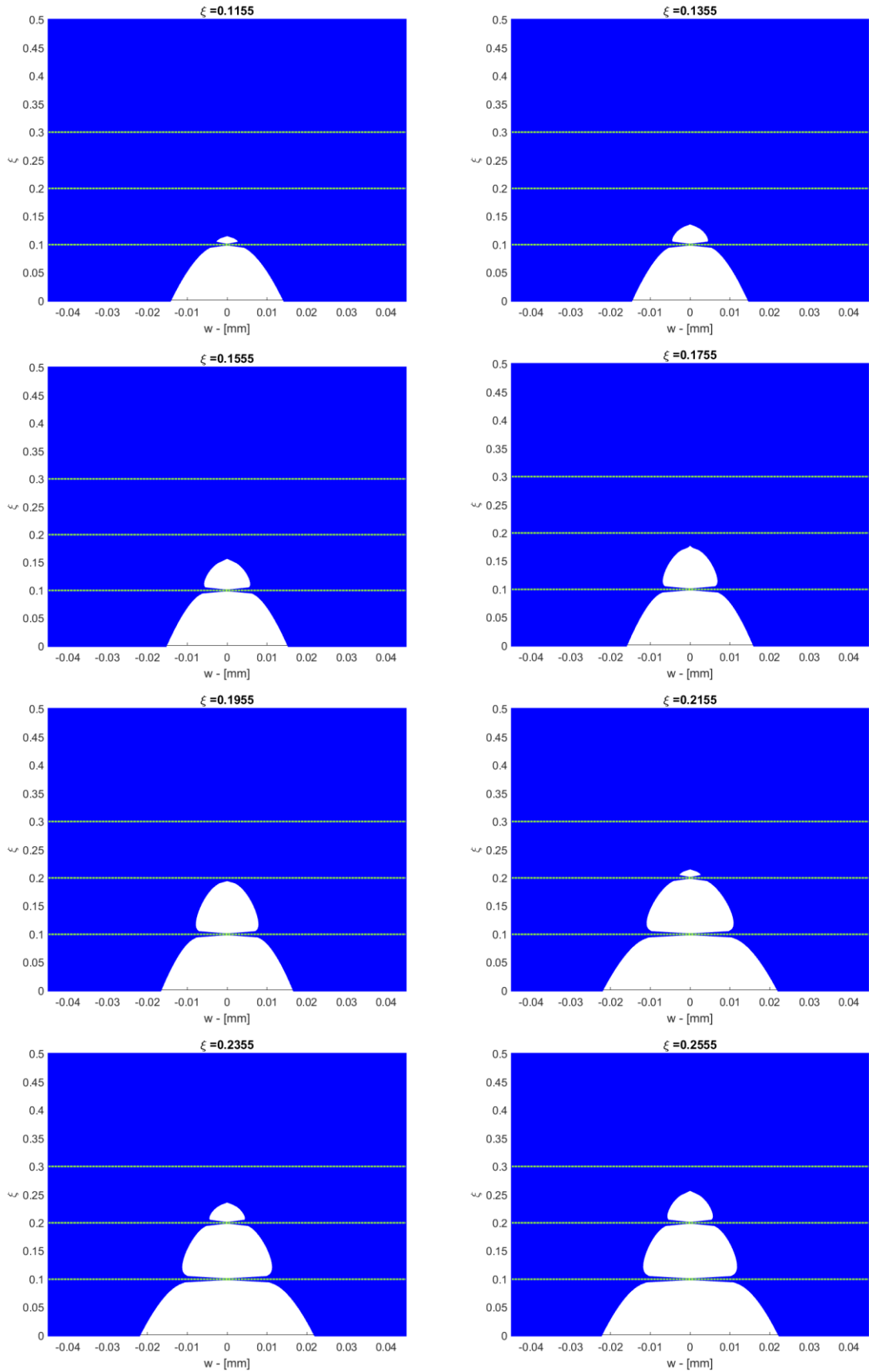


Figure 2.4: Crack profile from $\xi = 0, 1155$ to $\xi = 0, 2555$

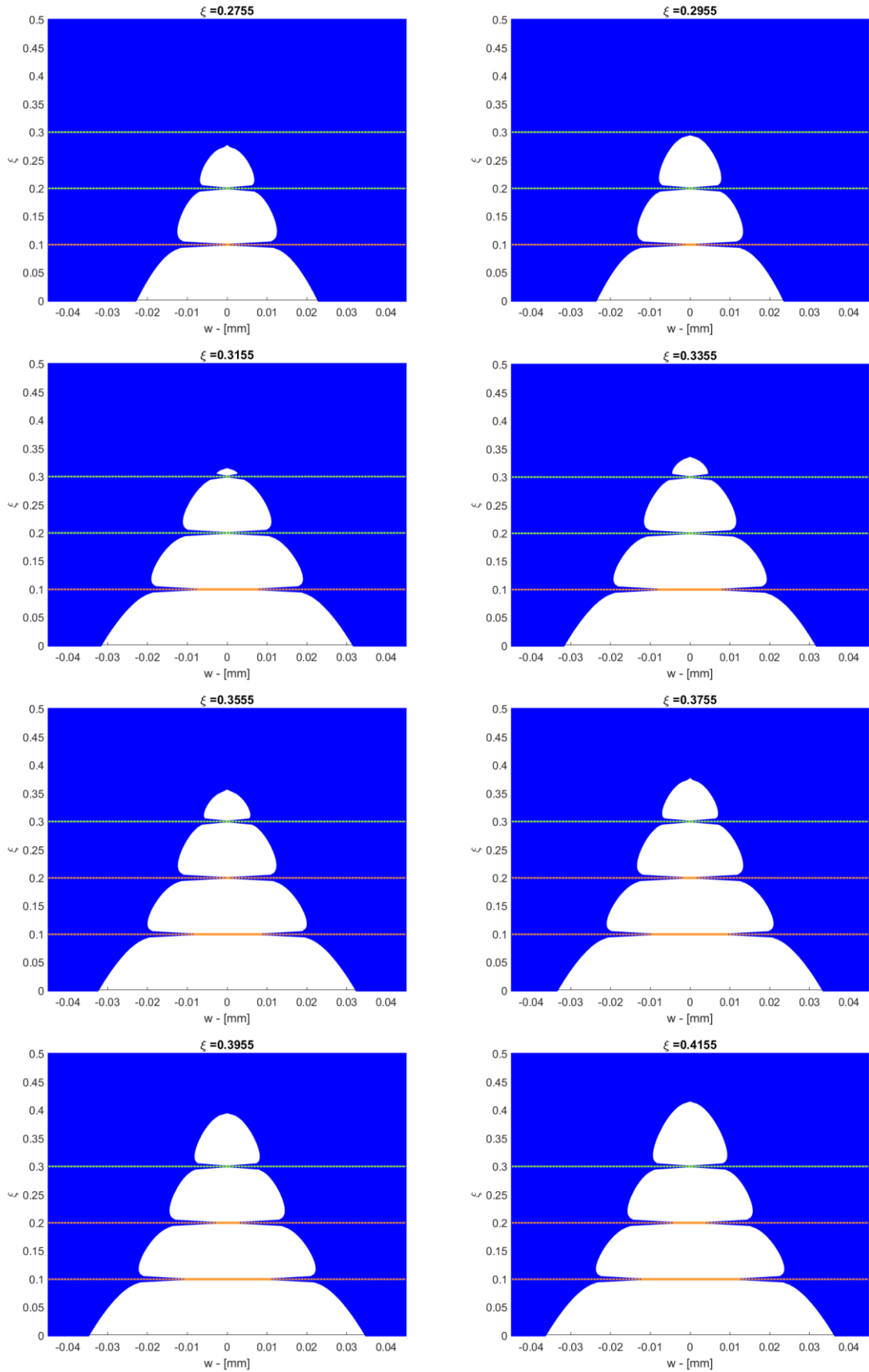


Figure 2.5: Crack profile from $\xi = 0, 1755$ to $\xi = 0, 4155$

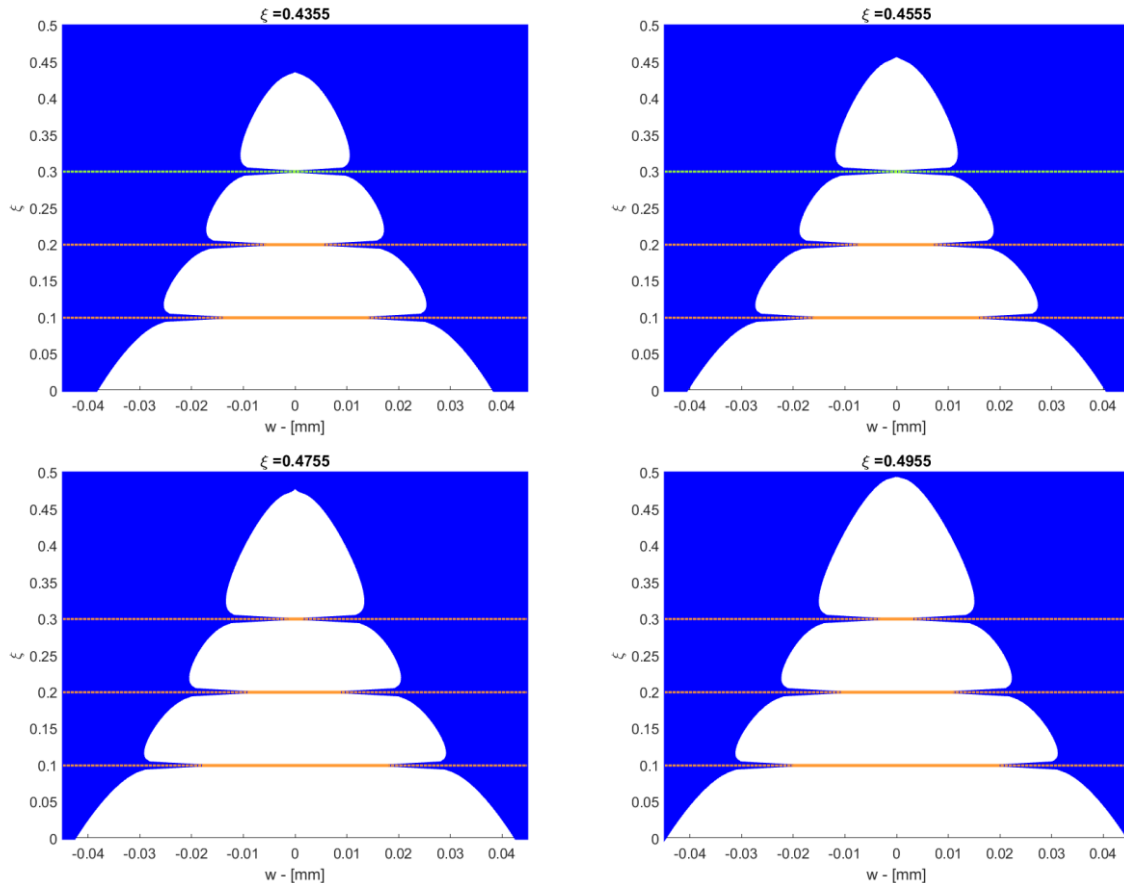


Figure 2.6: Crack profile from $\xi = 0,4355$ to $\xi = 0,4955$

Globally a strain-softening behaviour is shown by the system and it is correlated to the value of N_p . The influence of this number is condensed in Figure 2.7. A value of N_p lower than 0,7 produces a behaviour like the one just described. On the contrary a value of N_p higher than 0,7 gives rise to a global strain-hardening response. So a ductile to brittle transition is described. The value 0,7 divides the two behaviours because the ultimate bending moment has the same value approximately of the peaks given by the fiber actions. This condition represents the minimum reinforcement.

The three curves are superposed at the beginning because the value of the fiber reactions is the same until they attain their limit.

Even if the maximum crack depth considered in the calculation is the same, the curve with the highest value of N_p shows a larger deformation if it is compared to the other two.

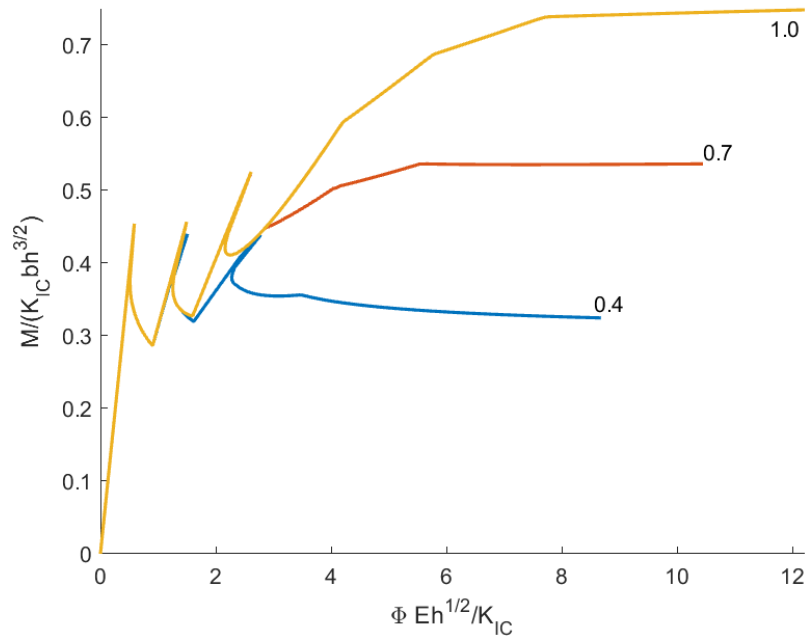


Figure 2.7: N_p influence on moment-rotation diagram ($N_p = 0, 4; 0, 7; 1, 0$).

2.1.3 Numerical errors

The value of the increment $\Delta\xi$ and the distance between the crack tip and the closest active fiber have a strong influence on the numerical results.

In particular is $\Delta\xi$ is too high, the graph $M - \phi$ loses its meaning and it is not possible any more to identify the peaks due to the bridging action of the fibers. On the contrary, if its value is too small, the graph is described accurately, but computational time increases.

As seen in section [1.3.2], the shape function $Y_p(\xi, \zeta_i)$ has a singularity for $\xi = \zeta_i$, in correspondence of the position of the fiber. Figure 1.3 shows that the function tends to infinity very quickly and this causes the numerical issues. It is sufficient that $\xi - \zeta_i < 1 \cdot 10^{-4}$ to observe the peaks of the curve rising very much losing their meaning.

In the present analysis the following values are normally used:

$$\Delta\xi = 0,005 \quad (2.8)$$

$$\xi - \zeta_i > 0,05 \Delta\xi \quad (2.9)$$

These issues are showed in Figure 2.8 and Figure 2.9 using a beam with the same characteristics of that of the examples in section [2.1.2]. The first picture is obtained with a value of $\Delta\xi$ lower than usual and equal to 0,0005. In this case it is possible to notice the peaks becoming too high because of the shape function $Y_p(\xi, \zeta_i)$ singularity when the crack tip is too close to a fiber. On the contrary in the second picture the interval $\Delta\xi$ is too high (0,05) and the peaks are not any more recognizable. The right $M - \phi$ response is the one showed in Figure 2.1 achieved with a $\Delta\xi$ equal to 0,005.

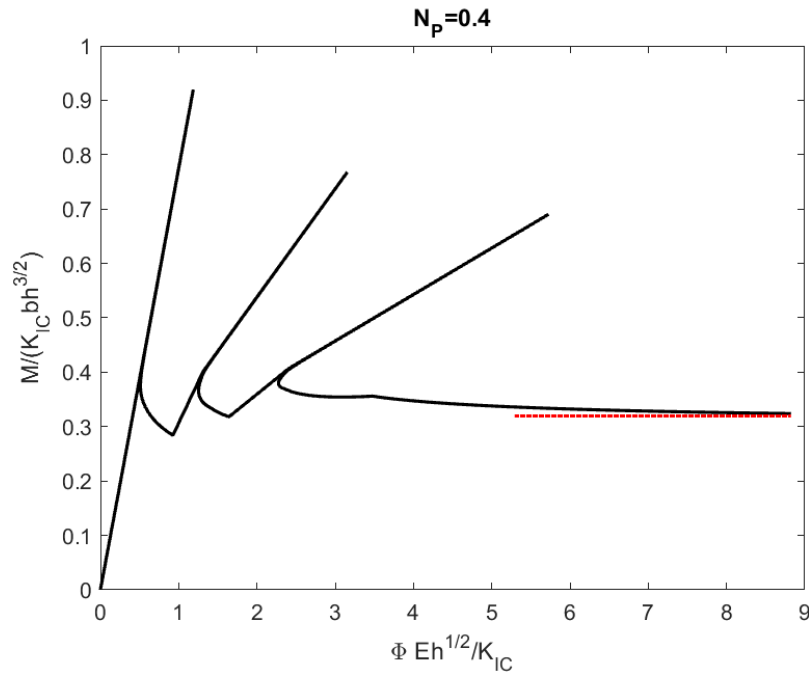


Figure 2.8: Moment-rotation diagram affected by the numerical singularity.

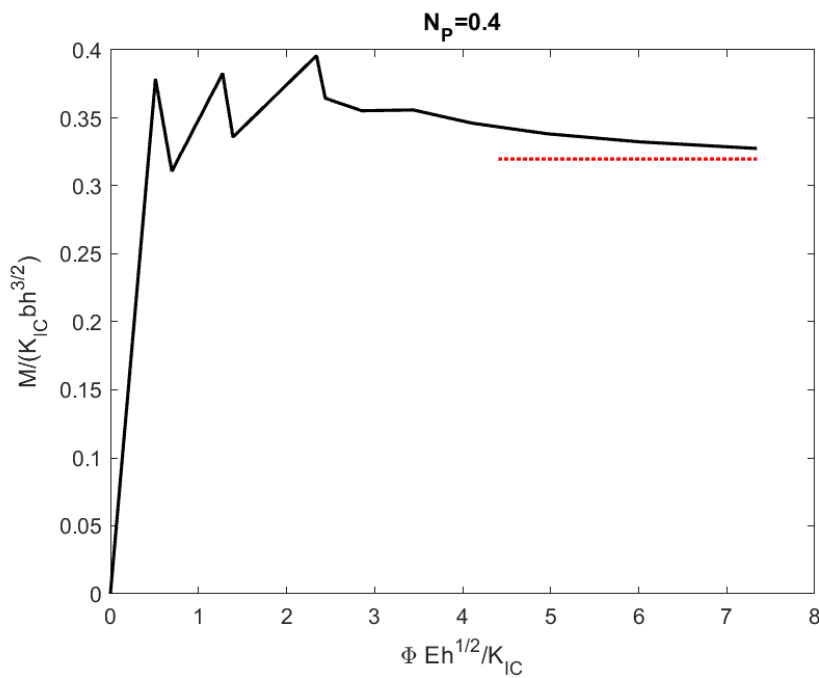


Figure 2.9: Moment-rotation diagram affected by an insufficient number of points.

2.2 Cyclic loading

The proposed algorithm describes the behaviour of the system subjected to a generic cyclic loading without the necessity to evaluate the plastic and shake-down moments. The process can be simulated both for loading and deformation control with two distinct but similar algorithm.

2.2.1 Force-controlled algorithm

This algorithm is based on the one proposed by Puzzi (Puzzi, 2004) and on the compatibility equation illustrated in [1.4.2].

The input parameters are the same as the monotonic case in [2.2.1], but the loading history in terms of bending moment values has to be added. For example, in Figure 2.10 the moment starts from zero, it reaches the maximum value, and it decreases up to a minimum value. Then it begins pulsating between these two extremes for a certain number of cycles.

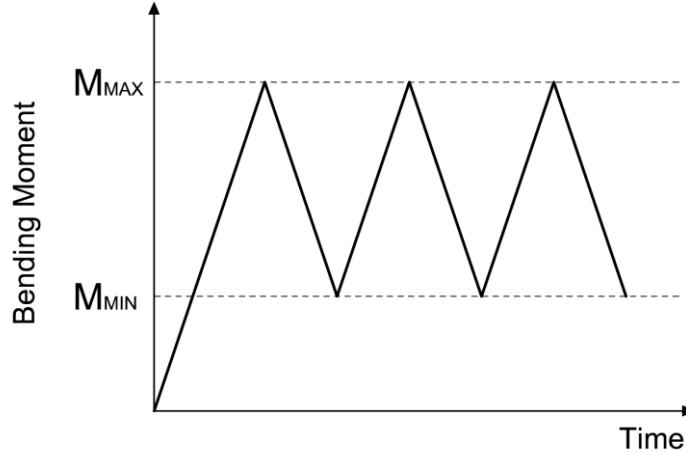


Figure 2.10: Load history in terms of bending moment.

It is important to choose the number of divisions of each monotonic part in order to describe accurately the moment–rotation response. This issue will be analysed in [2.2.10].

The initialization of the shape functions and the one of the compliances are the same as the monotonic loading.

In this case the values of the initial conditions M_0 , ϕ_0 , $\{P_0\}$ have to be taken into account, setting them equal to zero at the beginning.

Initially all the reinforcements are in the elastic field and again $\{c\}$ is the vector of active fibers while $\{f\}$ is empty.

For each value $M^{(k)}$ of the load history the fiber reactions are evaluated. At the beginning they all behave elastically and so it can be done solving the following linear system obtained from Eq. (1.78):

$$[\lambda](\{P\} - \{P_0\}) = \{\lambda_M\}(M - M_0) \quad (2.10)$$

If the reaction of a fiber overcomes its ultimate force, it is set equal to this value and the fiber is moved among the plasticized ones, updating $\{c\}$ and $\{f\}$.

The calculation of the elastic fiber forces is repeated using the following linear system obtained from the second equation of (1.79):

$$[\lambda_{cc}](\{P_c\} - \{P_{0,c}\}) = \{\lambda_{Mc}\}(M - M_0) - [\lambda_{cf}](\{P_f\} - \{P_{0,f}\}) \quad (2.11)$$

If none of the reactions exceeds the plastic force, it is possible to stop the procedure. Otherwise it is necessary to continue iterating, updating the yielded fibers and recalculating the reactions with Eq. (2.11).

Then, rotation $\phi^{(k)}$ can be obtained from Eq. (1.80).

Now fracture propagation should be taken into account. The cracking moment M_F is evaluated according to Eq. (1.61). If the value of the applied bending moment is higher than M_F , the crack propagation is triggered and the crack length is increased. In order to rise the cracking moment it is necessary to include at least a new fiber. This is the only chance to increase this value, because M_F decreases if ξ increases, while in this way a new term is added to the summation. If there are no more fibers, the crack advancing can be taken into account simply considering $\xi = \xi + \Delta\xi$. It is useful only if the ultimate bending moment is higher than the applied one, otherwise the structure fails. Anyway the crack depth changes and it is necessary to update the shape functions and the compliances taking into account the new fibers too. Then, the forces in the reinforcements are recalculated again using the procedure explained before and the cracking moment is recalculated too with these new values. Then, the condition $M^{(k)} < M_F$ is checked for a second time. If it is not respected, it is necessary to increase the crack length and the procedure is repeated. Otherwise it is possible to calculate the rotation using the new value of the forces.

When the reinforcement reactions are known, the crack openings are evaluated according to Eq. (1.37).

If the loading process is inverted, all the variables with the subscript 0 have to be set equal to their values at the end of the previous monotonic part. It is necessary to reset the number of elastic and yielded fibers too, because, when a fiber undergoes unloading, even if it is yielded, it will behave elastically until its compression limits is attained.

Failure can occur if the prefixed maximum value of ξ is reached. In this case the calculation is stopped. On the contrary it is possible to consider the next value of bending moment, repeating the procedure illustrated above.

Now the algorithm is illustrated in a synthetic form:

1. Initialization
 - a. Initialization of parameters and load history
 - b. Calculation of shape functions and compliances
 - c. Initialization of $\{c\}$ and $\{f\}$
2. For each value of moment $M^{(k)}$
 - a. Iterative procedure to find the fiber reactions $\{P\}^{(k)}$
 - i. Computation of forces with Eq. (2.10) or (2.11)
 - ii. Update $\{c\}$ and $\{f\}$, partitioned matrix and vector and reactions of the fibers for which $P_i^k > P_{p,i}$ or $P_i^k < -P_{p,i}$

- iii. Stop if all the reactions are lower or equal to their ultimate value
 - b. Computation of crack propagation moment M_F with Eq. (1.61)
 - c. Enter the loop if $M^{(k)} > M_F$
 - i. Increase crack depth, exit if ξ_{stop} is reached
 - ii. Update active fibers, shape functions and compliances
 - iii. Recalculate forces (as done in 2-a)
 - iv. Recalculate M_F and exit if $M^{(k)} < M_F$
 - d. Computation of rotation $\phi^{(k)}$ with Eq. (1.80)
 - e. Check load inversion and, if it is inverted, update $M_0, \phi_0, \{P_0\}$
3. Plot $M - \phi$ values

This algorithm has been implemented in MATLAB language and the code is reported in Appendix 2.

2.2.2 Rotation-controlled algorithm

This algorithm is similar to the previous one, but first of all it is necessary to express the bending moment as a function of the rotation, that is the driving parameter. Starting from Eq. (1.39) the following relation is obtained:

$$M = \frac{1}{\lambda_{MM}} (\phi + \{\lambda_M\}^T \{P\}) \quad (2.12)$$

The previous equation can be written also in its incremental form:

$$M - M_0 = \frac{1}{\lambda_{MM}} [\phi - \phi_0 + \{\lambda_M\}^T (\{P\} - \{P_0\})] \quad (2.13)$$

Substituting Eq. (2.13) in Eq. (1.78) a new compatibility equation is attained.

$$\{w\} - \{w_0\} = \frac{\{\lambda_M\}}{\lambda_{MM}} [\phi - \phi_0 + \{\lambda_M\}^T (\{P\} - \{P_0\})] - [\lambda] (\{P\} - \{P_0\}) = \{0\} \quad (2.14)$$

$$\left([\lambda] - \frac{\{\lambda_M\} \{\lambda_M\}^T}{\lambda_{MM}} \right) (\{P\} - \{P_0\}) = \frac{\{\lambda_M\}}{\lambda_{MM}} (\phi - \phi_0) \quad (2.15)$$

The same can be done substituting Eq. (2.13) in the second equation of system (1.79).

$$\{w_c\} - \{w_{0,c}\} = \frac{\{\lambda_{Mc}\}}{\lambda_{MM}} [\phi - \phi_0 + \{\lambda_M\}^T (\{P\} - \{P_0\})] - ([\lambda_{cf}] \{P_f\} + [\lambda_{cc}] \{P_c\}) = \{0\} \quad (2.16)$$

Then, splitting the term $\{\lambda_M\}^T (\{P\} - \{P_0\})$, the following linear system is achieved:

$$\begin{aligned} & \left([\lambda_{cc}] - \frac{\{\lambda_{Mc}\} \{\lambda_{Mc}\}^T}{\lambda_{MM}} \right) (\{P_c\} - \{P_{0,c}\}) \\ & = \frac{\{\lambda_{Mc}\}}{\lambda_{MM}} (\phi - \phi_0) + \left(\frac{\{\lambda_{Mc}\} \{\lambda_{Mf}\}^T}{\lambda_{MM}} - [\lambda_{cf}] \right) (\{P_f\} - \{P_{0,f}\}) \end{aligned} \quad (2.17)$$

The value of the forces in the fibers can be computed solving system (2.15) if all the reinforcements are in the elastic field or (2.17) if at least one reinforcements is plasticized.

The input parameters are the same as the monotonic case [2.2.1], but the deformation history in terms of rotation angle values has to be added. For example, in Figure 2.11 the angle starts from zero, it reaches the maximum value and it decreases up to a minimum value. Then it begins pulsating between these two extremes for a certain number of cycles.

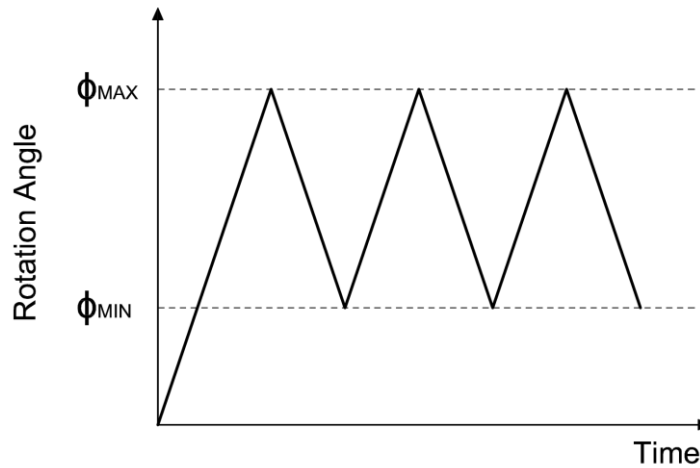


Figure 2.11: Deformation history in terms of rotation angle.

The algorithm is similar to the previous one shown in [2.2.1], but Eq. (2.15) and (2.17) are used instead of Eq. (2.10) or (2.11) in order to evaluate the reactions. At each step a value $\phi^{(k)}$ of the angle is considered.

Also the crack triggering is the same, but the new crack length is always determined by a increment $\Delta\xi$ fixed in advance.

$$\xi^{(k)'} = \xi^{(k)} + \Delta\xi \quad (2.18)$$

This is related to the deformation control assumed in this algorithm, that could admit load drops.

As remarked in [2.2.1], if the crack tip is too close to a fiber, the crack length should be increased of a fraction of $\Delta\xi$ in order to avoid numerical issues because of the shape function $Y_p(\xi, \zeta_i)$ singularity in correspondence of a fiber.

It is necessary to underline that the number of elastic and plasticized fibers ($\{c\}$ and $\{f\}$) has to be reset after crack advancing in order to take into account a possible bending moment drop.

When the fibers reactions are known, the bending moment $M^{(k)}$ is calculated from Eq. (2.13).

Again, if the loading process is inverted, all the variables with the subscript 0 have to be set equal to the value at the end of the previous monotonic part. Failure can occur if the prefixed maximum value of ξ is reached.

Now the algorithm is illustrated in a synthetic form:

1. Initialization
 - a. Initialization of parameters and rotation history
 - b. Calculation of shape functions and compliances
 - c. Initialization of $\{c\}$ and $\{f\}$
2. For each value of angle $\phi^{(k)}$
 - a. Iterative procedure to find the fiber reactions $\{P\}^{(k)}$
 - i. Computation of forces with Eq. (2.15) and (2.17)
 - ii. Update $\{c\}$ and $\{f\}$, partitioned matrix and vector and reaction of the fibers for which $P_i^k > P_{P,i}$ or $P_i^k < -P_{P,i}$
 - iii. Stop if all the reactions are lower or equal to their ultimate value
 - b. Computation of crack propagation moment M_F with Eq. (1.61) and applied moment $M^{(k)}$ with Eq (2.13).
 - c. Enter the loop if $M^{(k)} > M_F$
 - i. Increase crack depth, exit if ξ_{stop} is reached
 - ii. Reset active fibers, update shape functions and compliances
 - iii. Recalculate forces (as done in 2-a.)
 - iv. Recalculate M_F and $M^{(k)}$, exit if $M^{(k)} < M_F$
 - d. Check load inversion and, if it is inverted, update $M_0, \phi_0, \{P_0\}$
3. Plot $M - \phi$ values

This algorithm has been implemented in MATLAB language and the code is reported in Appendix 3.

2.2.3 Moment-rotation response and shake-down moments

As previously remarked the numerical results of the algorithms are expressed in terms of moment rotation diagram. If the crack propagation does not occur, for example because of a high fracture toughness, three different stages are evident as shown in Figure 2.12 in the case of a beam with two fibers:

- Linear elastic: $M < M_{P,1}$
- Linear hardening and elastic shake-down: $M_{P,1} < M < M_{SD,1}$
- Plastic shake-down: $M > M_{SD,1}$

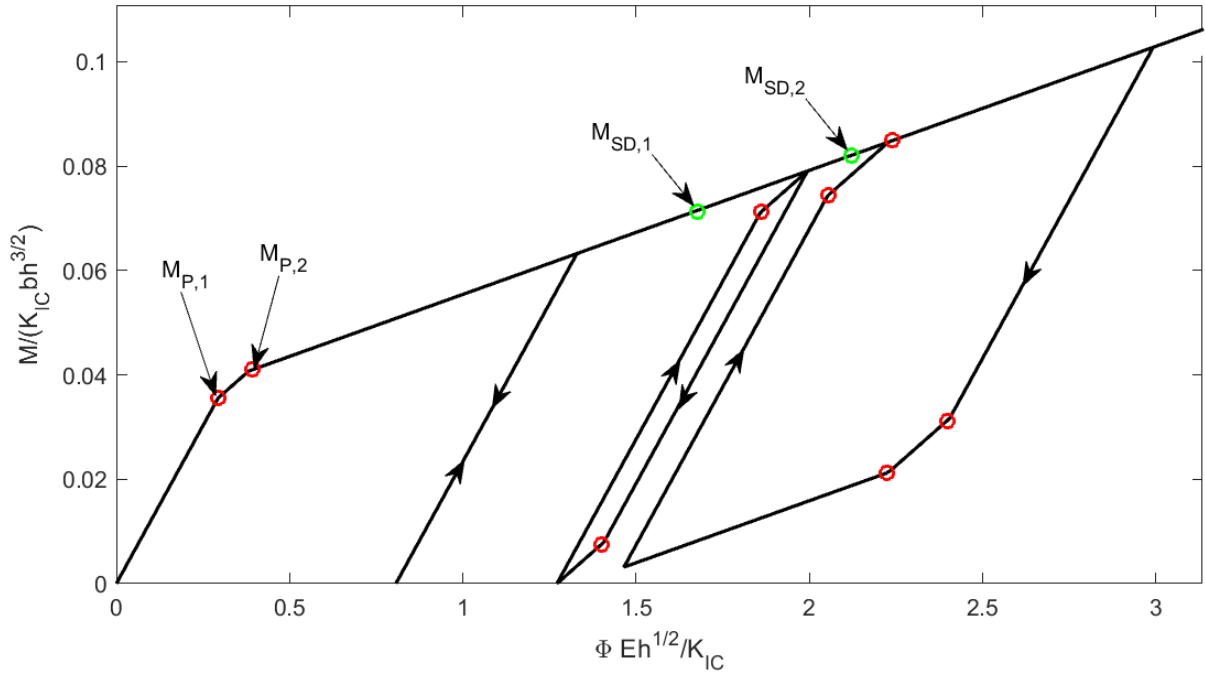


Figure 2.12: Moment-rotation response: shake-down and hysteresis.

The response is a linear function piecewise and each plasticization corresponds to a stiffness reduction. As it is possible to notice a fiber undergoes yielding in compression only when the corresponding shake-down moment is overcome. This is why the hysteretic cycle between $M_{SD,1}$ and $M_{SD,2}$ is characterized by only one fiber reaching its ultimate load, while in the one beyond $M_{SD,2}$ both fibers attain their compression limit. If none of the shake-down moments is reached, the unloading occurs on a single elastic branch without describing a hysteretic cycle and without dissipating energy.

Now the demonstration of the fact that the shake-down moment of a fiber is always the double of the respectively plastic moment is given.

First of all the reactions are calculated from Eq. (2.10).

$$\{P\} - \{P_0\} = [\lambda]^{-1} \{\lambda_M\} (M - M_0) \quad (2.19)$$

$$P_i - P_{0,i} = [\lambda]_i^{-1} \{\lambda_M\} (M - M_0) \quad (2.20)$$

Then the conditions $P_i = -P_{P,i}$, $P_{0,i} = P_{P,i}$, $M = 0$ and $M_0 = M_{SD,i}$ are considered and the correspondingly bending moment is evaluated.

$$-P_{P,i} - P_{P,i} = [\lambda]_i^{-1} \{\lambda_M\} (-M_{SD,i}) \quad (2.21)$$

$$M_{SD,i} = \frac{2P_{P,i}}{[\lambda]_i^{-1} \{\lambda_M\}} \quad (2.22)$$

The first shake-down moment is the minimum among these values and it is the double of the first plastic moment (Eq. (1.87) and (1.88)).

The following shake down moments are calculate with the same procedure, but considering Eq. (2.11) instead of Eq. (2.10).

$$\{P_c\} - \{P_{0,c}\} = [\lambda_{cc}]^{-1} \{ \{\lambda_{Mc}\} (M - M_0) - [\lambda_{cf}] (\{P_f\} - \{P_{0,f}\}) \} \quad (2.23)$$

$$P_i - P_{0,i} = [\lambda_{cc}]_i^{-1} \{ \{\lambda_{Mc}\} (M - M_0) - [\lambda_{cf}] (\{P_f\} - \{P_{0,f}\}) \} \quad (2.24)$$

Then the conditions $P_i = -P_{P,i}$, $P_{0,i} = P_{P,i}$, $M = 0$, $M_0 = M_{SD,i}$, $\{P_f\} = -\{P_{P,f}\}$ and $\{P_{0,f}\} = \{P_{P,f}\}$ are considered and the correspondingly bending moment is evaluated.

$$-P_{P,i} - P_{P,i} = [\lambda_{cc}]_i^{-1} \{ \{\lambda_{Mc}\} (-M_{SD,i}) - [\lambda_{cf}] (-\{P_{P,f}\} - \{P_{P,f}\}) \} \quad (2.25)$$

$$M_{SD,i} = \frac{2(P_{P,i} + [\lambda_{cc}]_i^{-1} [\lambda_{cf}] \{P_{P,f}\})}{[\lambda_{cc}]_i^{-1} \{\lambda_{Mc}\}} \quad (2.26)$$

The j -th shake-down moment is the minimum among these values and it is the double of the j -th plastic moment (Eq. (1.89) and (1.90)).

2.2.4 Snap-back and snap-through instability

If the same problem is analysed both with the crack length control scheme and with the deformation controlled algorithm, it is possible to observe the snap-back instability. It is a drop of the load value at a constant rotation.

In Figure 2.13 the result of crack length control scheme is superimposed over the one obtained with the deformation control algorithm.

The snap-back is represented by the vertical drops A-A', B-B' and C-C'.

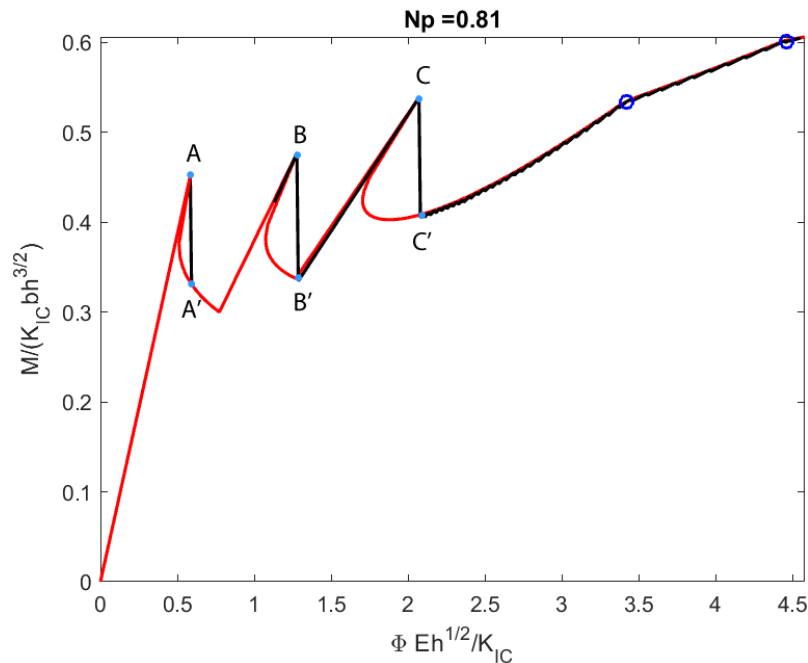


Figure 2.13: Snap-back instability underlined by the comparison between crack length control scheme (red) and rotation control (black).

If the same problem is analysed with the crack length control scheme and with the loading control algorithm, it is possible to observe the snap-through instability. It is a jump of the angle value at a constant load.

In Figure 2.14 the result of crack length control scheme is superimposed over the one obtained with the loading control algorithm.

The snap-through is represented by the horizontal jumps A-A', B-B' and C-C'.

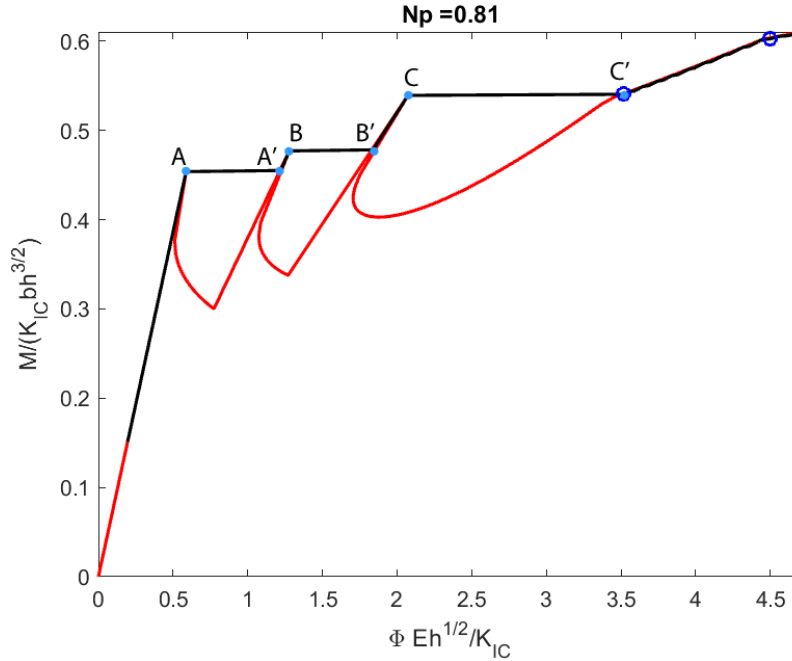


Figure 2.14: Snap-through instability underlined by the comparison between crack length control scheme (red) and loading control (black).

2.2.5 Energy dissipation

The energy dissipation is related to the presence of a hysteretic cycle and consequently to the shake-down moments overcoming.

$$M_{SD} \leq M_{max} < M_F \quad (2.27)$$

The dissipated energy is proportional to the area of the hysteretic cycle and it can be evaluated from the $M - \phi$ points obtained from the numerical algorithms. Only the ones between the step at the beginning of the cycle (s_b) and the one at the end (s_e) need to be considered.

$$W = \sum_{k=s_b}^{s_e} \frac{1}{2} (M^{(k+1)} - M^{(k)}) (\phi^{(k+1)} - \phi^{(k)}) \quad (2.28)$$

Eq. (2.28) represents the dissipated energy per cycle.

2.2.6 Influence of brittleness number, crack depth and fiber number

In this section the effect of the different geometric or mechanical properties on the system response is studied. In a first stage crack propagation is disregarded and the attention is focused on the hysteretic cycle shape.

The only effect of the brittleness number N_p is that on the dimension of the hysteretic cycle, while the shape is not affected by its variation. The same applies to the other part of the moment-rotation diagram. For example, if N_p doubles, the plastic and

shake-down moments double and this means that the dimension of the moment-rotation diagram doubles too. Consequently the dissipated energy, that is proportional to the area of the cycle, becomes four times higher. This effect is clearly visible in Figure 2.15, where three different values of N_p are considered. Each one is the double of the other. In this case the beam has four reinforcements.

For example the value of N_p (Eq. (1.76)) can be doubled by doubling the fiber limit force or by halving the fracture toughness. In the first case the plastic moments double while in the second case they remain equal and the diagram double because of the normalized axes. So only in the first case the increase of energy is real.

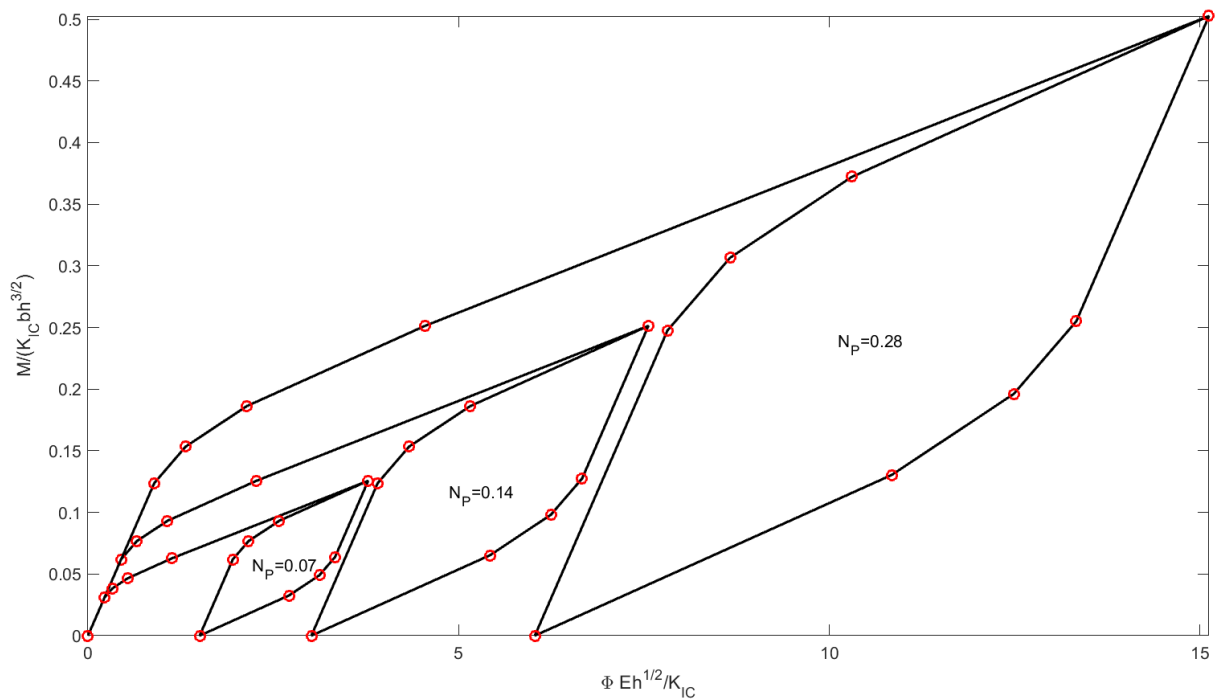


Figure 2.15: Influence of N_p on a beam with four fibers.

The area increase is related to the different maximum bending moment, that is equal to the last shake-down moment. If the two lowest N_p values are compared using the same maximum, the structure characterized by the highest brittleness value shows a smaller area.

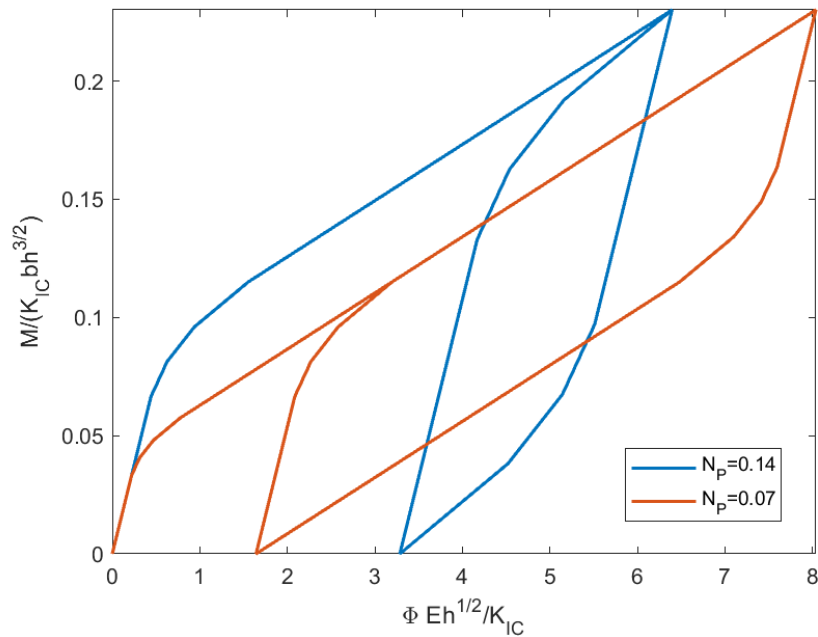


Figure 2.16: Influence of N_p on a beam with four fibers (the maximum moment is equal to the maximum shake-down-moment of the case $N_p = 0,14$).

In Figure 2.17 it is possible to notice the strong influence of the crack depth ξ on the shape of the moment-rotation diagram. In this example the position of the three fibers is kept constant, while the crack depth is varied. The fibers are equally spaced between the normalized depths equal to 0,05 and 0,25. When the crack depth ξ increases, the plastic and shake-down moments decrease, while the deformations become larger. At the same time the area of the hysteretic cycle is reduced and the stiffness decreases.

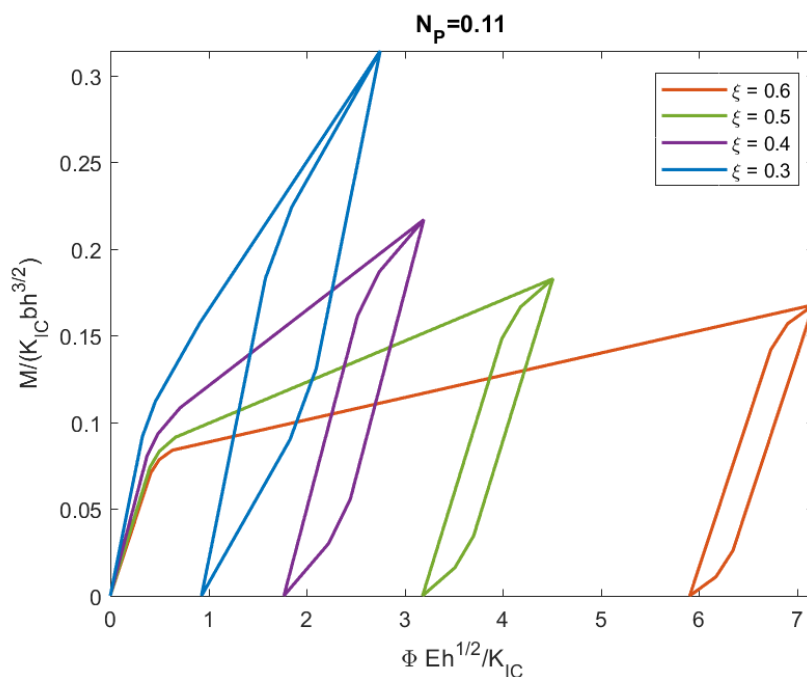


Figure 2.17: Influence of ξ on a beam with three fibers (in each case the maximum moment is equal to the maximum shake-down-moment).

The reduction of the hysteretic cycle area is only apparent and connected to the different maximum bending moment value, that in this case is equal to the last shake-down moment. If the two extreme cases ($\xi = 0,3$ and $\xi = 0,6$) are compared using the same maximum, the one with the deeper crack shows a much larger hysteretic cycle as it is remarked by Figure 2.18.

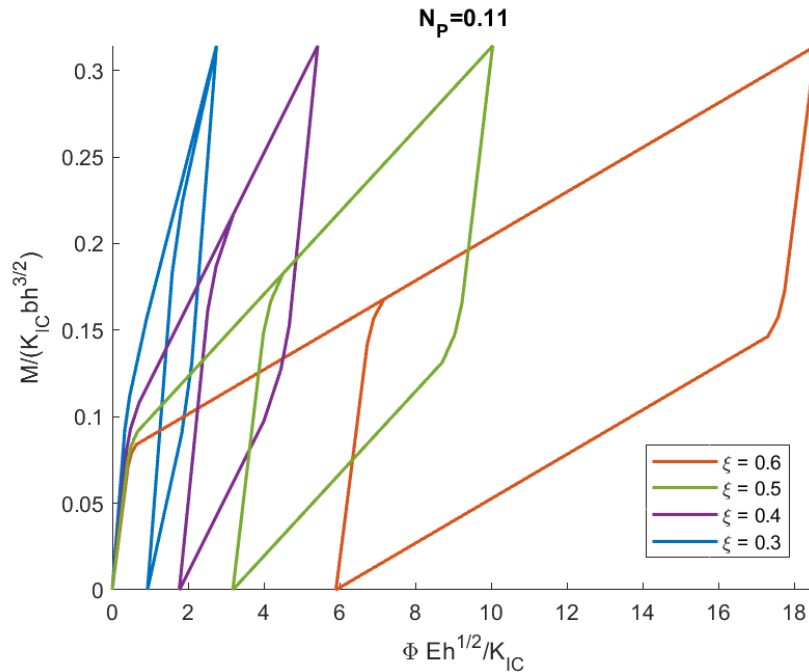


Figure 2.18: Influence of ξ on a beam with three fibers (the maximum moment is always equal to the maximum shake-down-moment of the case $\xi = 0,3$).

The effect of the fiber number m is examined in Figure 2.19. In this case the brittleness number N_p and the total reinforcement percentage are constant, while the number of fibers is increased diminishing the area of the single one. The maximum load of each case in Figure 2.19 is equal to the maximum shake-down moment. So it is possible to notice that, increasing the number of fibers, this value decreases and at the same time the stiffness increases. For high values of m the hysteretic cycles tend to the same shape and the difference between the shake-down moments is reduced.

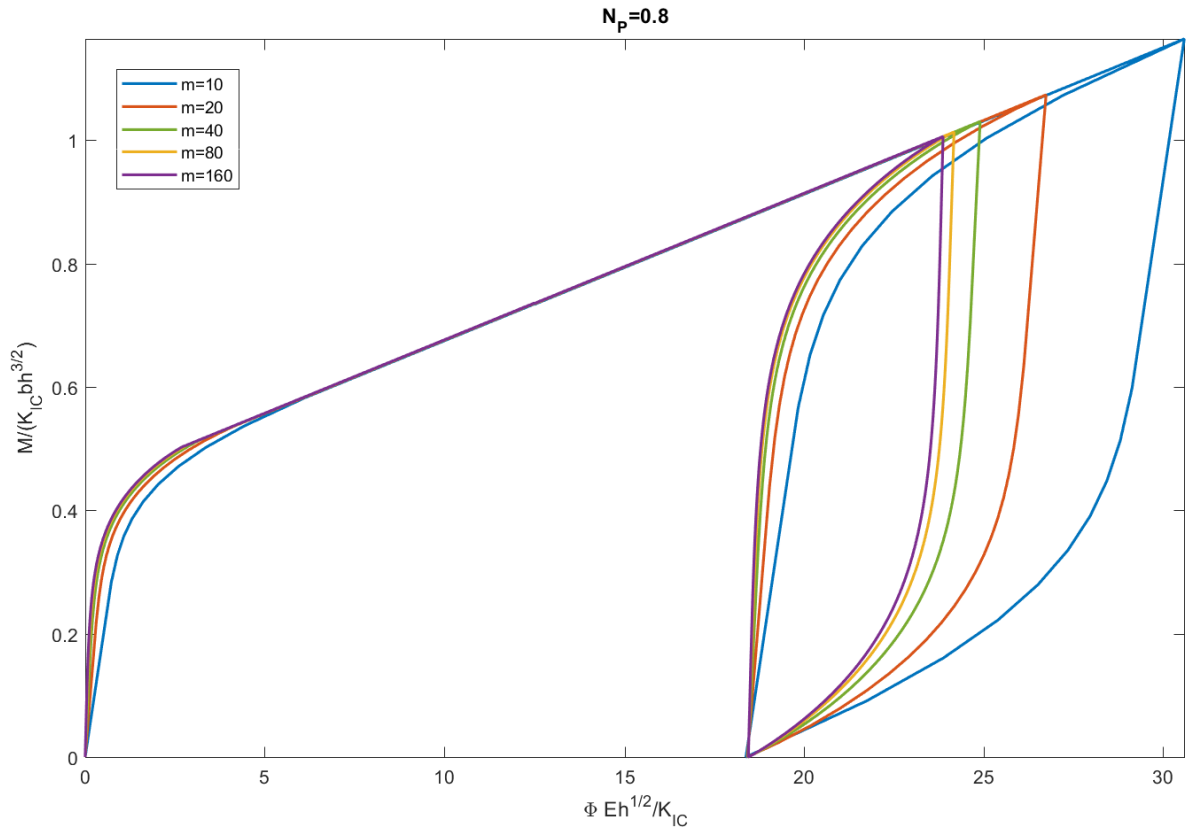


Figure 2.19: Influence of the number of fibers on a beam with a constant reinforcement percentage (in each case the maximum moment is equal to the shake-down-moment).

In Figure 2.19 the hysteretic cycles area becomes smaller as m increases, but it is related to the maximum bending moment value, that is considered. In Figure 2.20 the cases with 10 and 80 fibers are compared using the same maximum load and in this case the effect of the fiber number on hysteresis is evident. The area of the cycle attained with 80 fibers is larger and this produces an energy dissipation that is about 20% higher than the one obtained with 10 fibers. So, the fiber number increase has a positive effect on the behaviour of the system.

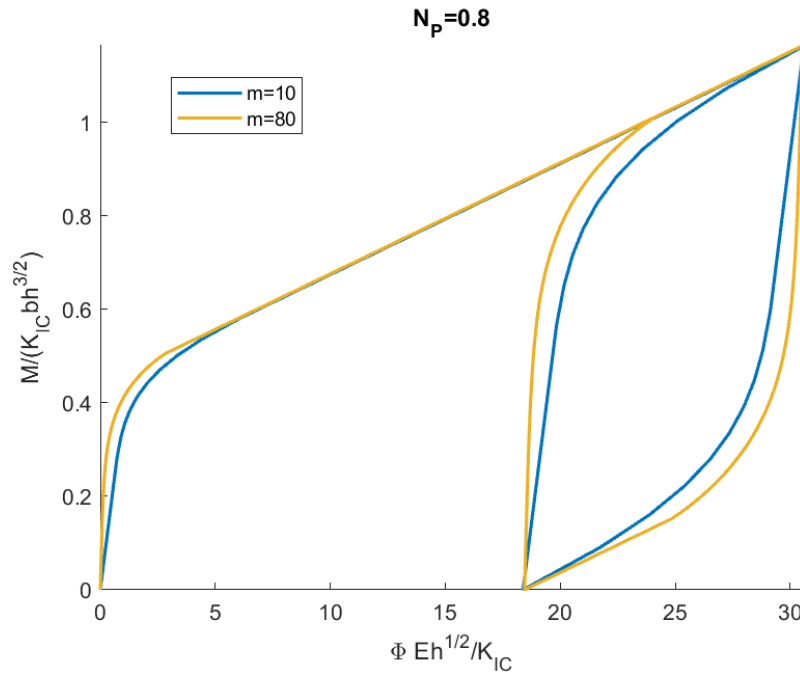


Figure 2.20: Influence of the number of fibers on a beam with a constant reinforcement percentage (the maximum moment is equal in both cases).

To explore the influence of the fiber number, of the brittleness number and of the crack depth a parametric study has been performed. First of all for each considered value of the crack depth (0,3; 0,5; 0,7) four different brittleness numbers have been taken into account (0,05; 0,1; 0,5; 1) and then the plastic, shake-down and cracking moments have been calculated for different numbers of fibers as explained respectively in [1.3.7], [1.4.3] and [1.3.9]. It is possible to increase the number of fibers keeping constant the reinforcement percentage and consequently N_p by diminishing the area of each one.

In Figure 2.21, Figure 2.22, Figure 2.23, Figure 2.24 the case of $\xi = 0,3$ is reported. The fiber number varies between 1 and 10 and they are equally spaced between the normalized position 0,05 and 0,25. For all the value of N_p the plastic and shake-down moments decrease rapidly, when m increases, and they tend to a horizontal asymptote. As explained before, for high numbers of fibers the variation is moderate and spreading the reinforcement area over a certain limit has no more influence. So, it is possible to suppose that the behaviour obtained using a high number of fibers tends to the one derived from a model with a continuous reinforcement expressed as a cohesive law. In the case $N_p = 0,05$ and $N_p = 0,1$ the crack propagation moment decreases slightly as m rises. In both cases, when fracture propagates, all the fibers have attained their limit ($M_F > M_{P,max}$), but only in the first one M_F is always higher than the shake-down moments. In the second case this occurs at least for one fiber when $m > 2$ ($M_F > M_{SD,min}$) and for all the fibers when $m > 6$ ($M_F > M_{SD,max}$).

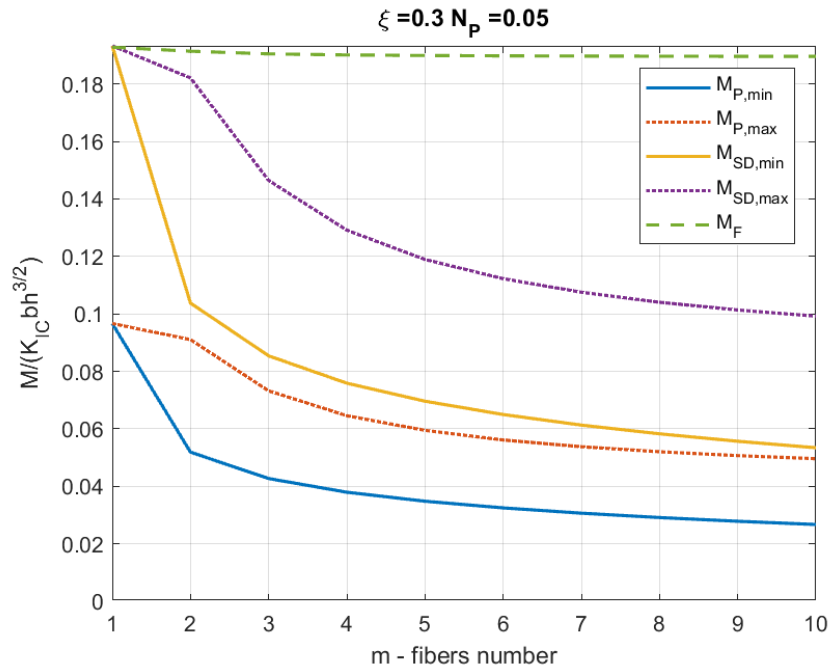


Figure 2.21: Plastic, shake-down and crack advancing moments at the variation of fiber number.

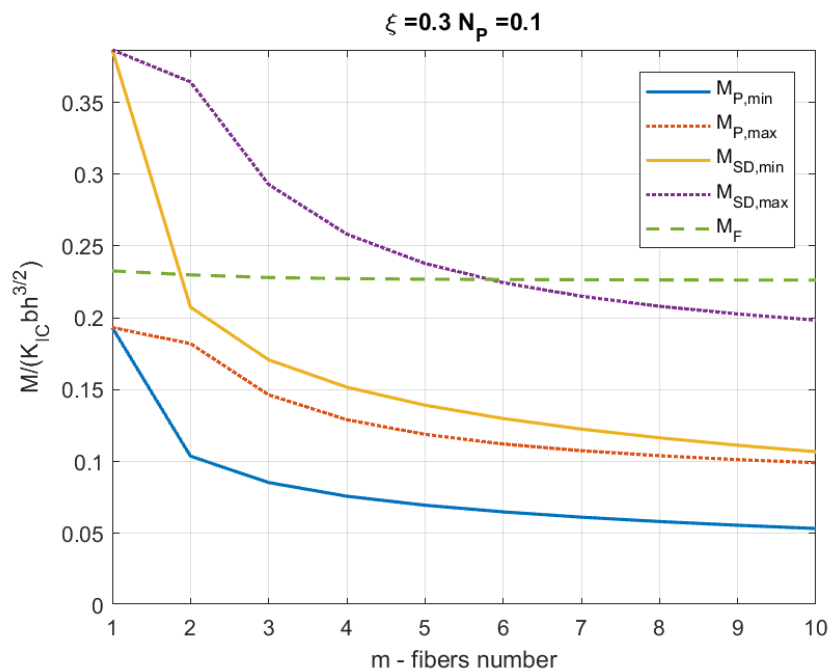


Figure 2.22: Plastic, shake-down and crack advancing moments at the variation of fiber number.

In the case $N_p = 0,5$ and $N_p = 1$ the crack propagation moment can be lower than the first plastic moment ($M_F < M_{P,min}$) for small number of fibers. This changes the previous trend of M_F and it is related to the fact that the crack propagation happens when not all the fiber are yielded. In these two cases shake-down is never reached ($M_F < M_{SD,min}$) and so hysteretic behaviour and dissipation are not possible for the considered fiber number range.

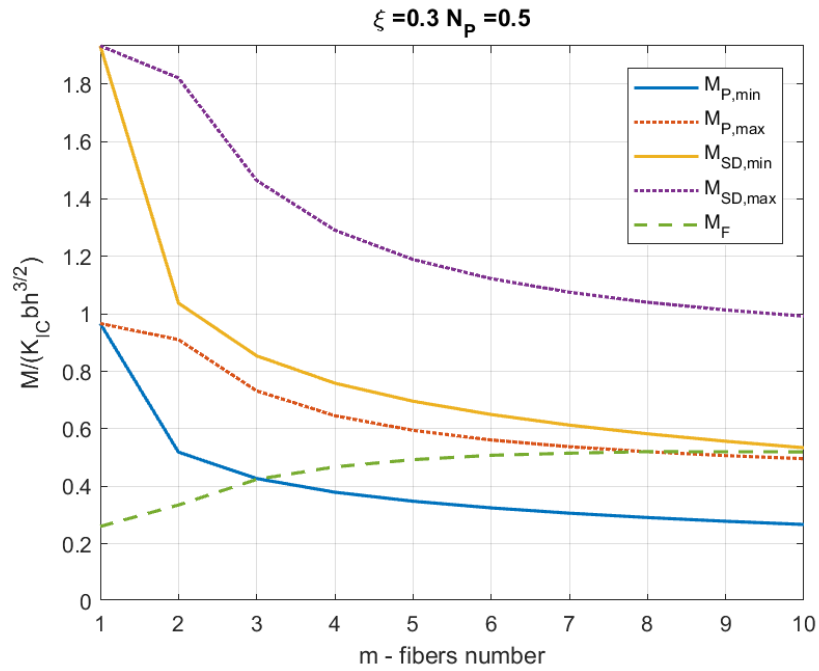


Figure 2.23: Plastic, shake-down and crack advancing moments at the variation of fiber number.

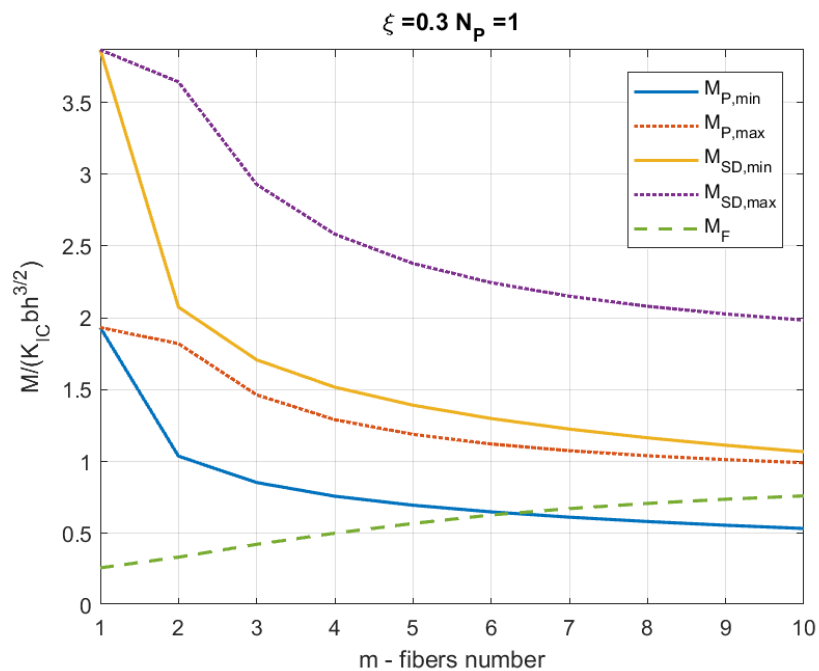


Figure 2.24: Plastic, shake-down and crack advancing moments at the variation of fiber number.

In Figure 2.25, Figure 2.26, Figure 2.27 and Figure 2.28 the case of $\xi = 0,7$ is showed. The fibers number varies between 1 and 15 and they are equally spaced between the normalized position 0,05 and 0,65. The remarks of the previous case are still valid, but now with $N_p = 0,05$ and one or two fibers the shake-down does not occur for all the reinforcements. The shake-down appears in the cases $N_p = 0,05$ for all the fibers ($M_F > M_{SD,max}$) only if there are more than four.

With this crack depth the last plastic moment is higher than the first shake-down moment for all the different considered values of the brittleness number if there are more than seven fibers.

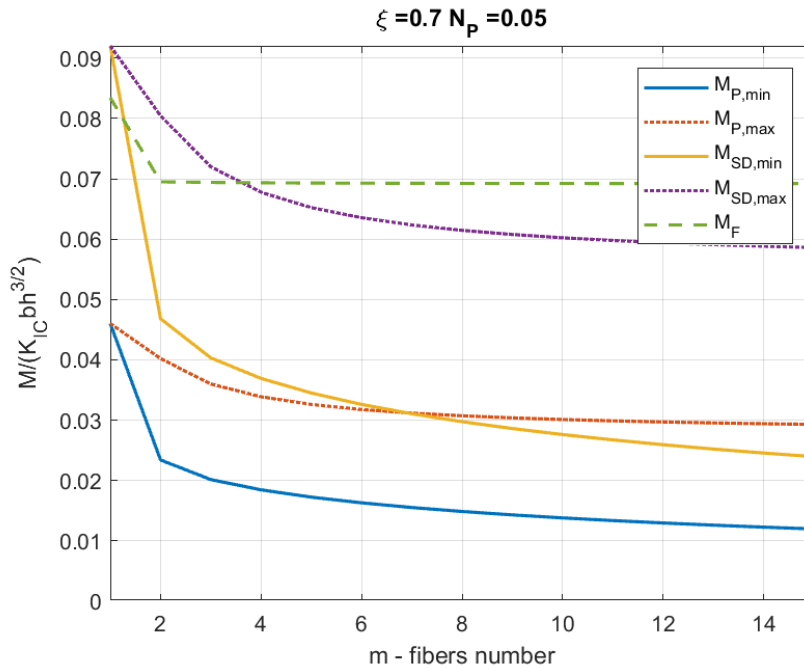


Figure 2.25: Plastic, shake-down and crack advancing moments at the variation of fiber number.

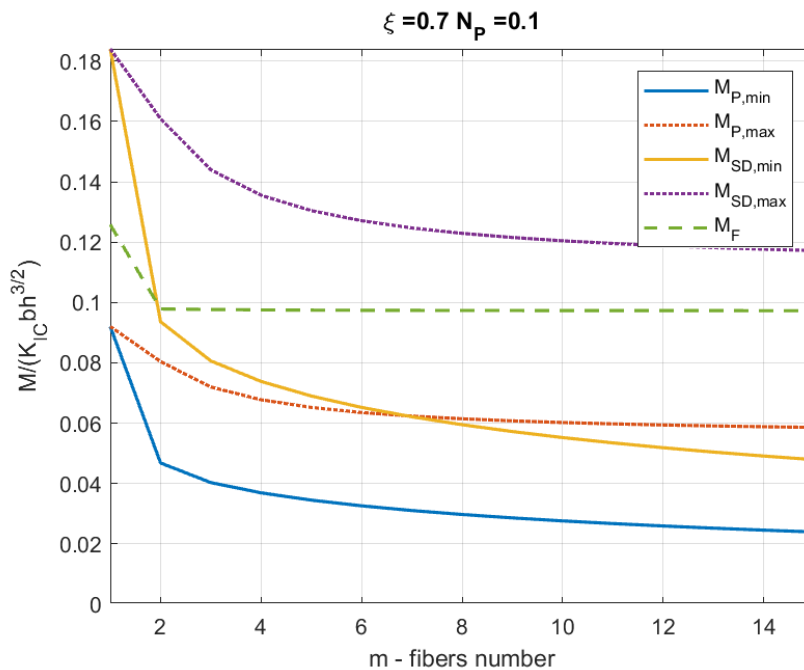


Figure 2.26: Plastic, shake-down and crack advancing moments at the variation of fiber number.

In this case the shake-down occurs also with a higher brittleness number: for $m > 7$ and $m > 8$ respectively in the case of $N_p = 0,5$ and $N_p = 1$.

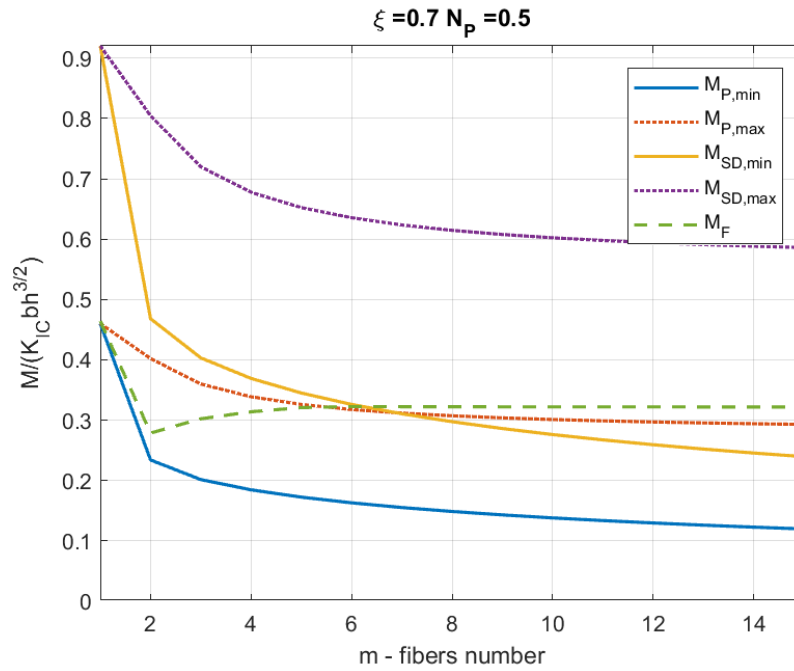


Figure 2.27: Plastic, shake-down and crack advancing moments at the variation of fiber number.

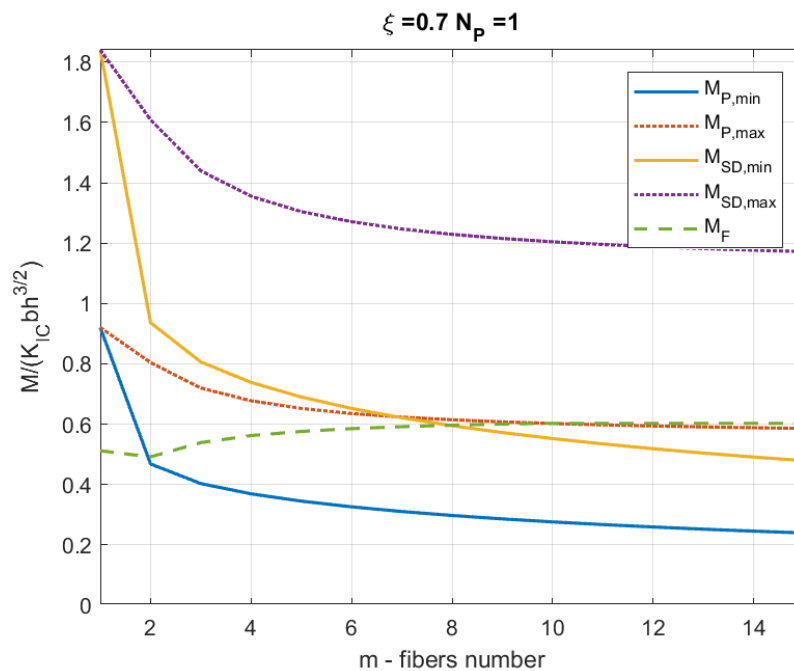


Figure 2.28: Plastic, shake-down and crack advancing moments at the variation of fiber number.

For the sake of completeness the diagrams of the intermediate case $\xi = 0,5$ are reported too in Figure 2.29, Figure 2.30, Figure 2.31 and Figure 2.32. In this case the fibers are equally spaced between 0,05 and 0,45. The behaviour in the cases $N_p = 0,05$ and $N_p = 0,1$ is similar to the one of $\xi = 0,3$, but with the second brittleness number nine fibers are necessary in order to get a cracking moment higher than the last shake-down one.

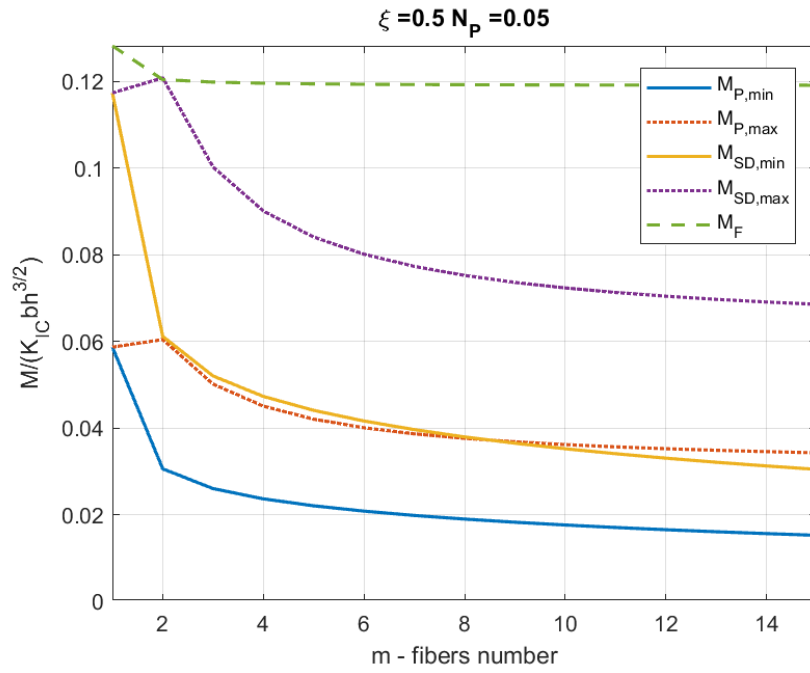


Figure 2.29: Plastic, shake-down and crack advancing moments at the variation of fiber number.

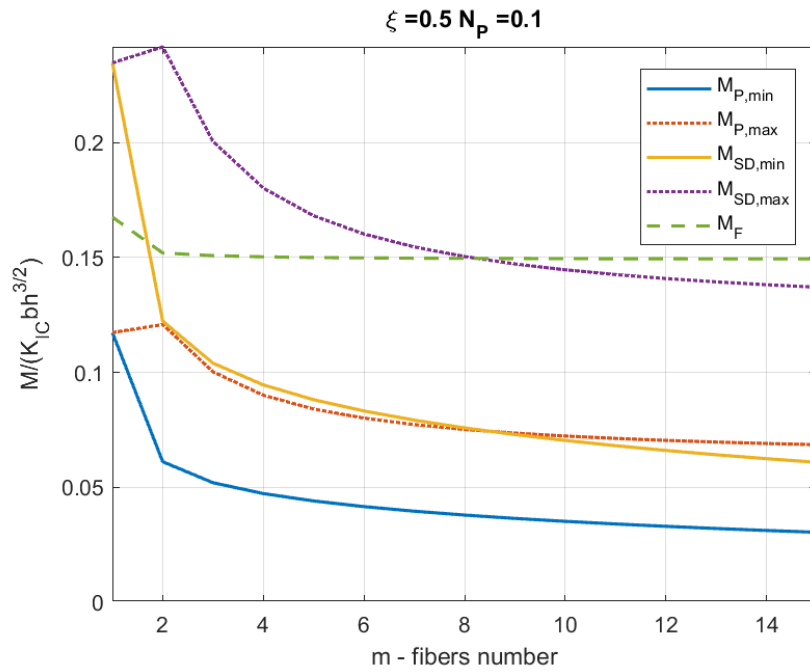


Figure 2.30: Plastic, shake-down and crack advancing moments at the variation of fiber number.

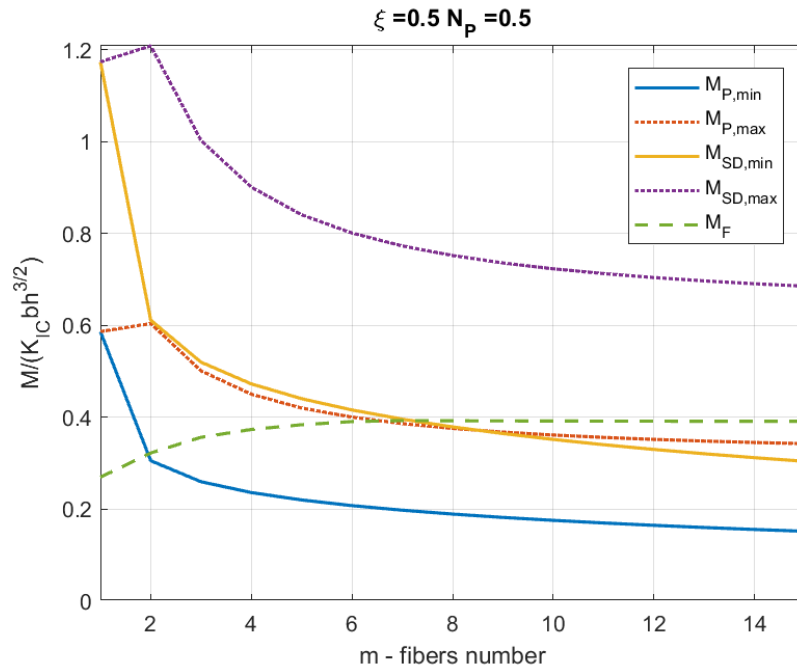


Figure 2.31: Plastic, shake-down and crack advancing moments at the variation of fiber number.

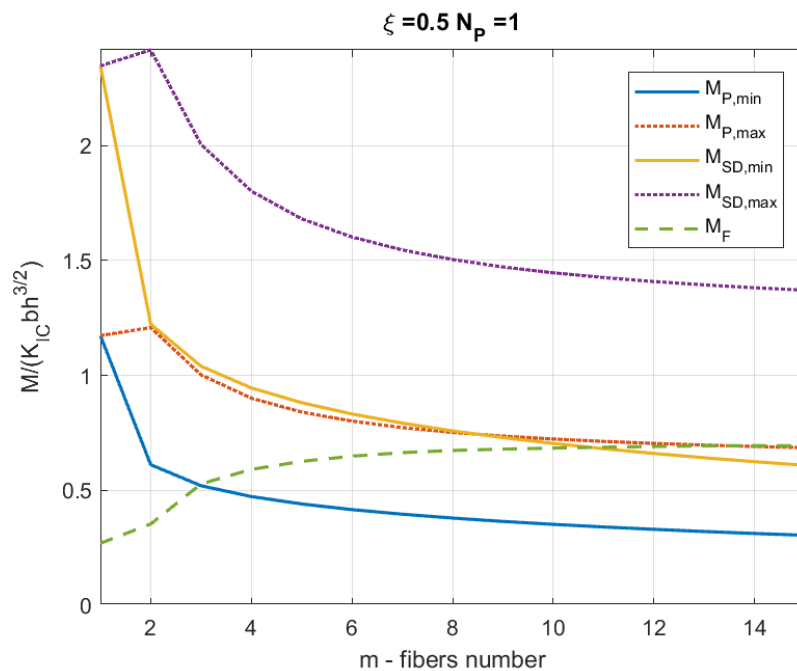


Figure 2.32: Plastic, shake-down and crack advancing moments at the variation of fiber number.

2.2.7 Case studies: loading control

An important difference between the two types of control is that the loading one is able to follow the response of the system up to large deformations only if it is characterized by a high value of N_p . In this case the ultimate bending moment is the highest load the system can bear. On the contrary for low value of N_p , when the highest peak is reached, it is not possible to increase the load anymore, because the ultimate bending moment is lower than the maximum one. This is related to the ductile to brittle transition described by N_p and to the different global behaviour of the

structure. The response is strain-hardening for high value of N_p , while it is strain-softening for low value of N_p as explained in [2.1.2].

If the rotation control is used instead, it is always possible to reach large deformations, because a load drop is allowed.

This means that it is more difficult to obtain a hysteretic cycle with the loading control algorithm, because for high value of N_p the shake-down moments are higher than the crack propagation one as remarked in [2.2.5].

In all the following moment-rotation diagrams the curve obtained with the loading or rotation control is always black and the one obtained with the crack length control scheme is red. In the points denoted by a blue circle a fiber reaches its tension or compression limit.

For example, a beam with ten equally spaced fibers is studied using the loading control. Its characteristics are summarized in Table 2.2. The mechanical properties correspond to those of a medium resistance concrete.

b	[cm]	25
h	[cm]	40
a/h		0,1
E	[GPa]	30
K_{IC}	[daN/cm ^{3/2}]	100
σ_y	[MPa]	450
m		10
ζ_{min}		0,1
ζ_{max}		0,5
r_i	[mm]	3,34
N_p		1,00

Table 2.2: Input data.

The loading history is described by the values in Table 2.3, that are referred to Figure 2.10.

M_{max}	[kNm]	42,00
M_{min}	[kNm]	0,00

Table 2.3: Loading input data.

The result in terms of moment-rotation response is showed in Figure 2.33. Nine snap-through instabilities occur before the load is inverted. If the load was further increased, a tenth snap-trough would appear. Only one shake-down moment is overcome and consequently only one fiber attains its compression limit giving rise to a hysteretic cycle. This is confirmed by Figure 2.34 in which the value of the reinforcement reactions normalized respect to their ultimate value are plotted against the normalized rotation. Only the first fiber ($\zeta = 0,1$) describes a cycle reaching its

compression limits, while the last fiber ($\zeta = 0,5$) does not plasticize even in tension and its maximum load is about $0,2 P_p$. The lower fibers ($\zeta \leq 0,28$) undergo a larger deformation in tension and so their reactions become negative after the load inversion, while the other fiber forces remain always positive. The jumps at constant load in the forces diagram correspond to each snap-through.

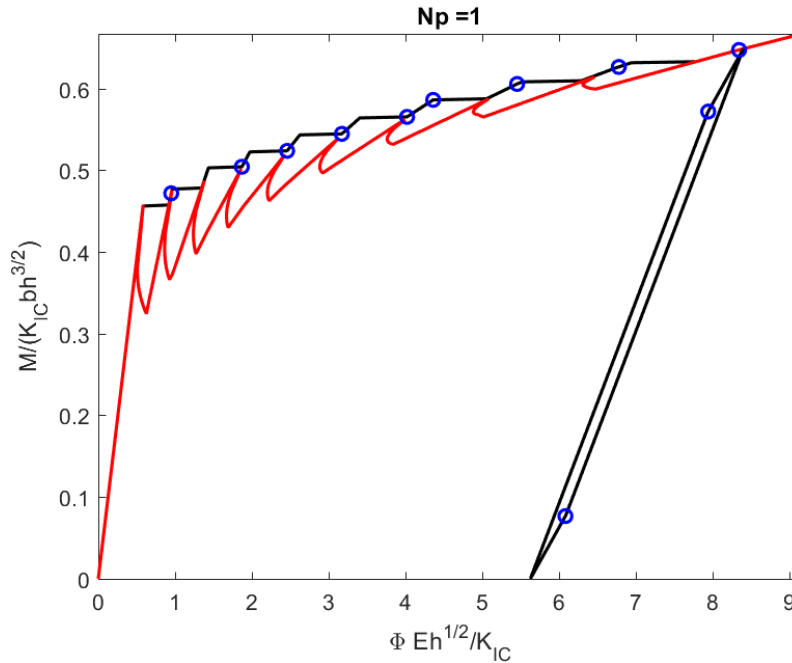


Figure 2.33: Moment-rotation diagram (loading control blue, crack length control scheme red).

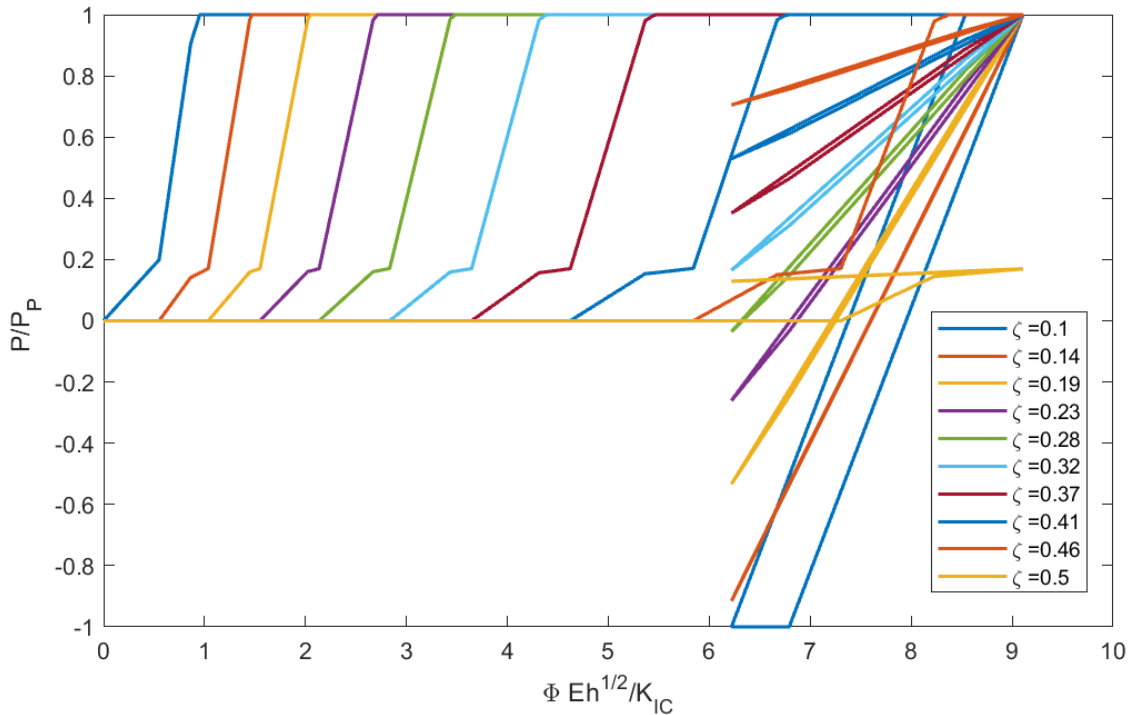


Figure 2.34: Fiber reactions

A negative minimum bending moment can be considered too. If the same system is reanalysed with the values in Table 2.4, a larger hysteretic cycle is obtained (Figure 2.35).

M_{max}	[kNm]	42,00
M_{min}	[kNm]	- 22,68

Table 2.4

In this case the minimum bending moment is about $M_{min} = -0,54M_{max}$ and this lets more fibers achieving their compression limit. As it can be deduced from Figure 2.36, only four fibers ($\zeta \geq 0,37$) do not attain their compression limit. It is possible to notice that the hysteretic cycle described by lower fibers is larger.

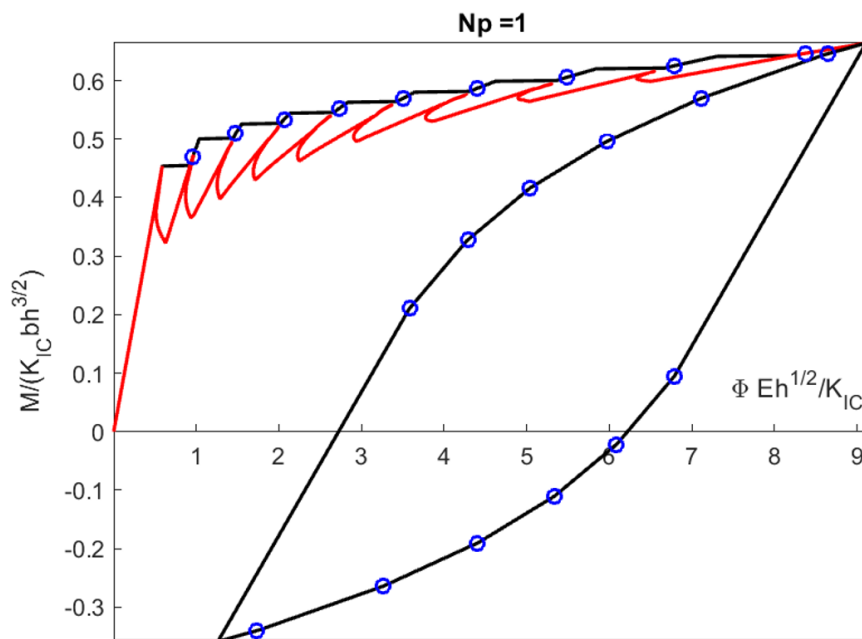


Figure 2.35: Moment-rotation diagram (loading control blue, crack length control scheme red).

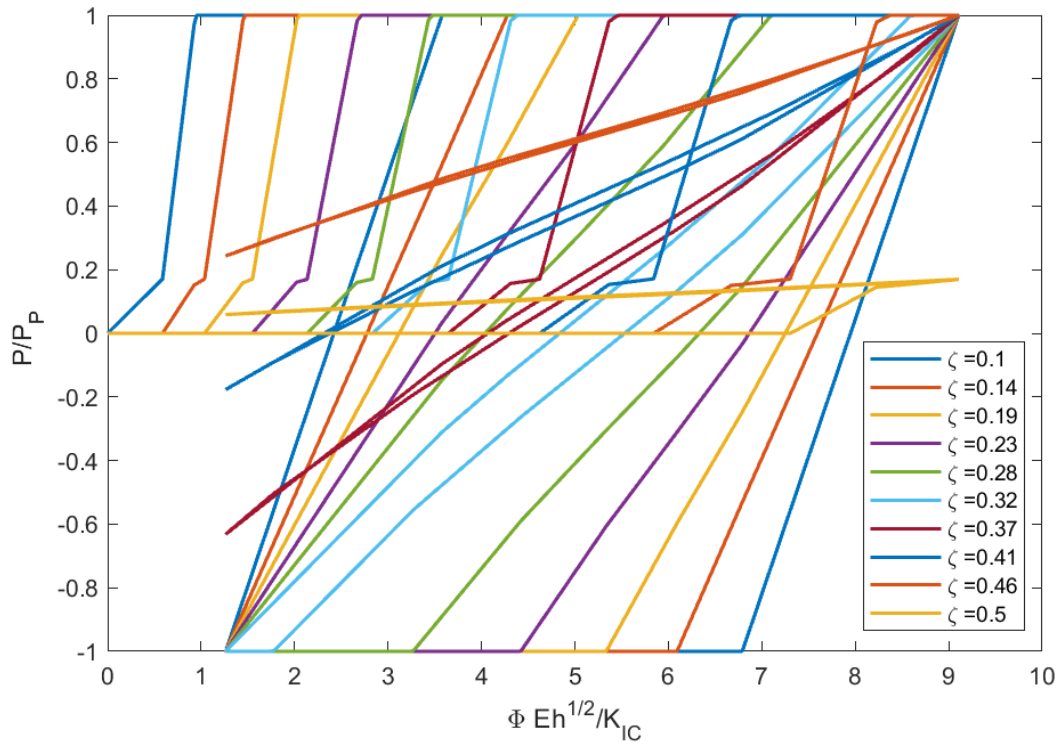


Figure 2.36: Fiber reactions

The minimum bending moment has been chosen in order to close completely the crack mouth, when this value is reached, and it is confirmed by the analysis of the crack opening profile (Figure 2.37, Figure 2.38, Figure 2.39 and Figure 2.40). In the loading phase the bridging action keeps the crack closed at the fiber level until the limit force is attained. As seen before the green fibers are in the elastic field, while the orange ones are plasticized. In the picture sequence the crack jumps to one fiber to another because of snap-throughs.

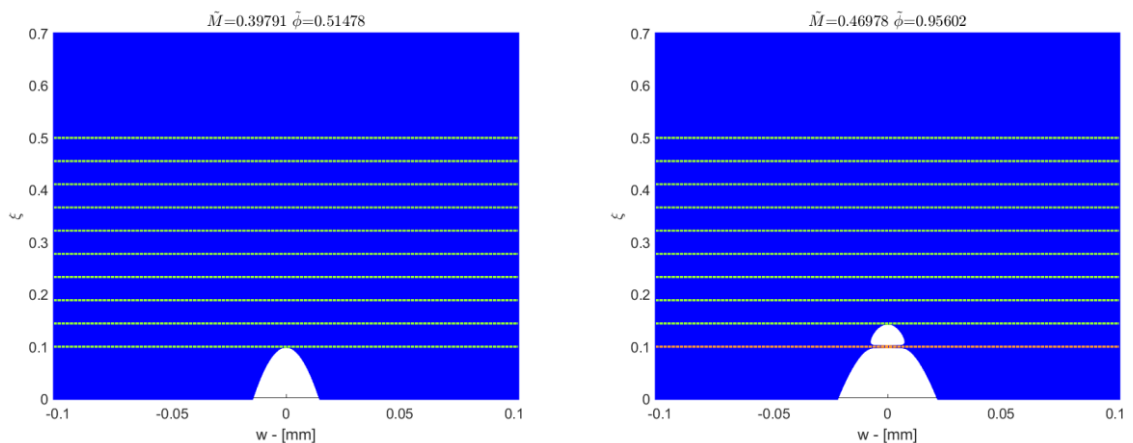


Figure 2.37: Crack propagation from the first to the second fiber.

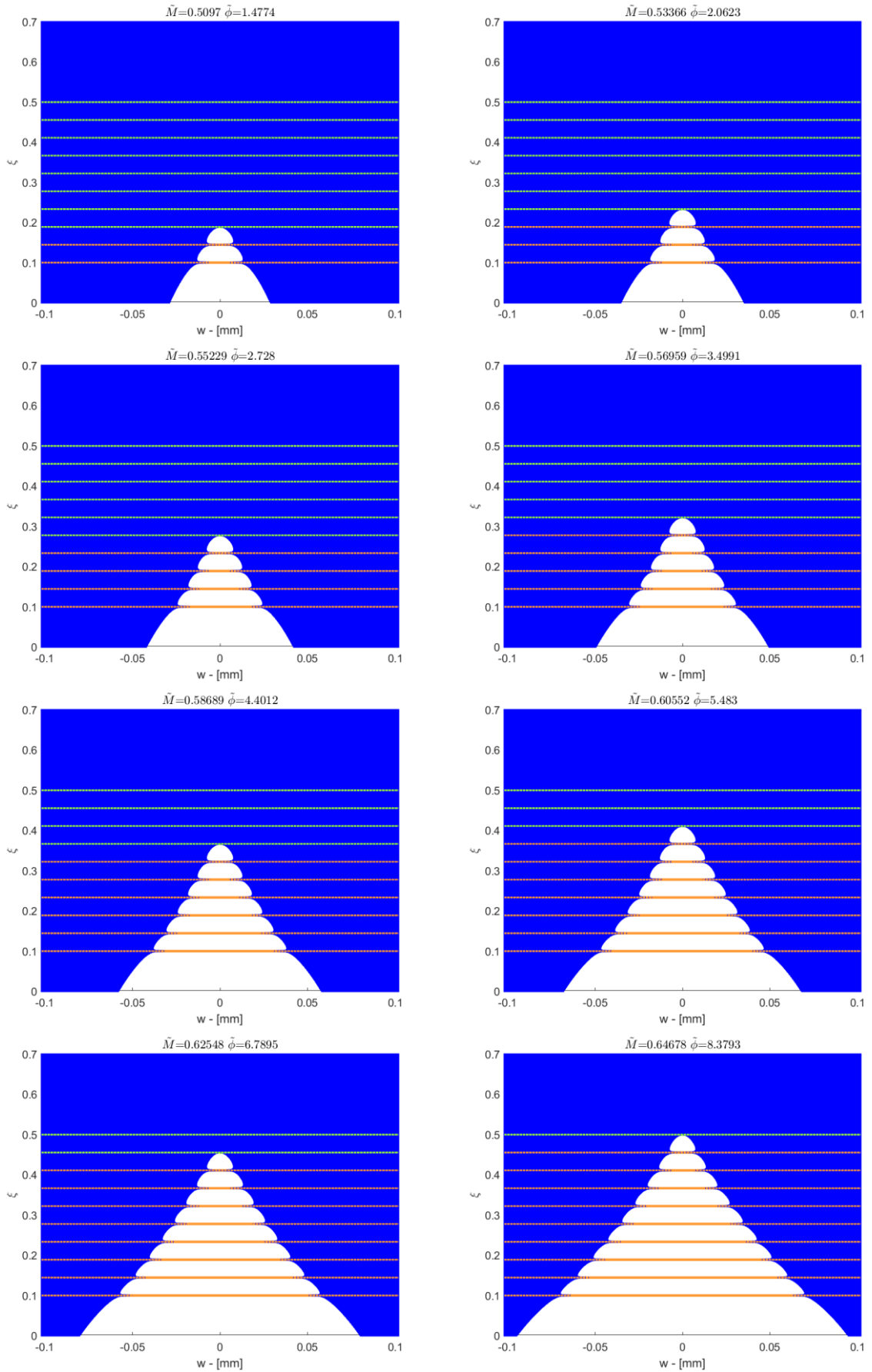


Figure 2.38: Crack propagation from the third to the tenth fiber.

At the beginning of the unloading phase all the fibers return in the elastic field because their reactions start decreasing. As a consequence of their rigid-perfectly plastic behaviour, they act as a strut and they keep the crack opened at their level. At a certain point the reactions become negative and eventually the compression limit is attained. When this condition is reached, the displacements start decreasing. At the end the crack mouth is closed, but the crack inside the beam is still opened. It is not possible to decrease the load any more, because overlapping arises. This problem is discussed in [2.2.11].

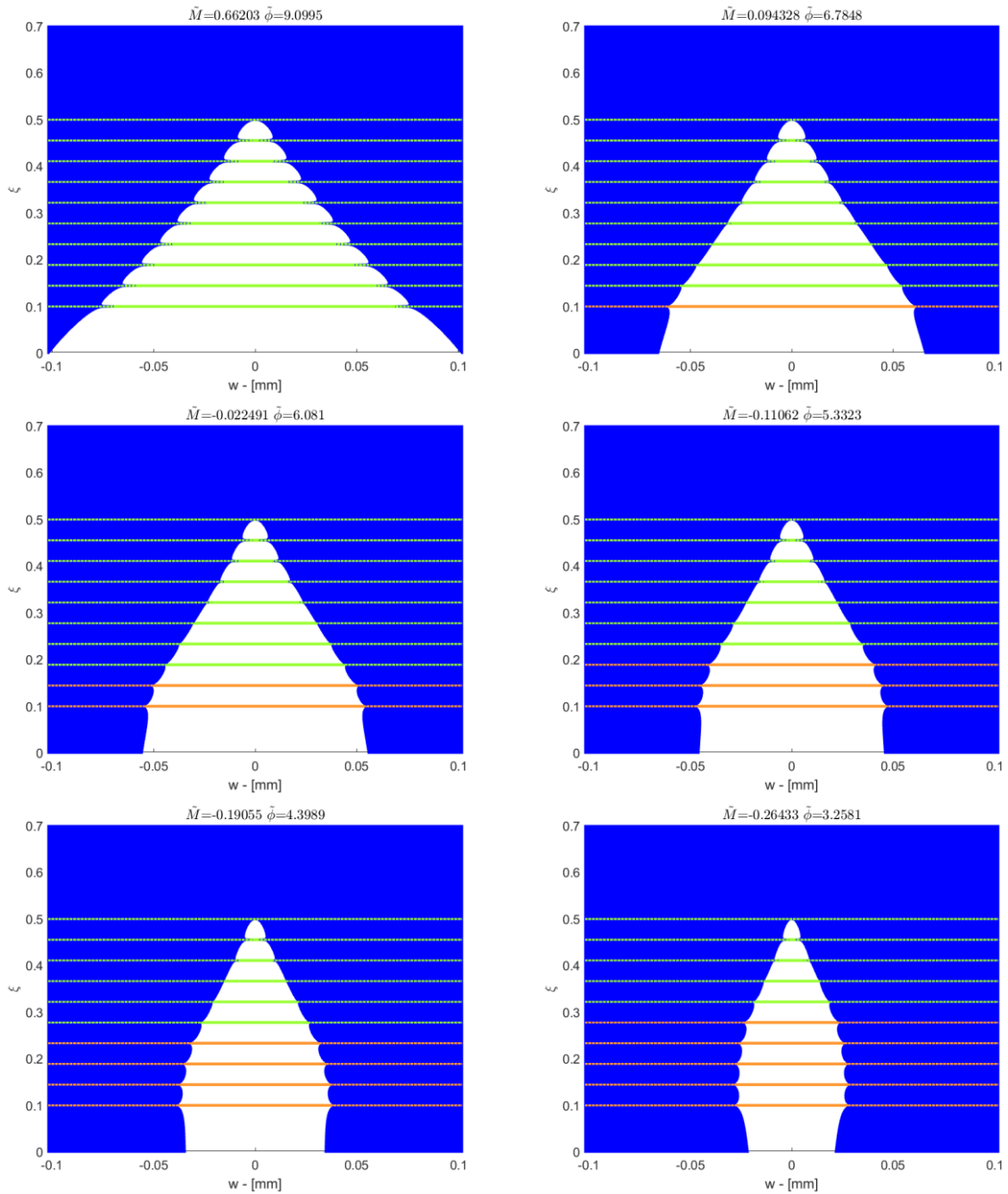


Figure 2.39: Crack closing up to $\tilde{M} = -0,26433$.

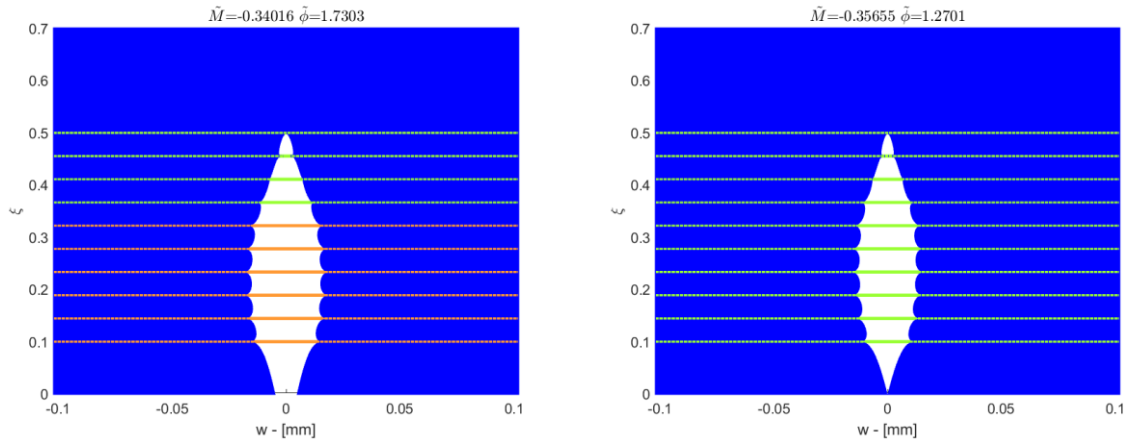


Figure 2.40: Crack closing up to $\tilde{M} = -0,35655$.

Now a beam with twenty equally spaced fibers is studied using the loading control again. Its characteristics are summarized in Table 2.5.

b	[cm]	25
h	[cm]	40
a/h		0,1
E	[GPa]	30
K_{IC}	[daN/cm ^{3/2}]	100
σ_y	[MPa]	450
m		20
ζ_{min}		0,1
ζ_{max}		0,5
r_i	[mm]	2,99
N_p		1,60

Table 2.5: Input data

The loading history is described by the values in Table 2.6, that are referred to Figure 2.10.

M_{max}	[kNm]	62,00
M_{min}	[kNm]	0,00

Table 2.6: Loading input data

The moment-rotation diagram (Figure 2.41) is characterized by many small snap-throughs and the overcoming of the shake-down moments of three fibers gives rise to a hysteretic cycle. Even if the reinforcement number is not so elevated, the response of the system tends already to a continuous one.

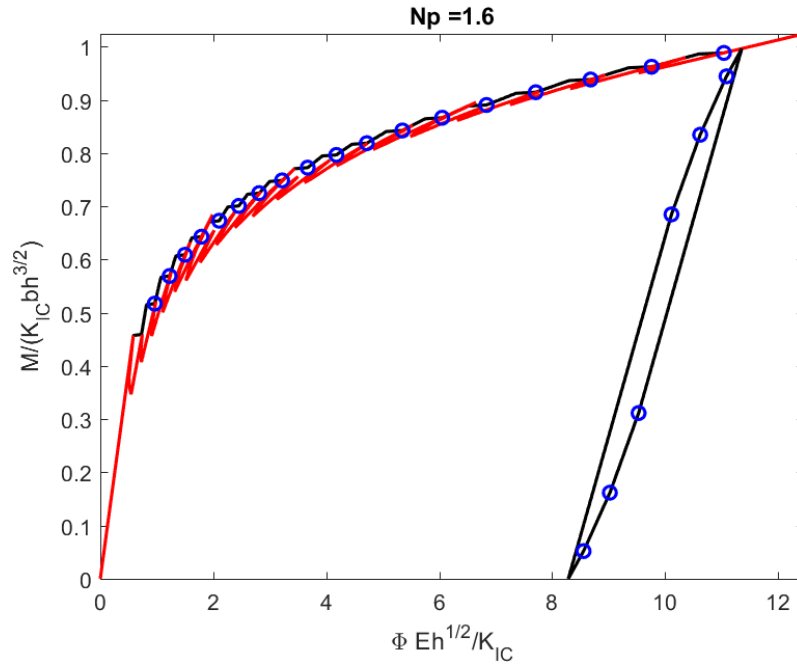


Figure 2.41: Moment-rotation diagram (loading control blue, crack length control scheme red).

2.2.8 Case studies: rotation control

In the following examples the rotation control will be used instead of the loading one.

A beam with three equally spaced fibers is analysed using the rotation control. Its characteristics are summarized in Table 2.7.

b	[cm]	25
h	[cm]	40
a/h		0,1
E	[GPa]	30
K_{IC}	[daN/cm ^{3/2}]	100
σ_y	[MPa]	450
m		20
ζ_{min}		0,1
ζ_{max}		0,5
r_i	[mm]	2,99
N_p		1,60

Table 2.7: Input data.

The maximum and minimum angle values are given in Table 2.8, that is referred to Figure 2.10.

ϕ_{max}	[rad]	0,00045
ϕ_{min}	[rad]	0,00012

Table 2.8: Rotation input data.

The moment rotation diagram is showed in Figure 2.42, where three snap-backs are visible. All the fibers overcome their shake-down moment attaining their compression limit in the unloading phase and giving rise to a hysteric cycle.

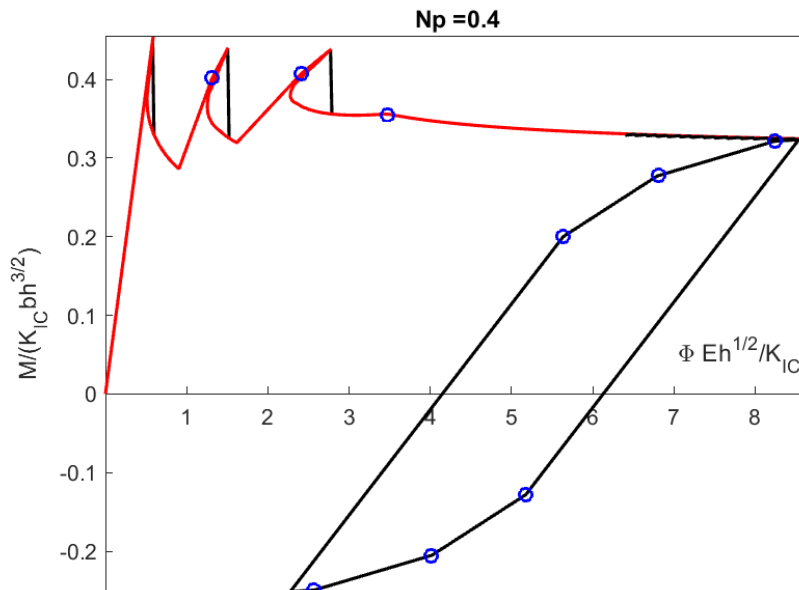


Figure 2.42: Moment-rotation diagram (rotation control blue, crack length control scheme red).

In Figure 2.43 the hysteric cycles described by the values of the reactions are visible. The one related to the lower fiber is larger.

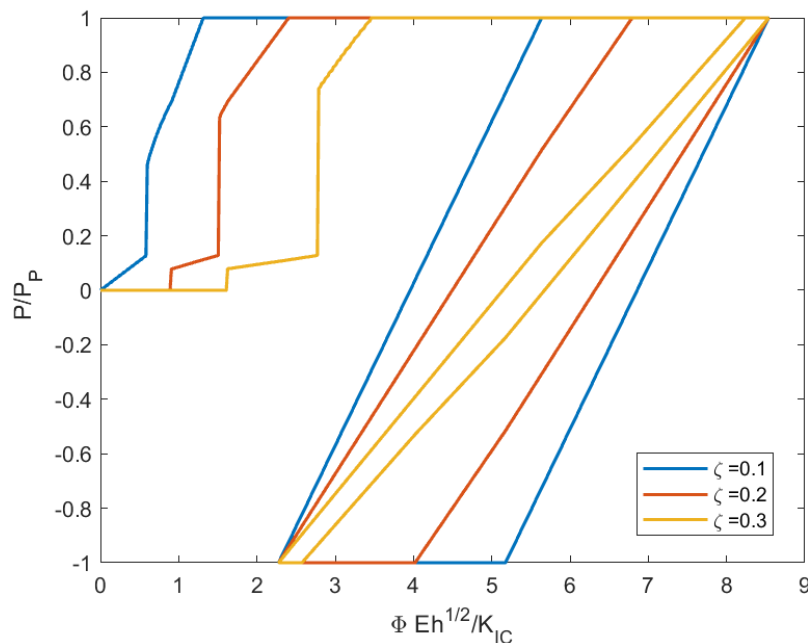


Figure 2.43: Fiber reactions

The crack openings profile is studied both in the loading and unloading phase (Figure 2.44 and Figure 2.45). The same remarks about the fiber behaviour are possible, but in this case the crack does not propagate to one fiber to another thanks to the rotation control.

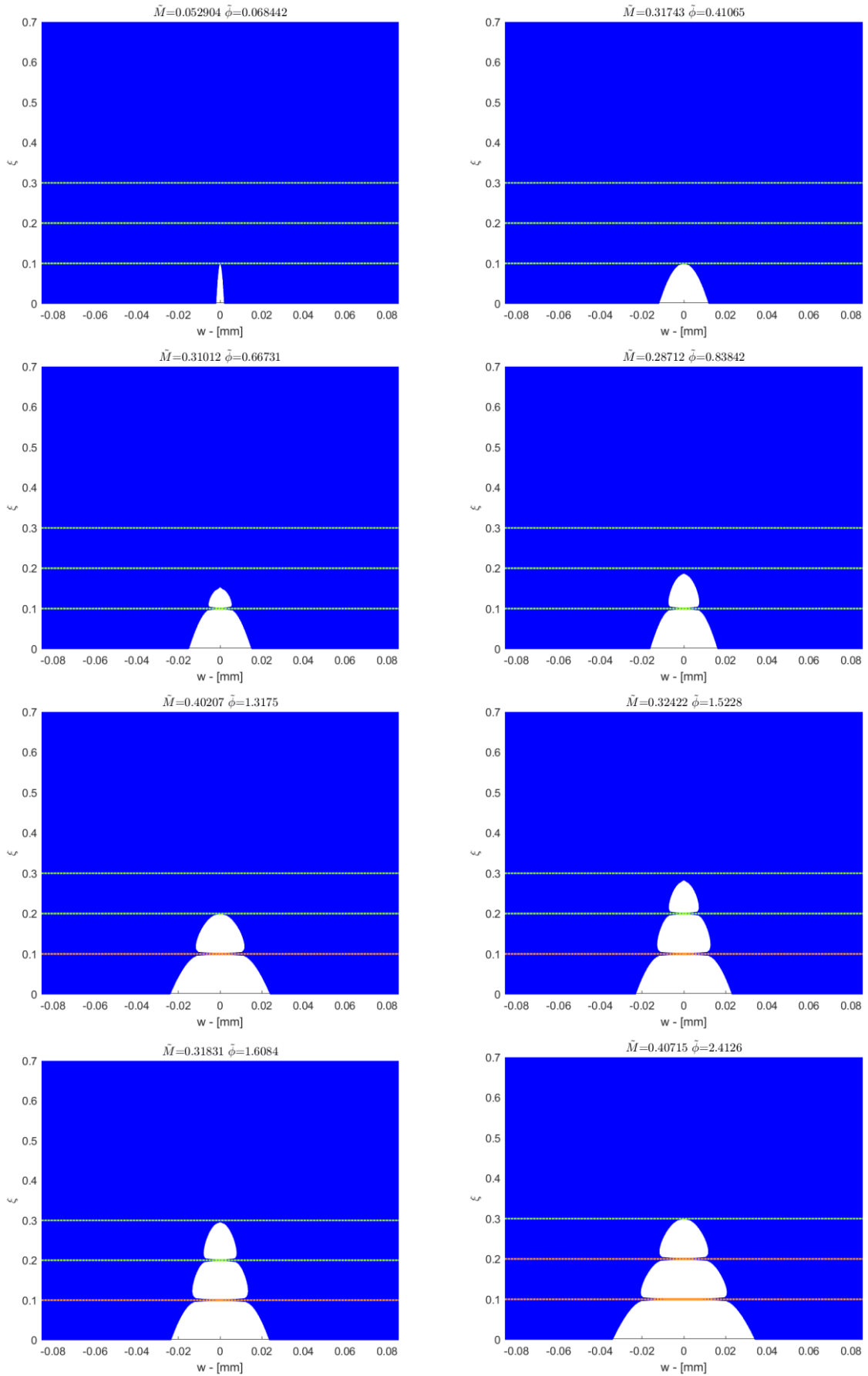


Figure 2.44: Crack profile from $\bar{\phi} = 0,068442$ to $\bar{\phi} = 2,4126$ (opening).

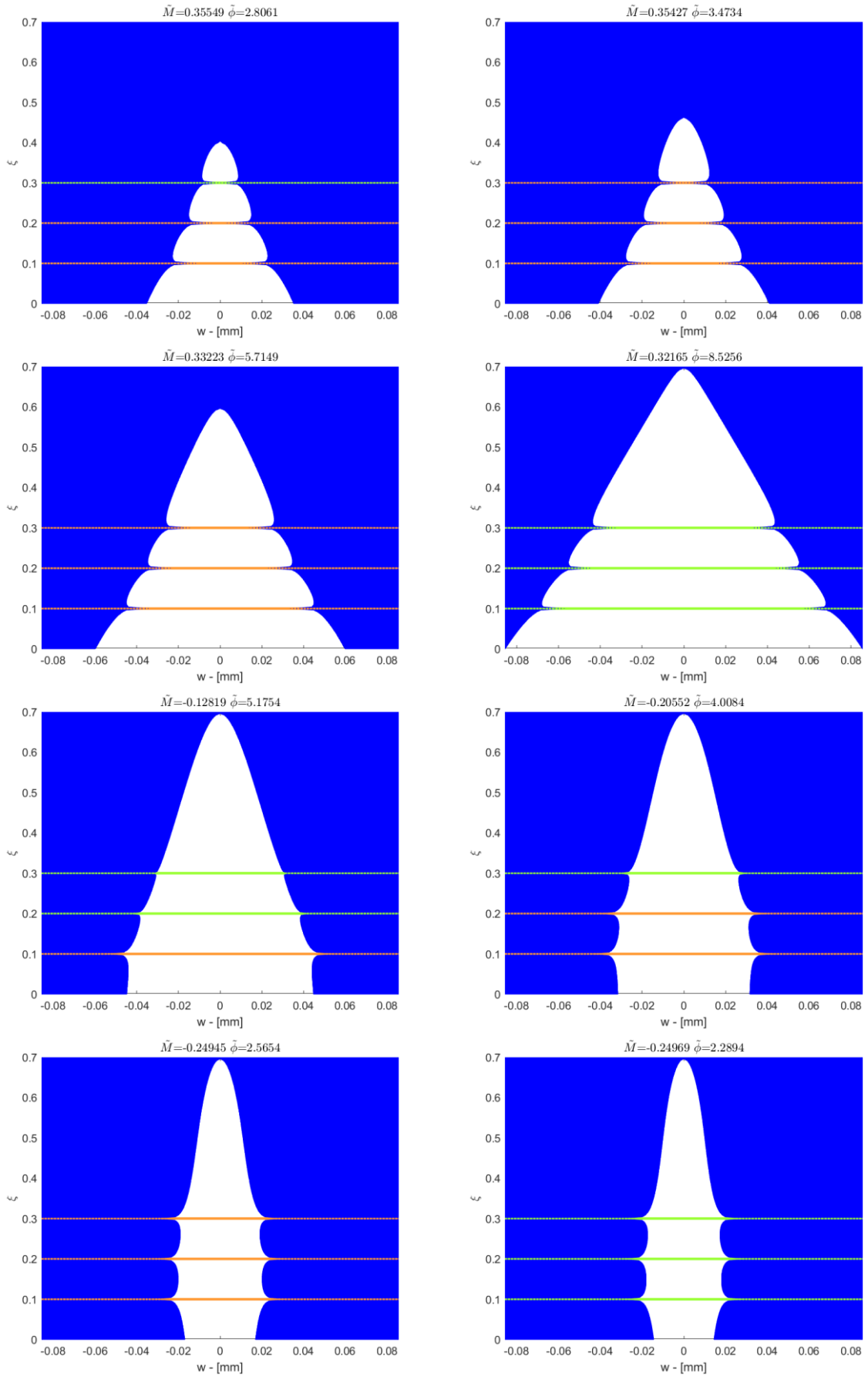


Figure 2.45: Crack profile from $\tilde{\phi} = 1, 3175$ to $\tilde{\phi} = 8, 5256$ (opening) and from $\tilde{\phi} = 5, 1754$ to $\tilde{\phi} = 2, 2894$ (closing).

2.2.9 Scale effects

If the brittleness number and the fiber number are varied, a scale effect arises. The following examples are used in order to explain this problem.

A beam with three equally spaced fibers is analysed with different percentages of reinforcement and consequently different brittleness numbers. The characteristics are illustrated in Table 2.9 and in Table 2.10 for the three cases.

b	[cm]	25
h	[cm]	40
a/h		0,1
E	[GPa]	30
K_{IC}	[daN/cm ^{3/2}]	100
σ_y	[MPa]	450
m		3
ζ_{min}		0,1
ζ_{max}		0,3

Table 2.9: Input data.

		Case - 1	Case - 2	Case - 3
r_i	[mm]	3,86	5,11	6,11
N_p		0,40	0,70	1,00

Table 2.10: Brittleness number.

The rotation angle history is described by the values in Table 2.11, that are referred to Figure 2.11. They are the same for all the cases.

ϕ_{max}	[rad]	0,00045
ϕ_{min}	[rad]	0,00000

Table 2.11: Rotation input data.

The moment-rotation responses of the three cases are displayed in Figure 2.46, Figure 2.47 and Figure 2.48. Each one is characterized by three snap-backs.

The first case shows a global strain-softening behaviour. As previously remarked in [2.2.6] a low brittleness number produces low plastic and shake-down moments. Consequently the hysteretic cycle area is large.

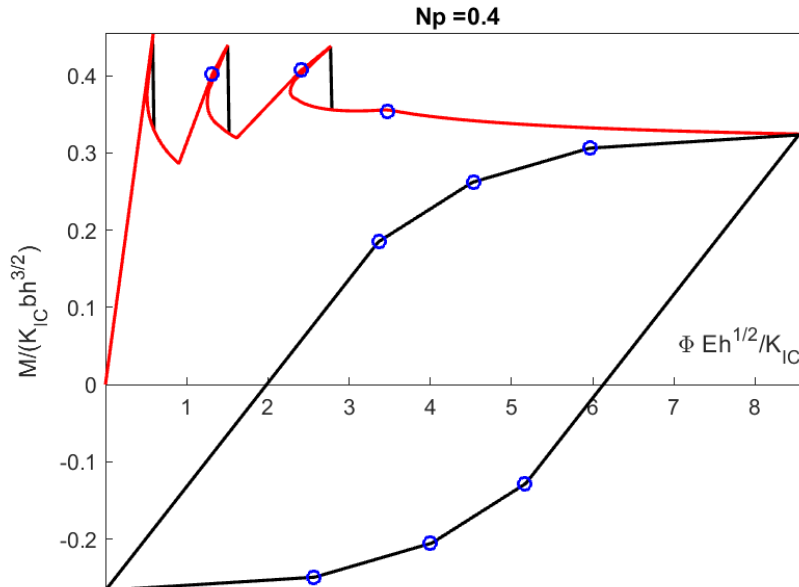


Figure 2.46: Moment-rotation diagram (rotation control blue, crack length control scheme red).

The value $N_p = 0,7$ divides the two possible behaviours of the system (strain-softening and strain-hardening). In this case the area of the cycle is reduced if compared to the previous one and the plastic moments are higher (blue circle) and they appear only after the three snap-backs.

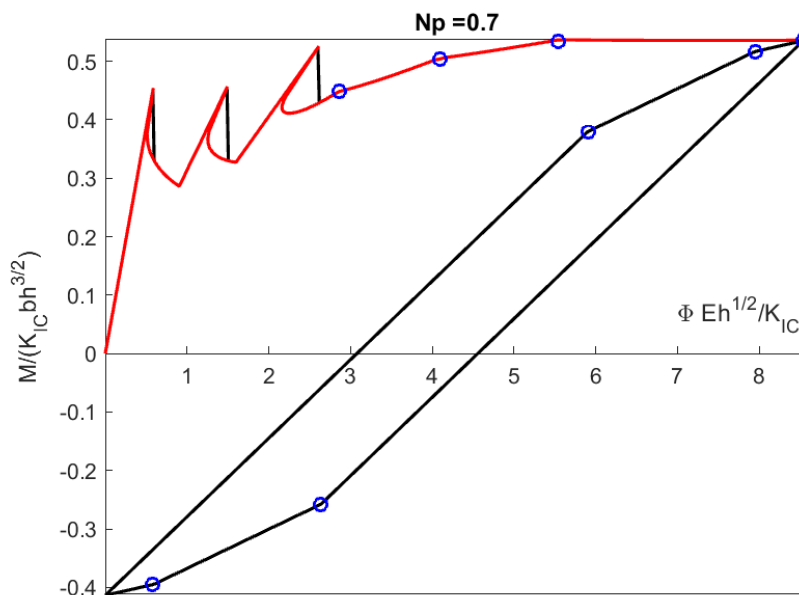


Figure 2.47: Moment-rotation diagram (rotation control blue, crack length control scheme red).

In the last case the behaviour is strain-hardening and the high brittleness number makes the hysteretic cycle almost vanish.

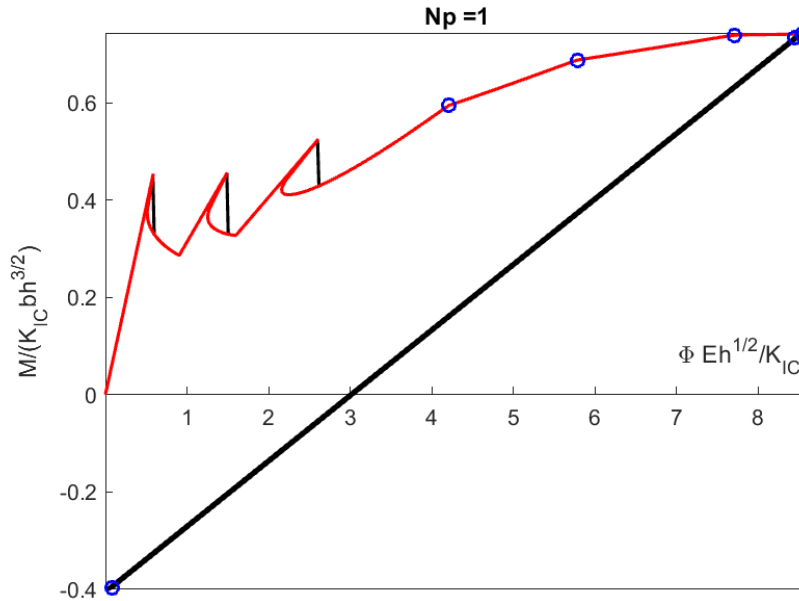


Figure 2.48: Moment-rotation diagram (rotation control blue, crack length control scheme red).

The comparison between the three hysteretic cycles in Figure 2.49 confirms the area reduction. The values are given in Table 2.12.

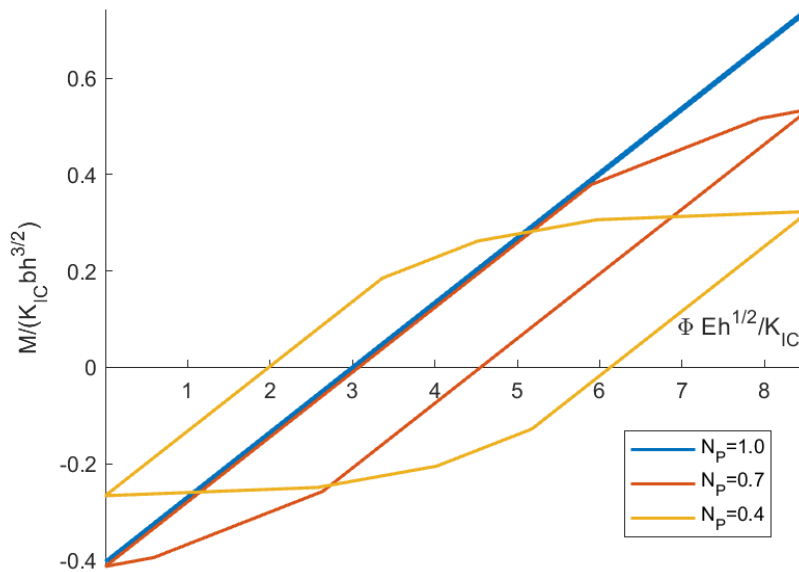


Figure 2.49: Hysteretic cycles comparison.

		Case - 1	Case - 2	Case - 3
N_p		0,40	0,70	1,00
Area	[daN cm rad]	73,32	40,50	1,76

Table 2.12: Cycles area.

In a similar way a beam with ten equally spaced fibers is analysed with the same previous percentages of reinforcement. The characteristics are illustrated in Table 2.13 and in Table 2.14 for the three cases.

b	[cm]	25
h	[cm]	40

a/h		0,1
E	[GPa]	30
K_{IC}	[daN/cm ^{3/2}]	100
σ_y	[MPa]	450
m		10
ζ_{min}		0,1
ζ_{max}		0,5

Table 2.13: Input data.

		Case -1	Case - 2	Case - 3
r_i	[mm]	2,12	2,80	3,34
N_p		0,40	0,70	1,00

Table 2.14: Brittleness number.

The rotation angle history is described by the values in Table 2.11, that are referred to Figure 2.11. They are the same for all the cases.

ϕ_{max}	[rad]	0,00035
ϕ_{min}	[rad]	0,00000

Table 2.15: Rotation input data.

The moment-rotation responses of the three cases are displayed in Figure 2.50, Figure 2.51 and Figure 2.52.

In the first case nine snap-backs are visible. The tenth would appear only for larger deformation. Eight fibers reach their compression limit and this produces a large hysteretic cycle. Again for low N_p values the behaviour is strain-softening.

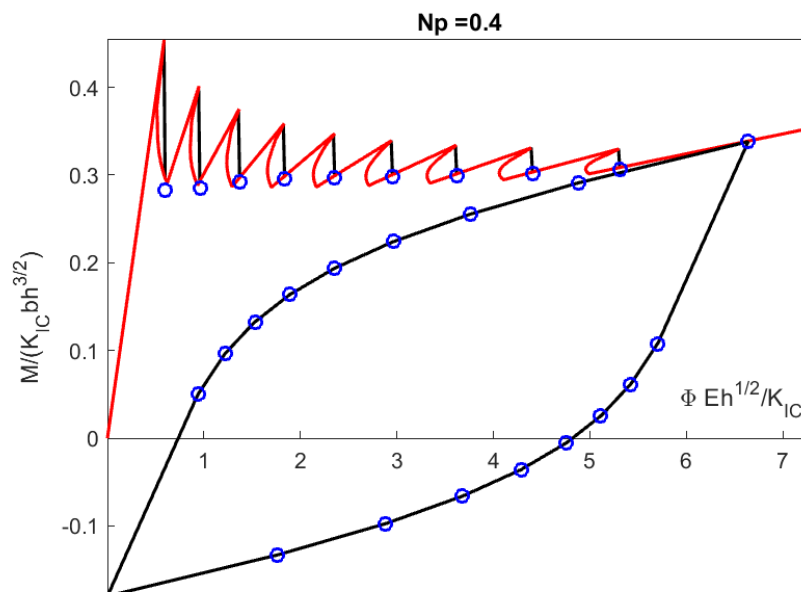


Figure 2.50: Moment-rotation diagram (rotation control blue, crack length control scheme red).

The second case is characterized by only seven fibers attaining their compression limit. This is due to the shake-down moments that are higher than before.

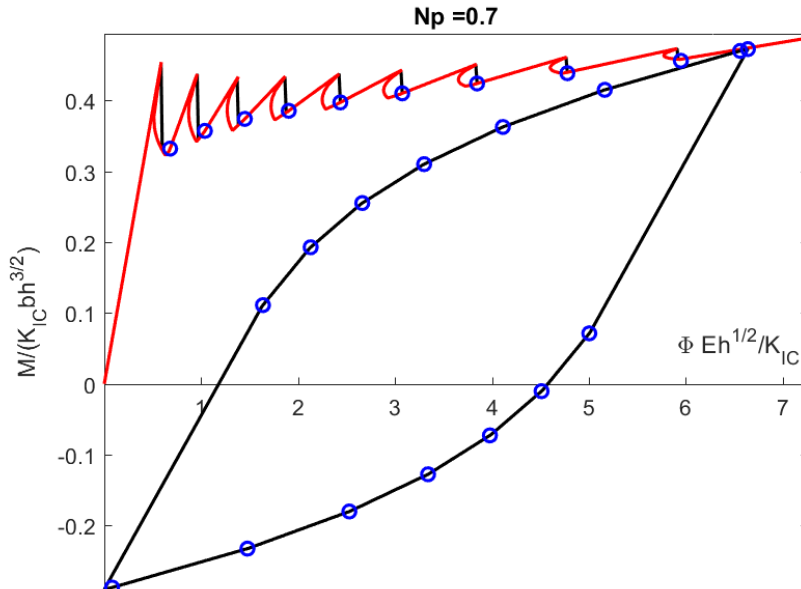


Figure 2.51: Moment-rotation diagram (rotation control blue, crack length control scheme red).

Increasing N_p only five fibers achieve their compression limit.

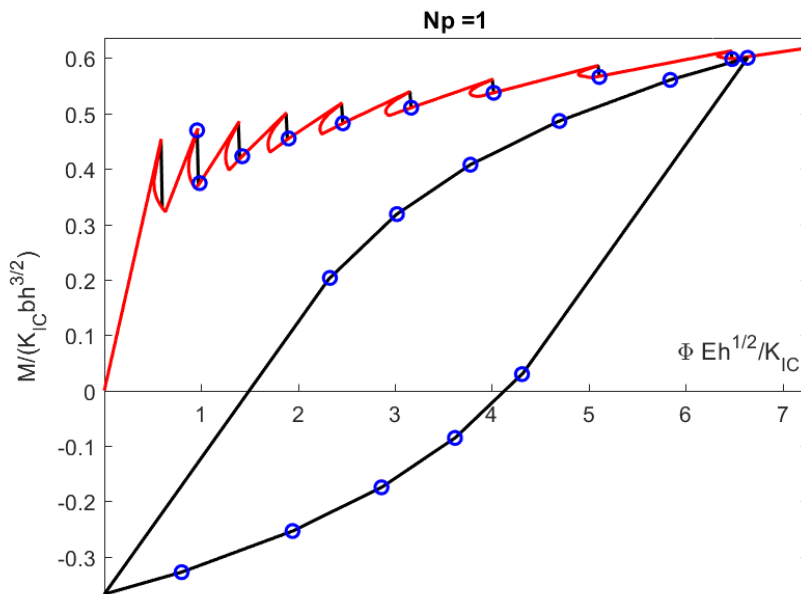


Figure 2.52: Moment-rotation diagram (rotation control blue, crack length control scheme red).

With ten fibers the dimension of the hysteretic cycle increases as the brittleness number rises. This is related to the higher number of reinforcements, as remarked in [2.2.6]. The comparison between the three cases is shown in Figure 2.53 and the values are given in Table 2.16. Anyway the cycle area difference between the three brittleness numbers is much smaller if it is compared to the case with three fibers.

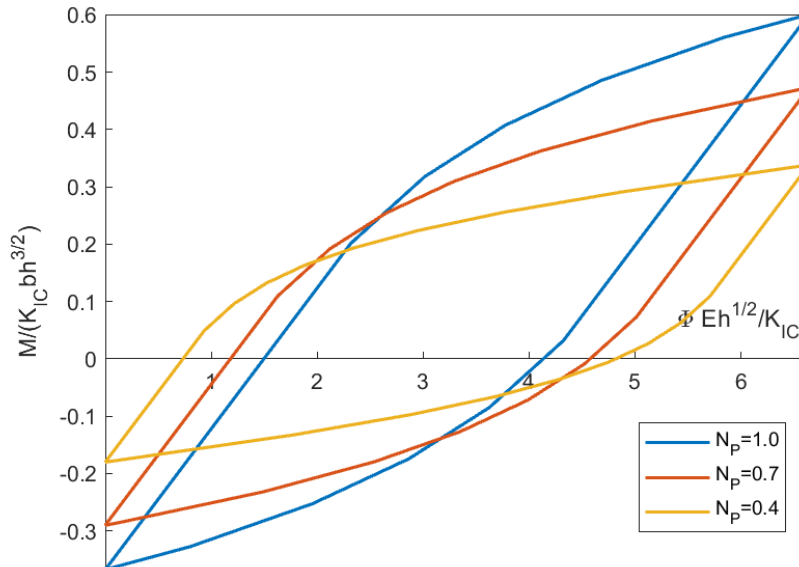


Figure 2.53: Hysteretic cycles comparison.

		Case - 1	Case - 2	Case - 3
N_p		0,40	0,70	1,00
Area	[daN cm rad]	52,36	64,06	64,37

Table 2.16: Cycles area.

It is necessary to remark that the first peak is always at the same level in each case because all the fiber are still in the elastic field. As the fibers yield, the behaviour starts changing, because the maximum attainable load in the reinforcements is different for each N_p value.

2.2.10 Numerical errors

The issues related to the distance between the crack tip and the closest fiber, described in [2.1.3] for the crack length control scheme, are still present in the loading and deformation controlled algorithms with the same effect.

In this case it is necessary to analyse the effect of the number of values used for describing the loading or rotation angle history. Again, if there is a lack of divisions, the shape of the peaks due to the fiber bridging actions is lost, but the influence on the shape of the hysteretic cycle must be checked too. The two algorithms do not compute plastic moments as reported in [1.3.7], but the plasticization is detected from the values of the reinforcement reactions. So, a possible difference can be found comparing the results of these two algorithms with the exact values of the plastic moments calculated with Eq.(1.50) and (1.55). This has been performed considering a beam with 20 fibers and using a high fracture toughness to avoid crack propagation. The results are showed in Figure 2.54: the black line is obtained with the exact values of the plastic moments, while the blue one is drawn with the loading controlled algorithm using 10 points to describe each loading or unloading segment. If the first loading branch is considered, it is possible to notice that the blue curve is unable to describe the right behaviour especially where the change in the slope is more marked. If the attention is focused on the hysteretic cycle, the one described by

the blue curve is inside the one described by the black curve. This leads to an underestimation of the dissipated energy, that is proportional to the cycle area. It is necessary to underline that this problem arises only if a high number of fibers is considered and at the same time the number of divisions is extremely low. If the rotation controlled algorithm is taken into account instead on the loading controlled one, the same result is attained.

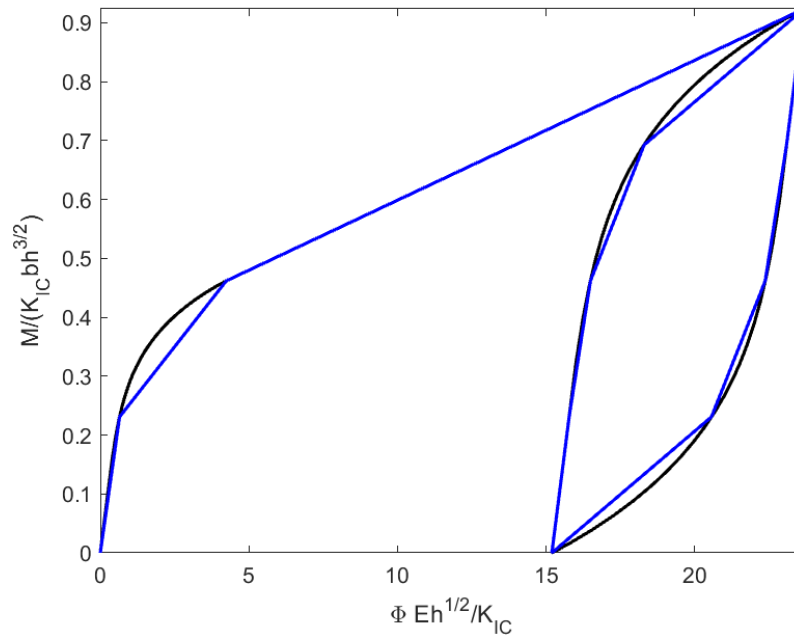


Figure 2.54: Influence of the number of points.

In all the case studies a number of division between 300 and 500 for each loading or unloading branch has been usually chosen without affecting the computation time. The same is valid for the rotations too.

Another issue is related to the crack advancing. When for a certain value of bending moment or rotation the cracking moment is lower than the applied moment, the crack length is increased of a quantity fixed in advance. This procedure is not completely correct because the new crack length should be calculated by equating the applied moment (or the moment as a function of the rotation) to the expression of the crack advancing moment. In other words, a new unknown (ξ) is added to the system, but at the same time a new equation ($M = M_F$) is added. If the value of ξ is fixed in advance, the solution is not the exact one, but in this way it is possible to avoid the calculation of ξ , that leads to a nonlinear procedure affecting too much the computation time. To check the influence of this problem it is possible to compare the curve obtained with the crack length control and the one given by the other two algorithms. The first represents the exact solution because in this case the crack depth is known. As it is possible to see in Figure 2.55, this issue causes some load drops in the softening branches. However, the overall behaviour tends to the correct one, especially if the $\Delta\xi$ value is small enough.

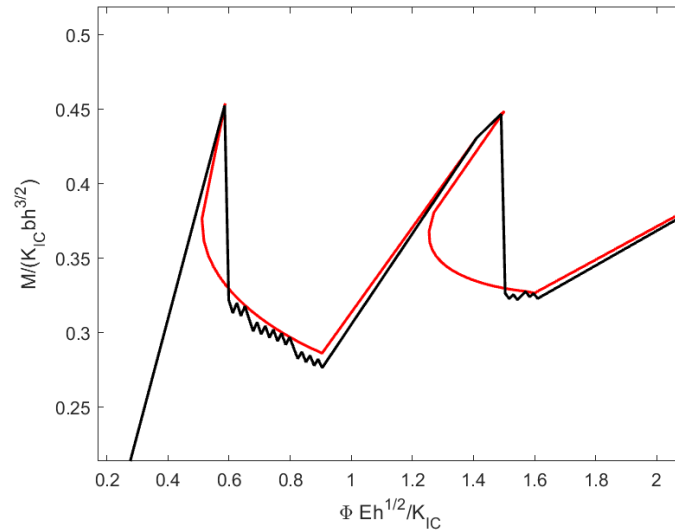


Figure 2.55: Effect of the crack advancing method (zoom on the softening branches).

2.2.11 Future developments

The proposed model does not take into account the admissible maximum stresses of the matrix both in tension and compression.

When the applied bending moment becomes negative, tension stresses arise at the top of the beam and they should be checked. They should be lower than the tension limit.

On the contrary, when the applied bending moment is positive, a compression stress is present at the top of the beam and the possibility of a collapse due to a crushing of the matrix should be considered. In this case overlapping model (Carpinteri, Corrado, Paggi, Mancini, 2009) can be applied.

Another issue related to the negative load values is the possible material interpenetration, that could occur during the crack closing. That can be avoided introducing a unilateral constraint along the crack faces when they come into contact or considering the overlapping model again.

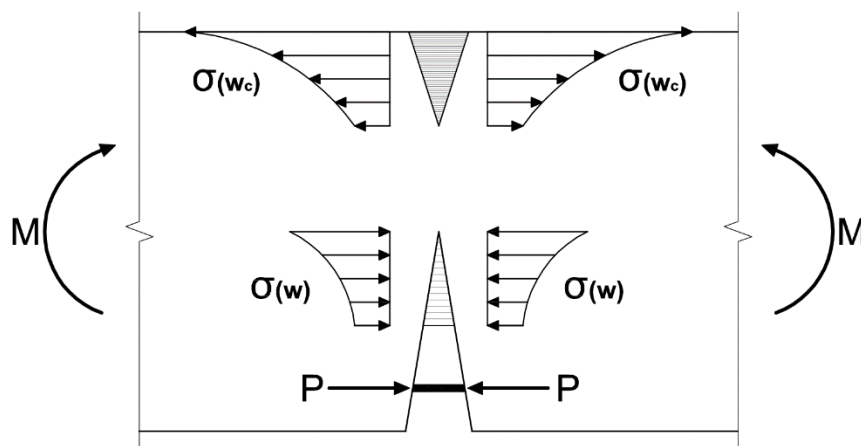


Figure 2.56: Positive bending moment

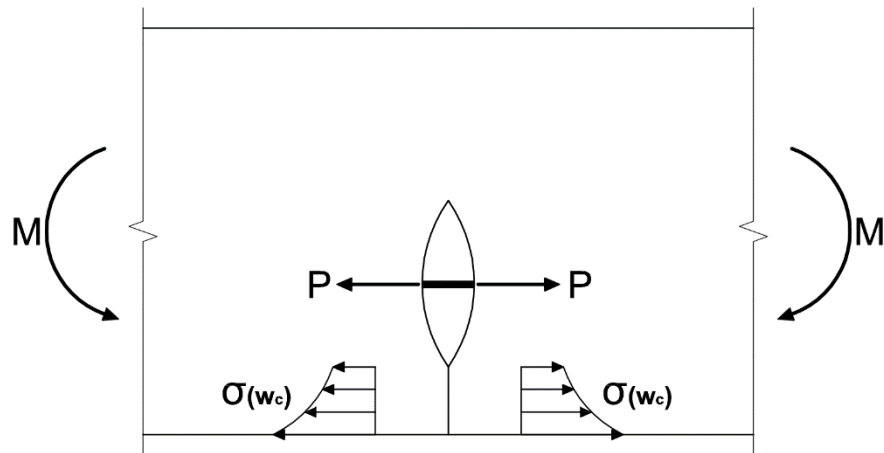


Figure 2.57: Negative bending moment

Figure 2.56 and Figure 2.57 summarize these issues. Also a cohesive option could be introduced to simulate a continuous bridging action.

After the first unloading-reloading cycle the structure continues to go along the same branch or hysteretic cycle if this process is repeated. For high number of cycle the problem of fatigue arises and this should be taken into account considering subcritical crack advancing. This should be done using Paris law. Furthermore, the degradation of the fiber properties could be modelled according to Woehler Theory.

Conclusion

The behaviour of fiber reinforced materials has been analysed using the Bridged Crack model. It respects both compatibility and equilibrium equations and it has been adapted to the case of cyclic loading too. The fracture propagation has been taken into account with reference to linear elastic fracture mechanics. Three different numerical algorithms, based on this theoretical approach, have been developed in order to study the response of these materials. They are based on three different driving parameters: crack length, applied bending moment and rotation. The system response has been studied especially regarding the problem of cyclic loading, shake-down and hysteresis. The influence of brittleness number, crack length, and fiber number has been illustrated, checking the variation of the hysteretic cycle area, that is proportional to the dissipated energy. The response of the system is shown in terms of moment-rotation diagram and the crack propagation has been studied considering its opening profile at different stages. In this way it has been possible to underline the snap-back and snap-through instabilities. The issues deriving from the numerical procedure have been discussed. Eventually some future developments have been addressed regarding matrix strength and fatigue problem.

References

- Agrawal, G.L., Tulin, L.G., Gerstle, K.H. (1965) "Response of Doubly Reinforced Concrete Beams to Cyclic Loading", *ACI Journal*, 62: 823-834.
- Ballarini, R., Muju, S. (1991) "Stability Analysis of Bridged Cracks in Brittle Matrix Composites", *ASME Paper*, 91-GT-094.
- Ballarini, R., Shah, S. P., and Keer, L. M. (1984) "Crack Growth in Cement Based Composites", *Engineering Fracture Mechanics*, 20: 433-445.
- Barenblatt, G. I. (1962) "The Mathematical Theory of Equilibrium Cracks in Brittle Fracture", *Adv. Appl. Mech.*, 7: 55-129.
- Bosco, C., Carpinteri, A. (1992) "Fracture behavior of beam cracked across reinforcement", *Theoretical and Applied Fracture Mechanics*, 17:61-68.
- Bosco, C., Carpinteri, A. (1995) "Discontinuous constitutive response of brittle matrix fibrous composites", *Journal of the Mechanics and Physics of Solids*, 43:261-274
- Bosco, C., Carpinteri, A., Debernardi, P.G. (1990a) "Fracture of reinforced concrete: Scale effects and snap-back instability", *Engineering Fracture Mechanics*, 35:665-677.
- Bosco, C., Carpinteri, A., Debernardi, P.G. (1990b) "Minimum reinforcement in high strength concrete", *Journal of Structural Engineering (ASCE)*, 116:427-437.
- Budiansky, B., Hutchinson, J. W., Evans, A. G. (1986) "Matrix Fracture in Fiber-Reinforced Ceramics", *J. Mech. Phys. Solids*, 34: 167-189.
- Cachim, P.B., Figueiras, J.A., Pereira, P.A.A. (2002) "Numerical modelling of fibre-reinforced concrete fatigue in bending", *International Journal of Fatigue*, 24: 381-387
- Carpinteri, A. (1981) "A fracture mechanics model for reinforced concrete collapse", *Proceedings of the I.A.B.S.E. Colloquium on Advanced Mechanics of reinforced Concrete*, Delft, pp. 17-30
- Carpinteri, A. (1984a) "Interpretation of the Griffith instability as a bifurcation of the global equilibrium", *Proceedings of the N.A.T.O. Advanced Research Workshop an Application of Fracture Mechanics to Cementitious Composites*, 287-316.
- Carpinteri, A. (1984b) "Stability of fracturing process in RC beams", *Journal of Structural Engineering (ASCE)*, 110: 544-558.
- Carpinteri, A. (1986) "Mechanical Damage and Crack Growth in Concrete: Plastic Collapse to Brittle Fracture", *Martinus Nijhoff*, Dordrecht.

- Carpinteri, A. (1988) "Snap-back and hyperstrength in lightly reinforced concrete beams", *Magazine of Concrete Research*, 40:209-215.
- Carpinteri, A. (1989a) "Post-peak and post-bifurcation analysis of cohesive crack propagation", *Engineering Fracture Mechanics*, 32:265-278.
- Carpinteri, A. (1989b) "Cusp catastrophe interpretation of fracture instability", *Journal of the Mechanics and Physics of Solids*, 37: 567-582.
- Carpinteri, A. (1992) "Reinforced Concrete Beam Behavior under Cyclic Loadings", In Al. Carpinteri, editor, *Applications of Fracture Mechanics to Reinforced Concrete*, Elsevier Applied Science, London and New York, pp. 547-578
- Carpinteri, A. (1999) "Nonlinear Crack Models for Nonmetallic Materials", Kluwer Academic Publishers, Dordrecht, The Netherlands.
- Carpinteri, A., Carpinteri, An. (1984) "Hysteretic behavior of RC beams", *Journal of Structural Engineering (ASCE)*, 110: 2073–2084.
- Carpinteri, A., Colombo, G. (1989) "Numerical analysis of catastrophic softening behaviour (snap-back instability)", *Computers and Structures*, 31: 607–636.
- Carpinteri, A., Corrado, M., Paggi, M., Mancini, G. (2009) "New model for the analysis of size-scale effects on the ductility of reinforced concrete elements in bending", *J. Eng. Mech.*, 135, 221-229.
- Carpinteri, A., Massabò, R. (1996) "Bridged versus cohesive crack in the flexural behavior of brittle-matrix composites", *International Journal of Fracture*, 81: 125-145.
- Carpinteri, A., Massabò, R. (1997a) "Continuous vs discontinuous bridged crack model of fiber-reinforced materials in flexure", *International Journal of Solids and Structures*, 34: 2321-2338.
- Carpinteri, A., Massabò, R. (1997b) "Reversal in failure scaling transition of fibrous composites", *Journal of Engineering Mechanics (ASCE)*, 123: 107-114.
- Carpinteri, A., Puzzi, S. (2003) "Hysteretic flexural behaviour of brittle matrix fibrous composites: the case of two fibers", *Proc. of 16th National (Italian) Congress of Theoretical and Applied Mechanics (AIMETA)*, CD-ROM, File 102, Ferrara.
- Carpinteri, A., Puzzi, S. (2004) "The Bridged Crack Model for the Analysis of FRC Elements Under Repeated Bending Loading," *Fibre-Reinforced Concretes*, Proc. of 6th RILEM Symposium on Fibre Reinforced Concrete, Varenna, Italy, R.I.L.E.M. Publications S.a.r.l., Bagnaux, M. Di Prisco, R. Felicetti, and G. A. Plizzari, eds., pp. 767–776.

- Carpinteri, A., Puzzi, S. (2007) "The bridged crack model for the analysis of brittle matrix fibrous composites under repeated bending loading", *Journal of Applied Mechanics*, 74: 1239-1246.
- Carpinteri, An., Spagnoli, A., Vantadori, S. (2004) "A fracture mechanics model for a composite beam with multiple reinforcements under cyclic bending", *International Journal of Solids and Structures*, 41: 5499-5515.
- Carpinteri, An., Spagnoli, A., Vantadori, S. (2005) "Mechanical Damage of Ordinary or Prestressed Reinforced Concrete Beams Under Cyclic Bending," *Eng. Fract. Mech.*, 72, pp. 1313–1328.
- Carpinteri, An., Spagnoli, A., Vantadori, S. (2006) "An elastic-plastic crack bridging model for brittle-matrix fibrous composite beams under cyclic loading", *International Journal of Solids and Structures*, 43: 4917-4936.
- Cotterell, B., Paravasivam, P., Lam, K. Y. (1992) "Modelling the Fracture of Cementitious Composites," *Mater. Struct.*, 25, pp. 14–20.
- Cox, B. N. (1991) "Extrinsic Factors in the Mechanics of Bridged Cracks," *Acta Metall. Mater.*, 39: 1189–1201.
- Cox, B. N., Marshall, D. B. (1991a) "Crack Bridging in the Fatigue of Fibrous Composites," *Fatigue Fract. Eng. Mater. Struct.*, 14: 847–861.
- Cox, B. N., Marshall, D. B. (1991b), "Stable and Unstable Solutions for Bridged Cracks in Various Specimens," *Acta Metall. Mater.*, 39: 579–589.
- Dugdale, D. S. (1960), "Yielding of Steel Sheets Containing Slits," *J. Mech. Phys. Solids*, 8: 100–104.
- Erdogan, F., Joseph, P. F. (1987) "Toughening of Ceramics Through Crack Bridging by Ductile Particles," *J. Mech. Phys. Solids*, 35: 262–270.
- Foote, R. M. L., Mai, Y. W., Cotterell, B. (1986) "Crack Growth Resistance Curves in Strain-Softening Materials," *J. Mech. Phys. Solids*, 6: 593–607.
- Guinea, G.V., Pastor, J.Y., Planas, J., Elices, M. (1998) "Stress intensity factor, compliance and CMOD for a general three-point-bend beam", *International Journal of Fracture*, 89: 103-116.
- Hillerborg, A. (1980) "Analysis of Fracture by Means of the Fictitious Crack Model, Particularly for Fibre Reinforced Concrete," *Int. J. Cem. Comp.*, 2: 177–184.
- Hillerborg, A., Modeer, M., and Petersson, P. E. (1976) "Analysis of Crack Formation and Crack Growth in Concrete by Means of Fracture Mechanics and Finite Elements," *Cem. Concr. Res.*, 6: 773–782.

- Jenq, Y. S., Shah, S. P. (1985) "A Two-Parameter Fracture Model for Concrete," J. Eng. Mech., 111: 1227–1241.
- Li, V. C., Liang, E. (1986) "Fracture Processes in Concrete and Fiber Reinforced Cementitious Composites," J. Eng. Mech., 112: 566–586.
- Mai, Y. W. (1991) "Fracture and Fatigue of Non-transformable Ceramics: The Role of Crack-Interface Bridging," Fracture Processes in Concrete, Rock and Ceramics, J. G. M. Van Mier, ed., E.&F.N. Spon, London, pp. 3–26.
- Marshall, D. B., Cox, B. N. (1987) "Tensile Fracture of Brittle-Matrix Composites: Influence of Fiber Strength," Acta Metall. 35: 2607–2619.
- Marshall, D. B., Cox, B. N., Evans, A. G. (1985) "The Mechanics of Matrix Cracking in Brittle Matrix Fiber Composites," Acta Metall., 33: 2013–2021.
- Massabò, R. (1993) "Meccanismi di rottura nei materiali fibrorinforzati", PhD. Thesis, Scuola di Dottorato, Politecnico di Torino.
- Matsumoto T., Li V.C. (1999) "Fatigue life analysis of fiber reinforced concrete with a fracture mechanics based model", Cement and Concrete Composites, 21: 249-261
- Milne, I., Ritchie, R.O., Karihaloo, B. (2003) Comprehensive structural integrity: fracture of materials from nano to macro / eds. in chief I. Milne, R.O. Ritchie and B. Karihaloo Amsterdam: Elsevier
- Murakami, Y. (1987) *Stress Intensity Factors Handbook*, Pergamon Press, Oxford.
- Paris, P. C., Erdogan, F. (1963) "A Critical Analysis of Crack Propagation Laws," ASME J. Basic Eng., 85: 528–534.
- Paris, P. C., Sih, G. C. (1965) "Stress analysis of cracks", *Fracture Toughness Testing and its Applications*, ASTM STP, 381:30-81.
- Petersson, P. E. (1981) "Crack Growth and Development of Fracture Zones in Plain Concrete and Similar Materials," Ph.D. thesis, Lund. Institute of Technology, Lund, Denmark.
- Puzzi, S. (2004) "Mechanics of grained or fibrous heterogeneous materials", PhD. Thesis, Scuola di Dottorato, Politecnico di Torino.
- Reis, J. M. L., Ferreira, A. J. M. (2003) "Fracture Behaviour of Glass Fiber Reinforced Polymer Concrete," Polym. Test., 22: 149–153.
- Rich, T. P., Cartwright, D. J. (1977). Case studies in fracture mechanics (No. AMMRC-MS-77-5). Army Materials And Mechanics Research Center Watertown Ma.

- Ruiz, G. (2001) "Propagation of a Cohesive Crack Crossing a Reinforcement Layer," *Int. J. Fract.*, 111: 265–282.
- Shah, S. P. (1988) "Fracture Toughness of Cement-Based Materials," *Mater. Struct.*, 21: 145–150.
- Sinclair, G.B., Messner, T.W., Meda, G. (1996) "Stress intensity factors for deep edge cracks in bending", *Engineering Fracture Mechanics*, 55: 19-24.
- Tada, H., Paris, P.C., Irwin, G. (1985) *The Stress Analysis of Cracks*, Paris Productions Incorporated (and Del Research Corporation), St. Louis, Missouri.
- Visalvanich, K., Naaman, A. E. (1983) "Fracture Model for Fiber Reinforced Concrete," *ACI J.* 80: 128–138.
- Wecharatana, M., Shah, S. P. (1983) "A Model for Prediction of Fracture Resistance of Fiber Reinforced Concrete," *Cem. Concr. Res.*, 13: 819–829.
- Wilson, W. K. (1970) "Stress intensity factors for deep cracks in bending and compact tension specimens", *Engineering Fracture Mechanics*, 2: 169-171.
- Zhang J., Stang H., Li V.C. (1999) "Fatigue life prediction of fiber reinforced concrete under flexural load", *International Journal of Fatigue*, 21: 1033-1049
- Zhang J., Stang H., Li V.C. (2001) "Crack bridging model for fibre reinforced concrete under fatigue tension", *International Journal of Fatigue*, 23: 655-670
- Zhang, J., Li, V. C. (2004) "Simulation of Crack Propagation in Fiber-Reinforced Concrete by Fracture Mechanics," *Cem. Concr. Res.*, 34: 333–339.

Appendix – MATLAB code

Appendix 1 – Crack Length Control Scheme

```

function [M_plot,phi_plot] =
Monotono(b,h,a,z,E,Kc,Pp,csi_max,delta_csi)
csi=a/h;
P=zeros(length(z),1);
if max(z(z<=csi))==csi
    csi=csi+0.1*delta_csi;
end
csi=csi:delta_csi:csi_max;
Mp=[];
phi_p=[];
M_plot=[];
phi_plot=[];
for i=1:length(csi)
    X=z<csi(i);
    x=z(X);
    if (csi(i)-max(x))<0.05*delta_csi
        csi(i)=csi(i)+0.1*delta_csi;
    end
    C_PP=c_PP(E,b,csi(i),x);
    C_MP=c_MP(E,b,h,csi(i),x);
    C_MM=c_MM(E,b,h,csi(i));
    y_M=Y_M(csi(i));
    y_P=Y_P(csi(i),x);
    c=1:length(x);
    f=[];
    C_cc=C_PP(c,c);
    C_cf=C_PP(c,f);
    C_Mc=C_MP(c);
    continua=1;
    while continua
        if isempty(f)
            MatrA=C_cc-C_Mc*y_P(c)'*h/y_M;
            TnB=C_Mc*(b*h^1.5*Kc/y_M);
            P(c)=MatrA\TnB;
        else
            try
                MatrA=C_Mc*y_P(c)'*h/y_M-C_cc;
                TnB=-(C_Mc*(b*h^1.5*Kc/y_M+h/y_M*y_P(f)')*P(f))-
C_cf*P(f));
                P(c)=MatrA\TnB;
            end
        end
        continua=0;
        [Pmax,k]=max(P);
        if Pmax>Pp(k)
            P(k)=Pp(k);
            f=sort([f,k]);
            c(c==k)=[];
            continua=1;
            C_cc=C_PP(c,c);
            C_cf=C_PP(c,f);
            C_Mc=C_MP(c);

```

```

end

[Pmin,k]=min(P);
if Pmin<0
    P(k)=Pp(k);
    f=sort([f,k]);
    c(c==k)=[];
    continua=1;
    C_cc=C_PP(c,c);
    C_cf=C_PP(c,f);
    C_Mc=C_MP(c);
end

end

M_fract(i)=b*h^1.5/y_M*(Kc+P(X) '*y_P/(b*h^0.5));
phi(i)=C_MM*M_fract(i)-C_MP'*P(X);
if i>1
    [M_plast, phi_plast]= M_plastici( x,Pp(X),C_PP,C_MP,C_MM );
    compresi=(M_plast>M_fract(i-1)) & (M_plast<M_fract(i));
    Mp=M_plast(compresi);
    phi_p=phi_plast(compresi);
else
    [M_plast, phi_plast]= M_plastici( x,Pp(X),C_PP,C_MP,C_MM );
    compresi=(M_plast<M_fract(i));
    Mp=M_plast(compresi);
    phi_p=phi_plast(compresi);
end
M_plot=[M_plot,Mp,M_fract(i)];
phi_plot=[phi_plot,phi_p,phi(i)];
end
end

function [Mp_min, phi,varargout] = M_plastici( x,Pp,C_PP,C_MP,C_MM )
P=zeros(length(x),1);
P_mem=zeros(length(x),length(x));
Mp=Pp./(inv(C_PP)*C_MP);
Mp(Mp<0)=max(Mp);
[Mp_min(1),k]=min(Mp);
n=length(x);
c=[1:k-1,k+1:n];
f=k;
C_cc=C_PP(c,c);
C_cf=C_PP(c,f);
C_Mc=C_MP(c);
P(f)=Pp(f);
try
P(c)=inv(C_cc)*(C_Mc*Mp_min(1)-C_cf*P(f));
end
phi(1)=C_MM*Mp_min(1)-C_MP'*P;
P_mem(:,1)=P;
for i=2:n
    Mp=(Pp(c)+inv(C_cc)*C_cf*Pp(f))./(inv(C_cc)*C_Mc);
    Mp(Mp<0)=max(Mp);
    [Mp_min(i),k]=min(Mp);
    f=sort([f,c(k)]);
    c(k)=[];

```

```

    C_cc=C_PP(c,c);
    C_cf=C_PP(c,f);
    C_Mc=C_MP(c);
    P(f)=Pp(f);
    P(c)=inv(C_cc)*(C_Mc*Mp_min(i)-C_cf*P(f));
    phi(i)=C_MM*Mp_min(i)-C_MP'*P;
    P_mem(:,i)=P;
end
end

```

Appendix 2 – Force-controlled algorithm

```

%BEAM
b=25;
h=40;
a=4;
csi=a/h;
%FIBERS
ri=0.3;
Ai=pi*ri^2;
x_min=0.1;
x_max=0.5;
m=10;
z=linspace(x_min,x_max,m)';
A=Ai*ones(m,1);
%MATERIALS
E=300000;
Kc=100;
fyi=4500;
fy=fyi*ones(m,1);
%LOAD
M_max=300000;
n_punti=500;
n_cicli=2;
%CRACK
delta_csi=0.005;
csi_max=0.7;

M=[linspace(0,M_max,n_punti),linspace(M_max,0,n_punti)];
M= repmat(M,1,n_cicli);
if max(z(z<=csi))==csi
    csi=csi+0.1*delta_csi;
end
Pp=fy.*A;
P=zeros(m,1);
plast=false(size(M));
crack=false(size(M));
X=z<csi;
x=z(X);
C_PP=c_PP(E,b,csi,x);
C_MP=c_MP(E,b,h,csi,x);
C_MM=c_MM(E,b,h,csi);
c=1:length(x);
f=[];
C_cc=C_PP(c,c);

```

```

C_cf=C_PP(c,f);
C_Mc=C_MP(c);
M_0=0;
phi_0=0;
P_0=zeros(m,1);
direzione_prec=1;
rotto=0;
P_mem=zeros(m,length(M));
for i=1:length(M)
    continua=1;
    while continua
        if isempty(f)
            P(c)=P_0(c)+inv(C_cc)*(C_Mc*(M(i)-M_0));
        else
            try
                P(c)=P_0(c)+inv(C_cc)*(C_Mc*(M(i)-M_0)-C_cf*(P(f)-
P_0(f)));
            end
        end
        continua=0;
        for j=1:length(P)
            if P(j)>Pp(j)
                P(j)=Pp(j);
                f=sort([f,j]);
                c(c==j)=[];
                continua=1;
                C_cc=C_PP(c,c);
                C_cf=C_PP(c,f);
                C_Mc=C_MP(c);
                plast(i)=true;
            end
            if P(j)<-Pp(j)
                P(j)=-Pp(j);
                f=sort([f,j]);
                c(c==j)=[];
                continua=1;
                C_cc=C_PP(c,c);
                C_cf=C_PP(c,f);
                C_Mc=C_MP(c);
                plast(i)=true;
            end
        end
    end
    if i<length(M) && M(i)<M(i+1)
        direzione=1;
    else
        direzione=0;
    end
    M_F=b*h^1.5/Y_M(csi)*(Kc+P(X)'*Y_P(csi,x)/(b*h^0.5));
    while M_F<M(i)
        csi_prec=csi;
        csi=min(z(z>csi))+0.1*delta_csi;
        crack(i)=true;
        if isempty(csi)
            csi=csi_prec+delta_csi;
            if csi>csi_max

```

```

        rotto=1;
        break;
    end
else
    X=z<csi;
    x=z(X);
    c=[c,length(x)];
end
C_PP=c_PP(E,b,csi,x);
C_MP=c_MP(E,b,h,csi,x);
C_MM=c_MM(E,b,h,csi);
C_cc=C_PP(c,c);
C_cf=C_PP(c,f);
C_Mc=C_MP(c);
continua=1;
while continua
    if isempty(f)
        P(c)=P_0(c)+inv(C_cc)*(C_Mc*(M(i)-M_0));
    else
        try
            P(c)=P_0(c)+inv(C_cc)*(C_Mc*(M(i)-M_0)-C_cf*(P(f)-
P_0(f)));
        end
    end
    continua=0;
    for j=1:length(P)
        if P(j)>Pp(j)
            P(j)=Pp(j);
            f=sort([f,j]);
            c(c==j)=[];
            continua=1;
            C_cc=C_PP(c,c);
            C_cf=C_PP(c,f);
            C_Mc=C_MP(c);
            plast(i)=true;
        end
        if P(j)<=-Pp(j)
            P(j)=-Pp(j);
            f=sort([f,j]);
            c(c==j)=[];
            continua=1;
            C_cc=C_PP(c,c);
            C_cf=C_PP(c,f);
            C_Mc=C_MP(c);
            plast(i)=true;
        end
    end
end
M_F=b*h^1.5/Y_M(csi)*(Kc+P(X)'*Y_P(csi,x)/(b*h^0.5));
end
phi(i)=phi_0+C_MM*(M(i)-M_0)-C_MP'*(P(X)-P_0(X));
P_mem(:,i)=P;
if rotto==1
    break;
end
if direzione_prec~=direzione

```

```

        M_0=M(i);
        phi_0=phi(i);
        P_0=P;
        direzione_prec=direzione;
        c=1:length(x);
        f=[];
        C_cc=C_PP(c,c);
        C_cf=C_PP(c,f);
        C_Mc=C_MP(c);
    end
    P_mem(:,i)=P;
end
plot(phi,M);

```

Appendix 3 – Rotation-controlled algorithm

```

%BEAM
b=25;
h=40;
a=4;
csi=a/h;
%FIBERS
ri=0.4;
Ai=pi*ri^2;
x_min=0.1;
x_max=0.3;
m=3;
z=linspace(x_min,x_max,m)';
A=Ai*ones(m,1);
%MATERIALS
E=300000;
Kc=100;
fyi=4500;
fy=fyi*ones(m,1);
%ANGLE
phi_max=0.00035;
n_punti=500;
n_cicli=2;
%CRACK
delta_csi=0.005;
csi_max=0.7;

phi=[linspace(0,phi_max,n_punti),linspace(phi_max,0,n_punti)];
phi= repmat(phi,1,n_cicli);
if max(z(z<=csi))==csi
    csi=csi+0.1*delta_csi;
end
Pp=fy.*A;
P=zeros(m,1);
plast=false(size(phi));
crack=false(size(phi));
X=z<csi;
x=z(X);
C_PP=c_PP(E,b,csi,x);
C_MP=c_MP(E,b,h,csi,x);
C_MM=c_MM(E,b,h,csi);
c=1:length(x);

```

```

f=[];
C_cc=C_PP(c,c);
C_cf=C_PP(c,f);
C_ff=C_PP(f,f);
C_Mc=C_MP(c);
C_Mf=C_MP(f);
M_0=0;
phi_0=0;
P_0=zeros(m,1);
direzione_prec=1;
rotto=0;
P_mem=zeros(m,length(phi));
for i=1:length(phi)
    continua=1;
    while continua
        if isempty(f)
            P(c)=P_0(c)+(-C_Mc*C_Mc'/C_MM+C_cc)\(C_Mc/C_MM*(phi(i)-
phi_0));
        else
            try
                P(c)=P_0(c)+(-C_Mc*C_Mc'/C_MM+C_cc)\
(C_Mc/C_MM*(phi(i)- phi_0+C_Mf'*(P(f)-P_0(f)))-C_cf*(P(f)-P_0(f)));
            end
        end
        continua=0;
        for j=1:length(P)
            if P(j)>Pp(j)
                P(j)=Pp(j);
                f=sort([f,j]);
                c(c==j)=[];
                continua=1;
                C_cc=C_PP(c,c);
                C_cf=C_PP(c,f);
                C_ff=C_PP(f,f);
                C_Mc=C_MP(c);
                C_Mf=C_MP(f);
                plast(i)=true;
            end
            if P(j)<-Pp(j)
                P(j)=-Pp(j);
                f=sort([f,j]);
                c(c==j)=[];
                continua=1;
                C_cc=C_PP(c,c);
                C_cf=C_PP(c,f);
                C_ff=C_PP(f,f);
                C_Mc=C_MP(c);
                C_Mf=C_MP(f);
                plast(i)=true;
            end
        end
    end
    end
    M(i)=M_0+(phi(i)-phi_0+C_MP'*(P(X)-P_0(X)))/C_MM;

    if i<length(phi)&&phi(i)<phi(i+1)
        direzione=1;
    end
end

```

```

else
    direzione=0;
end
M_F=b*h^1.5/Y_M(csi)*(Kc+P(X)'*Y_P(csi,x)/(b*h^0.5));
while M_F<M(i)
    csi=csi+delta_csi;
    X=z<csi;
    x=z(X);
    if (csi-max(x))<(0.05*delta_csi)
        csi=csi+0.1*delta_csi;
    end
    crack(i)=true;
    if csi>csi_max
        rotto=1;
        break
    end
    C_PP=c_PP(E,b,csi,x);
    C_MP=c_MP(E,b,h,csi,x);
    C_MM=c_MM(E,b,h,csi);
    c=1:length(x);
    f=[];
    C_cc=C_PP(c,c);
    C_cf=C_PP(c,f);
    C_ff=C_PP(f,f);
    C_Mc=C_MP(c);
    C_Mf=C_MP(f);
    continua=1;
    while continua
        if isempty(f)
            P(c)=P_0(c)+(-C_Mc*C_Mc'/C_MM+C_cc)\
(C_Mc/C_MM*(phi(i)-phi_0));
        else
            try
                P(c)=P_0(c)+(-C_Mc*C_Mc'/C_MM+C_cc)\
(C_Mc/C_MM*(phi(i)-phi_0+C_Mf'* (P(f)-P_0(f)))-C_cf*(P(f)-P_0(f)));
            end
        end
        continua=0;
        [Pmax,k]=max(P(X));
        if Pmax>Pp(k)
            P(k)=Pp(k);
            f=sort([f,k]);
            c(c==k)=[];
            continua=1;
            C_cc=C_PP(c,c);
            C_cf=C_PP(c,f);
            C_ff=C_PP(f,f);
            C_Mc=C_MP(c);
            C_Mf=C_MP(f);
        end
        [Pmin,k]=min(P(X));
        if Pmin<-Pp(k)
            P(k)=-Pp(k);
            f=sort([f,k]);
            c(c==k)=[];
            continua=1;
        end
    end
end

```

```

        C_cc=C_PP(c,c);
        C_cf=C_PP(c,f);
        C_ff=C_PP(f,f);
        C_Mc=C_MP(c);
        C_Mf=C_MP(f);
    end
end
M(i)=M_0+(phi(i)-phi_0+C_MP'(P(X)-P_0(X)))/C_MM;
M_F=b*h^1.5/Y_M(csi)*(Kc+P(X))*Y_P(csi,x)/(b*h^0.5);
end
if direzione_prec~=direzione
    M_0=M(i);
    phi_0=phi(i);
    P_0=P;
    direzione_prec=direzione;
    c=1:length(x);
    f=[];
    C_cc=C_PP(c,c);
    C_cf=C_PP(c,f);
    C_ff=C_PP(f,f);
    C_Mc=C_MP(c);
    C_Mf=C_MP(f);
end
if rotto ==1
    break;
end
P_mem(:,i)=P;
end
plot(phi,M);

```

Appendix 4 – Shape functions

```

function valore_funzione_forma = Y_M( e )
%Tada et al. 1985
% if e<=0.6
%     valore_funzione_forma=6*(1.99*e.^0.5-2.47*e.^1.5+12.97*e.^2.5-
23.17*e.^3.5+24.8*e.^4.5);
% else
%     valore_funzione_forma=3.99*(1-e).^(-1.5);
% end
%Guinea et al. (1998)
p_inf=1.99+0.83*e-0.31*e.^2+0.14*e.^3;
k_b=sqrt(e)./(1-e).^1.5.*(1+3*e)).*(p_inf);
valore_funzione_forma=6*k_b;
%Paris, Sih 1965
% c=2*(pi-2)/(3*(pi^2-8));
% valore_funzione_forma=6*sqrt(pi)*(1-e).^(-1.5).*c;
%Paris, Sih 1965 interpolati
% c=0.375 + 0.108*(exp(24*(4/3*e- 1)) - 1)/10^4;
% valore_funzione_forma=6*sqrt(pi)*(1-e).^(-1.5).*c;
end

function valore_funzione_forma = Y_P( e, x )
%Tada et al. 1985
g1=0.46+3.06*e+0.84*(1-e).^5+0.66*e.^2.*(1-e).^2;
g2=-3.52*e.^2;

```

```

g3=6.17-28.22*e+34.54*e.^2-14.39*e.^3-(1-e).^1.5-5.88*(1-e).^5-
2.64*e.^2.*(1-e).^2;
g4=-6.63+25.16*e-31.04*e.^2+14.41*e.^3+2*(1-e).^1.5+5.04*(1-
e).^5+1.98*e.^2.*(1-e).^2;
G=g1+g2.*x./e+g3.*(x./e).^2+g4.*(x./e).^3;
valore_funzione_forma=2./sqrt(pi*e).*(1-e).^(-1.5).*(1-(x./e).^2).^(-
0.5.*G;
end

```

Appendix 5 – Compliances

```

function cedevolezza_MM = c_MM( E,b,h,csi )
integrando=@(e) Y_M(e).^2;
cedevolezza_MM=2/(h^2*b*E)*integral(integrando,0,csi);
end

function cedevolezza_MP = c_MP( E,b,h,csi,zita )
cedevolezza_MP=zeros(length(zita),1);
for i=1:length(zita)
    integrando=@(e) Y_P(e,zita(i)).*Y_M(e);
    cedevolezza_MP(i)=2/(h*b*E)*integral(integrando,zita(i),csi);
    cedevolezza_MP(i)=real(cedevolezza_MP(i));
    if isnan(cedevolezza_MP(i))
        cedevolezza_MP(i)=0;
    end
end
end

function cedevolezza_PP = c_PP( E,b,csi,zita )
cedevolezza_PP=zeros(length(zita),length(zita));
delta=0.00001;
for i=1:length(zita)
    for j=i:length(zita)
        if i==j
            integrando=@(e) Y_P(e,zita(i)).*Y_P(e ,zita(j)+delta);
            cedevolezza_PP(i,j)=2/(b*E)*integral(integrando,zita(i)+delta,c
si);
        else
            integrando=@(e) Y_P(e,zita(i)).*Y_P(e,zita(j));
            cedevolezza_PP(i,j)=2/(b*E)*integral(integrando,max(zita(i),zita(j))
,csi);
        end
        cedevolezza_PP(i,j)=real(cedevolezza_PP(i,j));
        if isnan(cedevolezza_PP(i,j))
            cedevolezza_PP(i,j)=0;
        end
    end
end
end
cedevolezza_PP=cedevolezza_PP+cedevolezza_PP'-
diag(diag(cedevolezza_PP));
end

```